MODIFICATION OF STAINLESS STEEL SURFACES

FOR ADVANCED FUNCTIONALITIES

A Dissertation
Presented to
The Academic Faculty

by

Won Tae Choi

In Partial Fulfillment
of the Requirements for the Degree
Doctor of Philosophy in Chemical Engineering
in the School of Chemical & Biomolecular Engineering

Georgia Institute of Technology
May 2017

MODIFICATION OF STAINLESS STEEL SURFACES

FOR ADVANCED FUNCTIONALITIES

Approved by:

Dr. Dennis W. Hess, Advisor
School of Chemical & Biomolecular Engineering
Georgia Institute of Technology

Dr. Victor Breedveld, Advisor
School of Chemical & Biomolecular Engineering
Georgia Institute of Technology

Dr. Thomas F. Fuller
School of Chemical & Biomolecular Engineering
Georgia Institute of Technology

Dr. J. Carson Meredith
School of Chemical & Biomolecular Engineering
Georgia Institute of Technology

Dr. Preet M. Singh
School of Materials Science & Engineering
Georgia Institute of Technology

Date Approved: January 10, 2017

Dedicated to my loving family: Dad, Mom, Brother, and my Wife

Dr. Doo Jin Choi, Myunghye Lee, Wonjoong Choi, and Dr. Yeongseon Jang

ACKNOWLEDGEMENTS

First and foremost, I would like to express my greatest gratitude to my advisors Dr. Dennis W. Hess, and Dr. Victor Breedveld for all their guidance and support throughout my Ph.D. studies. I was motivated by their enthusiasm and attitude on science. Also, their guidance at each point of my Ph.D. works made me to be on a right track and this accomplishment possible. I will never be able to express my deepest appreciation to them for their patience, encouragement, and all I have learned for the past four years. I am grateful to my committee members, Dr. Preet M. Singh, Dr. Thomas F. Fuller, and Dr. J. Carson Meredith, for providing me their broad knowledge and contributions to my works. It was my pleasure to have these great professors as my thesis committee. I would like to thank to Dr. Preet M. Singh for valuable advice and generosity for allowing me to use resources and facilities in his lab. I would like to extend thank to Dr. Kkochnim Oh for helping me quickly start on my work.

I am grateful to all the past and present Hess and Breedveld group members, Dr. Kyung Hee Oh, Dr. Tae-seop Choi, Dr. Sricharan Yarlagadda, Dr. Zhenguan Tang, Lu Jiang, and Xiaolong Yang for valuable discussions and helpful hands. I will also remember our laughs and conversations we have had in the group. I also thank to my Georgia Tech Korean friends for their encouragements and support.

I want to express my sincerest appreciation to my parents, Dr. Doo Jin Choi, and Myunghye Lee, for their unconditional love and support to my academic endeavors. They showed me their passion and philosophy on education. They always told me a story. When a butterfly extract itself from its cocoon, it should experience and overcome the difficulty by itself, so

that gaining sufficient strength during the extracting, and flap the wings to fly. Like this, there is no shortcut and stepping on my own way is the fastest way to achieve anything. I would like to thank to my brother, Wonjoong Choi, for his care and being there for me, and I always care him, too. I am thoroughly grateful to my parents in-law, Gubong Jang and Chunbun Yoon, and sisters in-law, Hye-ryeon Jang and Hye-eun Jang, for their constant support, and pray.

Finally, to my loving wife Dr. Yeongseon Jang, I owe many things: her love, support, understanding, and encouragements. I am grateful to her for being my wife, and I would like to say that absolutely none of this work would have been possible without you.

TABLE OF CONTENTS

LIST OF TABLES

LIST OF FIGURES

SUMMARY

In industry, business, and homes worldwide, metal alloys called stainless steels are used extensively. Stainless steel is a generic term for a large family of iron-based alloys containing a minimum of 10.5% chromium content by weight. The primary alloying element, chromium, forms a thin passive layer of chromium oxide/hydroxide when exposed to air and moisture, which is dense and impervious to water and air, thereby protecting the bulk metal beneath the surface layer. Stainless steel alloy composition, along with surface properties such as surface chemistry and topography, significantly impact the reliability and performance of stainless steels in their myriad applications. Typically, a smooth stainless steel surface with chromium enrichment is desired because of the enhanced corrosion resistance it displays. Recently, much attention has focused on controlling both surface structure and chemistry to achieve advanced functionalities such as liquid repellency, anti-bacterial, and anti-fouling properties. Most such studies have been conducted on soft materials like paper/cellulose and polymers. However, the extensive and varied applications of stainless steels often require exposure to complex and harsh environments such as corrosive liquids, seawater, food and beverages, and body fluids. As a result, considerable interest has developed in stainless steel surface modifications to achieve advanced functionalities beyond corrosion resistance alone. In this thesis, studies are described in which stainless steel surfaces are modified to control hydrophobicity, corrosion resistance, and anti-bacterial properties. Among the many different types of stainless steels, stainless steel 316L(SS316L) was chosen as the starting

material because of its extensive use in many industries, including maritime, bio-medical, and infrastructure applications.

Metals and metal alloys are composed of grains with different orientations; grain boundaries represent interfaces between the grains. These grain boundaries have high interfacial energy and relatively weak atomic bonding, which renders them more susceptible to etching or dissolution under certain conditions than the grains themselves. The etching at different rates can therefore results in surface roughening. Here, electrochemical etching has been employed to modify SS316L surfaces. Variation in the applied anodic potential during electrochemical etching altered the etch selectivity between grains and grain boundaries, thereby producing various surface structures on SS316L. A relationship between the applied anodic potential and SS316L surface topography was established, which served as the basis to control roughness and thereby develop advanced functionalities.

A super-hydrophobic stainless steel surface offers benefits in many applications including efficient fluid transport in pipes through drag reduction and effective drainage and cleaning of storage tanks. Generation of a hierarchical structure that combines nanoscale and microscale surface roughness is critical to achieve super-hydrophobicity. Based upon the established relationship, a two-step electrochemical etching process was developed for SS316L by consecutively using two different applied anodic potentials; this sequence accentuated both nanoscale and microscale roughness on SS316L surfaces. Deposition of a thin fluorocarbon layer on the hierarchically structured SS316L yielded super-hydrophobicity with a static contact angle of 163.9 ° ± 1.2 and a roll-off angle of 10.7 ° ± 2.9 with 4 μL water droplets.

Despite the corrosion resistance of stainless steel surfaces, they are not fully corrosion-proof in corrosive environments such as seawater. Seawater is a solution with approximately 0.6 M sodium chloride and diverse maritime bio-organisms, which trigger local breakdown of passive layers and cause localized corrosion. In order to improve the localized corrosion resistance, electrochemical surface modification was conducted on SS316L with an anodic potential of 1.3 V vs. SCE, which resulted in a microscale grain boundary etched surface. Corrosion tests performed in 0.6 M sodium chloride solution displayed superior corrosion resistance with a narrow distribution of high breakdown potentials (0.96 to 1.05 V vs. SCE) compared to that of as-received SS316L (0.32 to 0.86 V vs. SCE). In addition, the grain boundary etched SS316L exhibited hydrophobicity with a static water contact angle of 135.7° ± 2.6. This unique combination of hydrophobicity and microscale topography on the SS316L surface offers the potential to reduce adhesion of marine organisms, which further deters localized corrosion and improves the reliability of this material in the maritime industry.

Pathogenic bacterial adhesion on stainless steel surfaces is problematic because the existence of bacteria on implants, surgical tools, and biomedical devices can cause infectious diseases. Nanoscale surface topography can reduce bacterial adhesion by generating repulsive forces for bacteria and by inducing stress to the cell membrane where bacteria are attached. Nano-textures were achieved on SS316L surface by the electrochemical surface modification at an anodic potential of 2.2 V vs. SCE. *E.coli*, a gram-negative bacterium was used to investigate bacterial adhesion on SS316L, and a significant reduction in *E.coli* adhesion was observed on the nano-textured SS316L surface compared to an as-received SS316L surface. However, no difference in adhesion and

metabolic activity of fibroblast (NIH-3T3) cells between nano-textured and as-received SS316L surfaces was observed. Therefore, the nano-textured SS316L surface can reduce bacterial adhesion while maintaining adhesion and biocompatibility with desired cells.

A patterned surface with dissimilar wettability has many potential applications such as diagnostic sensors and microfluidic platforms. Copper is a relatively cheap engineering metal due to its abundance. A simple method to fabricate a hydrophobic pattern on super-hydrophobic copper surface was devised as a proof of concept. A commercially available marker pen was utilized to directly draw patterns on copper surface, which served as masking layer, thereby growing nanowire selectively on background region in an aqueous solution. Fluorocarbon film deposition on the copper surface resulted in hydrophobic pattern/super-hydrophobic background copper surface. Diverse patterns including dot, line, and curve were attained on copper surface to demonstrate droplet manipulations.

CHAPTER 1. INTRODUCTION

1.1 History of Stainless Steels

In 1821, French metallurgist Pierre Berthier, first discovered corrosion resistance of iron-chromium alloys against acid attacks and suggested use of the alloys in cutlery. However, the alloys in the 19th century were too brittle to be practical because of high carbon content. Since then, extensive research has led to the invention of stainless steels. In 1913, Harry Brearley, a lead scientist of Brown-Firth research laboratory in England, created a steel alloy with 12.8% chromium and 0.24% carbon, which is argued to be the first stainless steel.[1] Stainless steel was first applied to cutlery, and different grades of stainless steels with ductility and improved corrosion resistance were invented, which paved a road to countless applications including scalpels, engines of aircrafts, cars, chemical tanks, milk tanks, Swiss Army knife, and architectural projects like the Chrysler building in New York and St. Paul's Cathedral in London. Today, there are more than 150 grades of stainless steel and global production of the stainless steels in 2015 reportedly exceeded 41.5 million tons.[2] Worldwide, stainless steels are used daily everywhere: in industry and in homes.

1.2 Stainless Steel Grades

Stainless steel is a generic term for a large family of iron-based alloys containing a minimum of 10.5% chromium content by weight.[3] Chromium is the primary element to impart corrosion resistance by formation of a thin passive layer of chromium oxide/hydroxide, which is impervious to water and air, thereby protecting the bulk metal underneath.[4] If the passive layer is damaged by abrasion or scratches, the layer self-repairs when in contact with oxygen from air or water.[5] Furthermore, addition of other metallic or non-metallic elements to stainless steels can improve desired physical properties.[6-7] For instance, nickel addition improves ductility,[8] and molybdenum enhances corrosion resistance by stabilizing the passive layer.[9] Small amounts of carbon and manganese increase the mechanical strength of stainless steels because having differently sized atoms in the lattice prevents lattice layers from sliding over each other easily. In all these cases, alloy compositions determine the corrosion resistance and physical properties of stainless steels.

Stainless steels can be classified into four categories by crystal structure: austenite, ferrite, martensite, and duplex, which have face centered cubic (FCC), body centered cubic (BCC), body centered tetragonal (BCT), and mixed FCC/BCC microstructures, respectively (Figure 1).[3, 5, 10] Ranges of chemical compositions of the various stainless steel groups are shown in Table 1.[5, 7]

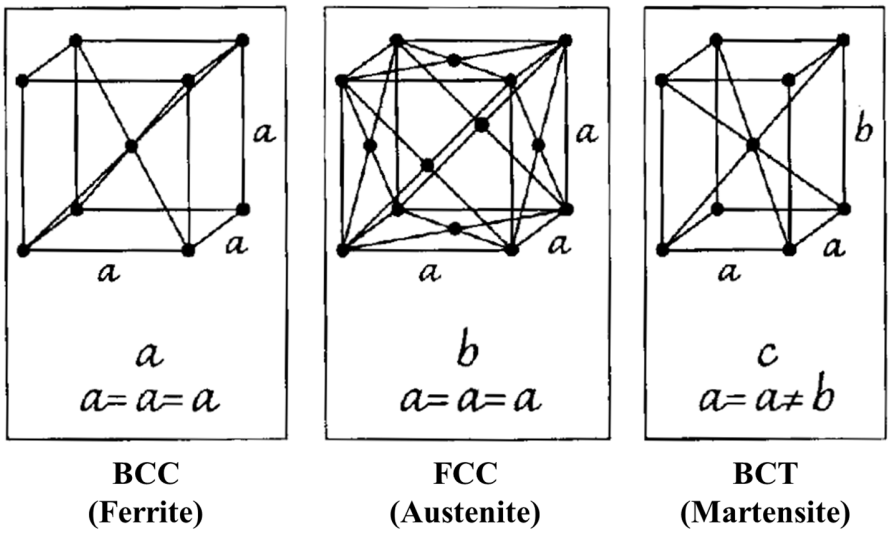

Figure 1. Crystal structures of stainless steels. (Adapted from reference [3])

Table 1. Chemical compositions of stainless steels (%)

	Cr	Ni	C	Other Elements
Austenite	16-28	3.5-32	< 0.08	Mn, N
Ferrite	10.5-27	No or Little	< 0.08	Mo < 4
Martensite	12-14	< 2	0.1-1	Mo 0.2-1
Duplex	19-32	1.4-7	< 0.03	Mo 0.3-4

1.2.1 Austenitic Stainless Steels

Austenitic stainless steels are the most common group of stainless steels at more than 70% of total stainless steel production.[5] Austenitic stainless steels have a relatively high chromium content, and thus offer superior corrosion resistance. Nickel and/or manganese stabilize the austenitic crystal structure over a wide range of temperatures, from cryogenic conditions to the alloy melting point, and provide good ductility.[11] Because of the beneficial combination of superior corrosion resistance and ductility, austenitic stainless steels are widely used in piping, vessels, cookware, food and beverage equipment, processing equipment, and medical devices.[3, 10]

1.2.2 Ferritic Stainless Steels

Ferritic stainless steels have lower chromium and nickel contents compared to austenitic stainless steels, which leads to reduced corrosion resistance and lower ductility, but are usually lower in price than austenitic grades.[5] Ferritic stainless steels are commonly used in automotive exhaust systems, sinks, and other less expensive consumer products such as appliances and flatware.[3]

1.2.3 Martensitic Stainless Steels

Martensitic stainless steels are not as corrosion resistant as the other grades of stainless steels, but have improved mechanical strength and hardenability due to their high carbon contents.[5] Martensitic stainless steels are used extensively in cutlery, automotive, aerospace, sport equipment, and surgical tools.[3]

1.2.4 Duplex Stainless Steels

Duplex stainless steels contain a mixture of austenite and ferrite, and exhibit roughly twice the mechanical strength of austenitic stainless steel, while high chromium and molybdenum contents yield improved corrosion resistance.[5, 12] They are mainly used in high-strength applications where better corrosion resistance is required, for example in the petrochemical industry in heat exchangers, pressure vessels and tanks.[3]

1.3 Essential Properties of Stainless Steels

In many applications, including petrochemical, maritime, and biomedical industries, stainless steel surfaces are exposed to liquids and bio-organisms. Controlling interactions with these media is of critical importance for many stainless steel applications. In this section, three key properties are described in more detail: corrosion resistance, wettability, and biofouling, in order to highlight the necessity to control these properties.

1.3.1 Corrosion Resistance of Stainless Steels

The most defining property of stainless steels is corrosion resistance. Corrosion is defined as the deterioration of a material due to (electro)chemical reactions with its environments.[13-14] Corrosion is a major problem in almost all application, including vehicles, buildings, bridges, home appliances, pipelines, and water purification systems.[14] In extreme cases, material failures triggered by corrosion can result in disasters and expensive recurring costs. For example, the San Francisco Bay Bridge collapsed due to bolt failure.[15] In 2016, the estimated corrosion-related cost in the US was $1.1 trillion, which is about 6.1% of US GDP.[16] However, many corrosion-related problems can be predicted and prevented to ensure public safety save economic budgets. One of the most effective solutions is use of corrosion resistant alloys, of which stainless steels are prime examples. When ordinary carbon steels are exposed to air and moisture, they form rusts, which are flaky and provide no protection to the underlying metal. In contrast, stainless steels form a dense passive layer of chromium oxide that protects the metal beneath. Nevertheless, even stainless steels can corrode in corrosive environments such as strong acid media and high salinity, thereby limiting the applicability of stainless steels in such

environments. In the following sections, fundamentals of corrosion phenomena are discussed.

1.3.1.1 General Corrosion

Corrosion can be classified into two different types: general and localized corrosion. General corrosion, also known as uniform corrosion, represents relatively uniform loss of metals across the entire surface.[13] This mainly occurs when stainless steels are exposed to highly acidic conditions.[17] Because of the evenly receding characteristic, it is relatively easy to predict the metal loss through corrosion, which makes disastrous failure rare.

1.3.1.2 Localized Corrosion

Localized corrosion is an accelerated form of corrosion at discrete sites of passive metals where the protective passive layer has broken down. [13, 18-19] Pitting corrosion is the most common form of localized corrosion. This mechanism produces hole or cavities in the material, and is more dangerous than general (or uniform) corrosion damage because it is more difficult to detect and a single small, narrow pit can lead to failure of an entire engineering system. Local defects on passive layer and non-metallic inclusions such as manganese sulfide on stainless steels are common pitting initiation sites because they are electrochemically more active than the surrounding material.[19-20] Once pitting corrosion begins, localized production of metal cations facilitates migrations of aggressive chloride anions in order to maintain charge neutrality, thereby further accelerating the pitting corrosion. The occurrence of pitting corrosion is strongly dependent on the surface quality of stainless steels: smooth stainless steel surfaces with a homogeneous passive layer are generally desired for better localized corrosion resistance. Therefore, surface finishing

techniques play a pivotal role in localized corrosion behavior, as will be discussed in section 1.4 in greater detail.

1.3.2 Wetting on Stainless Steel Surfaces

Wettability of liquids on stainless steel surfaces is significant in many industrial applications. In particular, surface wettability plays critical roles in heterogeneous condensation[21-22] and liquid mobility on the surface.[23-24] Condensation is the change of physical state of matter from gas phase to liquid phase and vapor condensation on a solid surface is relevant in many stainless steel industrial applications including heat exchanger,[21] desalination,[25] and water harvesting system.[26] Enhancing condensation rate can significantly improve efficiency of such applications. Surface wettability is one of the key factors determining condensation behavior. On highly wetting surface, film-wise condensation occurs, where a thin liquid film covers the solid surface. In this type of condensation, large thermal resistance associated with the condensate film limits overall heat transfer efficiency.[21] Whereas, drop-wise condensation occurs on non-wetting surface, where droplets can be shed away easily to expose solid surface for nucleation of droplets, thereby improving condensation rates.[21] Drag is a resistant force against an object moving through the fluid. Fluid drag reduction is beneficial for many stainless steel applications including marine vessel and liquid transporting pipe. Extremely non-wetting surface can retain air bubble at the solid surface when submerged in or contacted with water, which permits slip (or drag reduction) to occur across the surface.[23-24] Therefore, surface wettability is an essential property to be considered in many stainless steel applications; below, fundamentals wetting phenomena are briefly discussed to provide the framework for surface modifications that will be pursued in this thesis.

1.3.2.1 Wetting on Ideal Surfaces

Wetting captures how strongly liquids want to maintain contact with a solid surface as a result of intermolecular interactions. An ideal solid surface is rigid, flat, perfectly smooth and chemically homogeneous. The behaviour of a liquid droplet on an ideal solid surface (rigid, flat, perfectly smooth, chemically homogeneous) can be described by Young's equation for the equilibrium contact angle (θ_Y):[27]

$$\gamma_{lv}\cos\theta_Y = \gamma_{sv} - \gamma_{ls} \quad (1)$$

in terms of interfacial energies of solid-liquid (γ_{SL}), solid-vapor (γ_{LV}), and liquid-vapor (γ_{LV}), where γ_{ij} depends on the chemistries of the reactive interfaces. Equation (1) can also be interpreted as a force balance between surface tension forces on the three phase contact line (Figure 2).

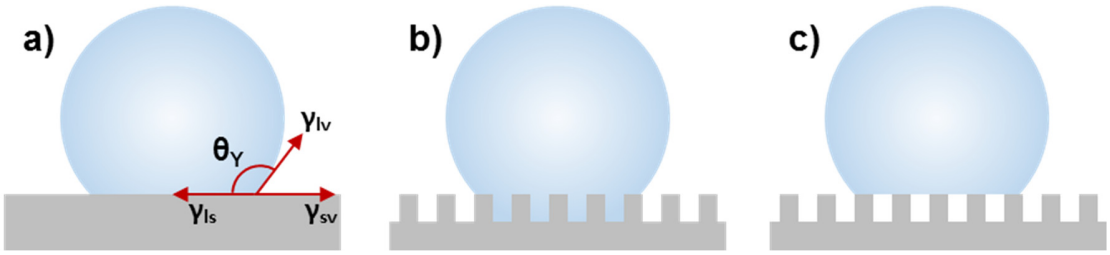

Figure 2. Liquid droplet placed on solid substrate (a) Ideal wetting, (b) Wenzel state, (c) Cassie-Baxter state.

1.3.2.2 Wetting on Non-ideal Surfaces

In reality, however, most solids are naturally rough, which causes deviations from the contact angle value predicted by Young's equation. To account for the effects of surface roughness, two models have been introduced: Wenzel and Cassie-Baxter models. In the Wenzel model, a liquid droplet completely wets the rough surface; as a result, surface roughness amplifies the wetting behavior of an ideal solid surface by increasing the contact area (Figure 2). According to this model, the solid-liquid interfacial area is enlarged by a factor *r*, the ratio of the actual surface area to the apparent, projected area. Wenzel proposed that the apparent contact angle on rough surfaces (θ) can be related to the contact angle on an ideal surface (θ_Y) is described by equation (2):[28]

$$\cos\theta = r\cos\theta_Y \tag{2}$$

Cassie and Baxter took into account chemical heterogeneities of surfaces. Averaging the surface energies of the respective area factions, ϕ_i, yields equation (3):

$$\cos\theta = \sum_i \phi_i \cos\theta_i \tag{3}$$

where θ is the apparent contact angle on a rough surface, and θi is the equilibrium contact angle corresponding to area fraction *i* ($\sum \phi_i = 1$). On a rough, non-wetting surface, the liquid droplet can sit on top of the roughness structures with underlying trapped air (Figure 2). In that scenario, a two-component composite interface is formed consisting of solid-liquid and air-liquid contact areas, where the air-liquid part is regarded complete non-wetting

(θi = 180°), so that the apparent contact angle (θ) of the rough surface can be expressed as equation (4):[29-30]

$$\cos\theta = r\,\phi\cos\theta_Y + \phi - 1 \quad (4)$$

where ϕ is the solid-liquid interface areal fraction, and r represents the roughness of the solid in contact with the liquid.

1.3.2.3 Contact Angle Hysteresis

Surface heterogeneities of either chemical or structural origin can pin a contact line.[31] A liquid droplet spreading across the surface can therefore be halted by the defects. The same concept applies to a receding droplet.[32] As a result, a droplet on an inclined surface, which has both advancing and receding contact lines, can remain stationary if two different contact angles provide a net force to counteract gravity (Figure 3). The maximum/minimum contact angles observed on an inclined surface are defined as the advancing/receding contact angles ($\theta_{adv}/\theta_{rec}$) and the difference between these two contact angles is defined as the contact angle hysteresis.[33-34]

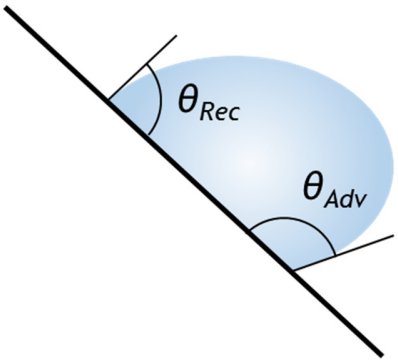

Figure 3. Contact angle hysteresis with advancing and receding contact angles.

1.3.2.4 Super-hydrophobic Surface

Super-hydrophobic surfaces show water contact angles greater than 150º; the term is often also reserved for surfaces with low (<10 º) contact angle hysteresis and thus associated with droplet roll-off.[34-35] A water droplet placed such a super-hydrophobic surface retains a nearly spherical shape and displays high mobility, which offers many potential applications such as self-cleaning[36] and fluid drag reduction.[23] It should be noted that "sticky super-hydrophobic" surfaces with high contact angles and strong droplet adhesion also exist. Roll-off super-hydrophobic properties exist on various surfaces in nature such as plant leaves and water strider legs; Neinhuis and Barthlott therefore coined the term "lotus effect" to highlight the similarity to wetting properties of a lotus leaf.[37] These researchers revealed that the roll-off super-hydrophobicity of the lotus leaf is attributed to hierarchical structure composed of randomly oriented hydrophobic wax tubules on top of papillae (Figure 4).[34] When water droplet is placed on a roll-off super-hydrophobic surface, air-pocket can be retained underneath the water droplet. Wetting behavior of liquid on a solid surface having a composite interface can be described by Cassie-Baxter model, and large apparent contact angle (θ) can be achieved by reducing liquid-solid contact area fraction (ϕ) (Figure 5). Hierarchical structure can effectively reduce liquid-solid area fraction (ϕ), thereby increasing water contact angle (θ) (Figure 6). Consider three ideal surfaces: microscale, nanoscale, and hierarchical structures. Microscale structure consists of an array of microscale flat topped pillars with uniform spacing. Nanoscale structure exhibits a nano-array of flat topped nano-pillars. Hierarchical structure represents dual structures having nano-pillar array on top of the micro-pillars. Also, assume that there is no sagging of liquid and liquid can only contact to top flat part of the surface structure.

Both microscale and nanoscale structures can attain liquid-solid contact area fraction of 0.5, while hierarchical structure displays liquid-solid contact area fraction of 0.25. Therefore, surface structure with multiple scales can effectively reduce liquid-solid contact area fraction and achieve super-hydrophobicity. Since then, great efforts have been devoted to fabricate hierarchical structures to develop artificial super-hydrophobic surfaces on different substrates.

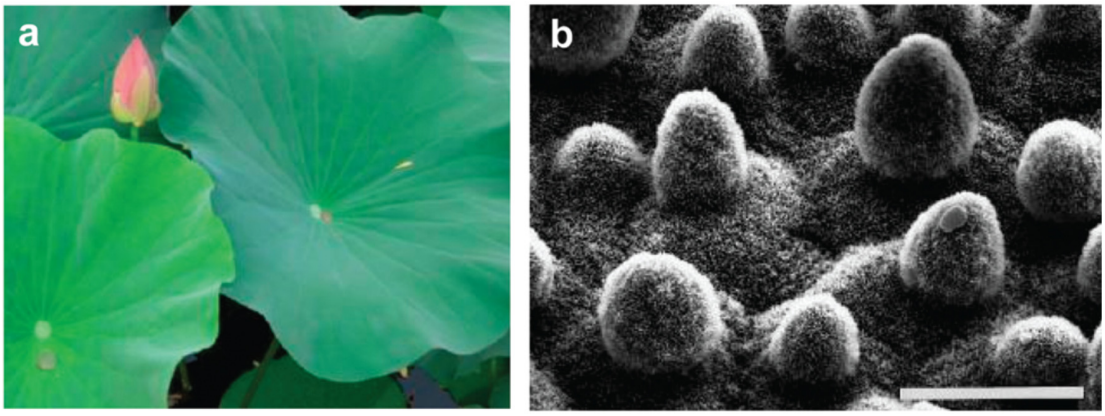

Figure 4. Super-hydrophobic surface in nature. (a) Lotus leaf, (b) Microstructure of lotus leaf observed by scanning electron microscopy. Scale bar is 20 μm (Adapted from reference [34]).

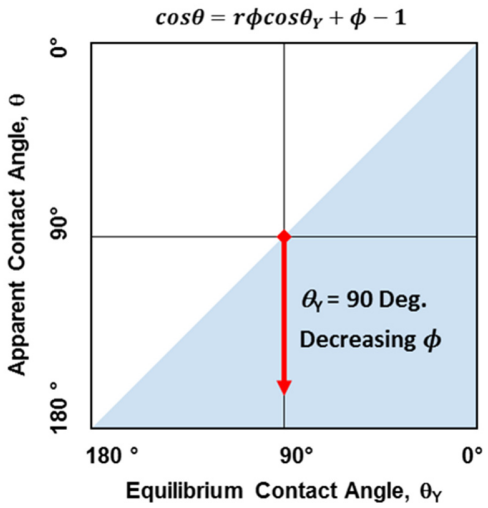

Figure 5. Cassie-Baxter model. Effect of solid-liquid contact area fraction on apparent contact angle.

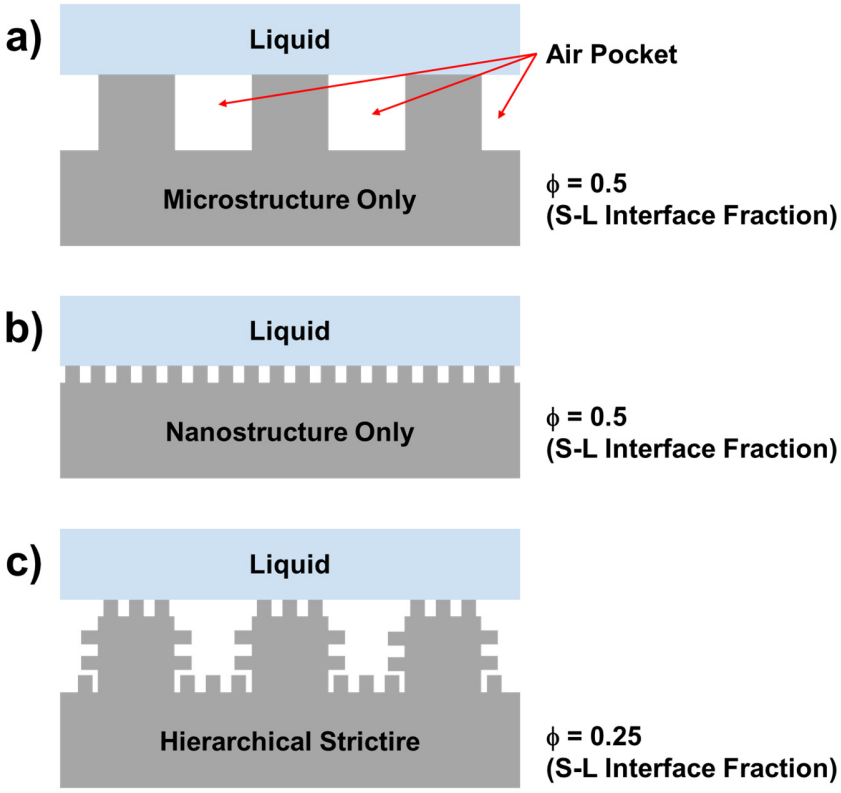

Figure 6. Hierarchical surface structure for super-hydrophobicity. Liquid placed on (a) micro-structured surface, (b) nanostructured surface, (c) micro- and nanoscale hierarchically structured surface.

1.3.3 Biofouling on Stainless Steel Surfaces

Biofouling refers to the accumulation and growth of undesired bio-organisms on clean solid surfaces.[38-39] This occurs both in marine and physiological environments, and is problematic in many common stainless steel applications such as ship hulls[39] and biomedical devices.[40] Marine biofouling and medical biofouling usually have different characteristics. Medical biofouling typically occurs in the form of bacterial biofilm,[40-41] while marine biofouling accompanies macrofouling by barnacles and mussels.[39, 42] The process of marine biofouling is shown in Figure 7.[42] First, organic molecules including proteins and polysaccharides adhere to the surface and form a conditioning film which facilitates subsequent attachment of marine bacteria; this can occur within a few minutes. Then, bacteria and diatoms attach to surface and begin colonization and form biofilm within hours. Finally, macro-foulants such as visible algae, barnacles, and tube worms begin to attach.

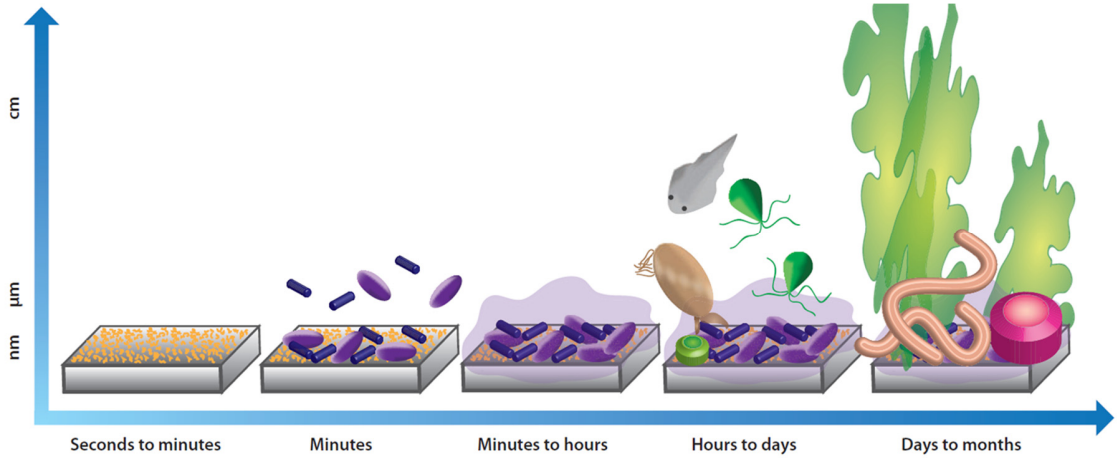

Figure 7. Marine biofouling process with time scale (Adapted from reference [42]).

Marine biofouling incurs massive costs to military and commercial marine vessels. Fouling on ship hulls by various marine organisms from light slime to heavy barnacles increases surface roughness and adds weight to the vessels, which leads to increased hydrodynamic drag and increased fuel consumption. The estimated annual costs due to fouling is $1 billion.[39] In medical biofouling, bacterial biofilm formation is a major concern because it is associated with infectious diseases.[38, 43-44] Adhesion of pathogenic bacteria and biofilm formation on stainless steel biomedical devices such as implants, catheters, prosthetic devices, and stents can cause infectious diseases. If biomedical devices are microbially contaminated, replacements and antibiotic therapy are required, which is a significant source of additional health care costs.[38] Therefore, much attention has been devoted to the development of antifouling surfaces by pursuing two major strategies: coatings and surface topography.

1.3.3.1 Coating-based Antifouling

The commonly used chemical strategy is to apply surface coatings that either resist the adhesion of bio-foulants or degrade them once attached. Coatings with embedded and/or slowly releasing biocides like copper- and tin-based metallic compounds are effective,[45] but such chemical compounds can have serious toxic effects on marine life.[46] Therefore, alternatives to replace these chemicals are required to address environmental concerns.[42] Similarly, in medical biofouling, anti-microbial coatings are used that include silver or antibiotics.[47] Silver-impregnated surfaces can slowly release silver ions, which prevent bacterial adhesion by killing bacteria. Although chemical coating methods are effective in terms of anti-fouling, they have some considerable drawbacks, including the emergence of

anti-biotic resistant pathogens, toxicity to mammalian cells, and potential delamination of the coatings.[44, 48]

1.3.3.2 Surface Topography-based Antifouling

Current research is now focusing on developing non-toxic, environmentally benign/biocompatible antifouling surfaces, inspired by marine species that naturally resist biofouling.[40] For example, barnacle biofouling is evident on whales but not on sharks even though they live in the same marine environments.[49] Shark skin has very specific microscale topography that helps to prevent biofouling and to maintain clean skin (Figure 8).[39, 49]

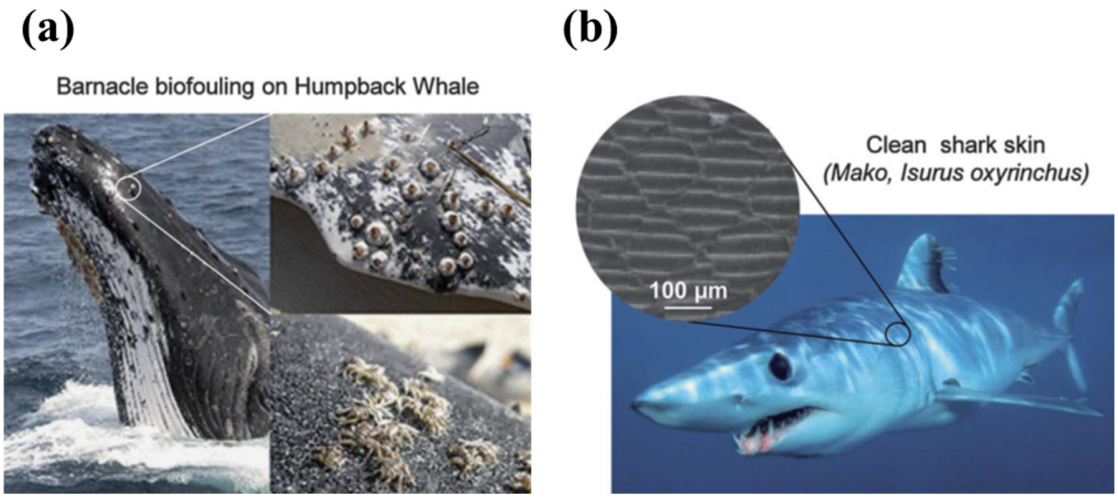

Figure 8. Biofouling in marine environments. (a) Barnacle biofouling on Humpback whale, (b) Clean shark skin (Adapted from reference [49]).

Carman et al. first created microscale topography on polymer surface by mimicking shark skins and demonstrated significant antifouling performance.[50] Since then, many studies have been devoted to the creation of microscale topography by mimicking natural marine species such as crab shells[51] and clam shells.[52] The anti-fouling mechanisms of such

microscale topographies has not been elucidated, but reduction in attachment points is one of the potential factors to be accounted.[40] When the foulants are larger than the surface texture, the topographic surface can provide reduced attachment points to the foulants, thereby reducing adhesion strength. Because there are broad size range of foulants in maritime environment (Figure 9), a multi-scale hierarchical structure is generally desired to achieve versatile antifouling performance. In particular, these strategies to control surface structures for preventing biofouling have been recently highlighted again with the development of nano-technology.

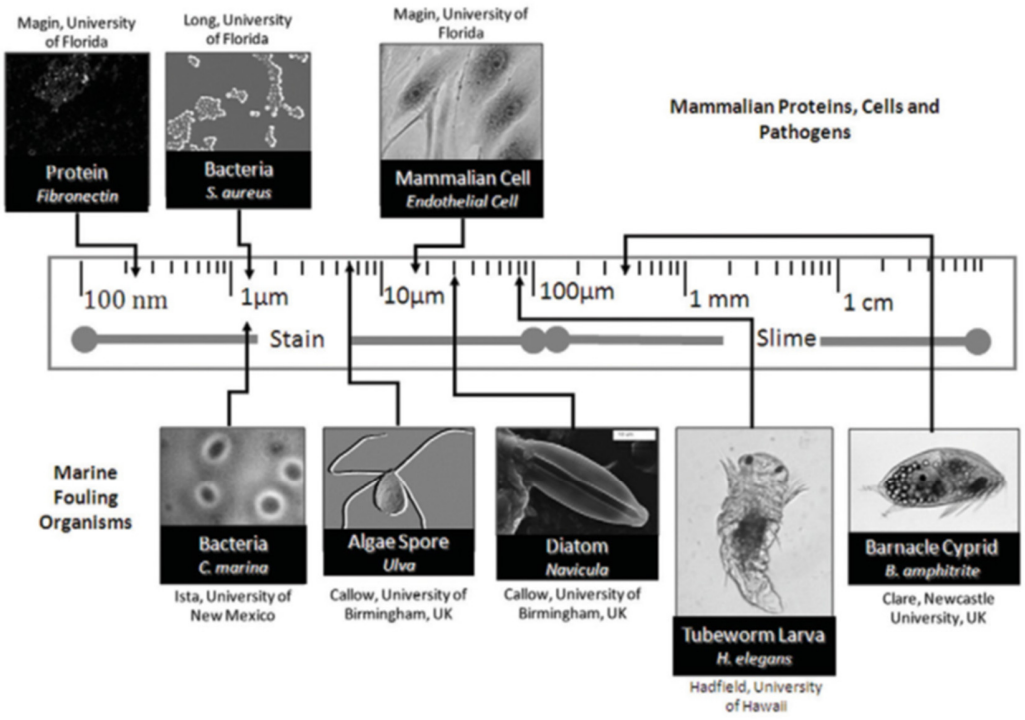

Figure 9. Diverse kinds of marine organisms (Adapted from reference [39]).

1.4 Surface Modifications of Stainless Steels

As stated above, three key properties (corrosion resistance, wettability, and interaction with bio-organisms) are largely dependent on surface chemistry and topography. In this section, stainless steel surface modification techniques are presented that have been developed by other researchers in attempts to modify and control these properties. The surface modification techniques include surface finishing and surface structural modification. Surface finishing techniques generate a smooth and chemically homogeneous stainless steel surface to improve wear and corrosion resistance. While, surface structural modifications mainly focus on creating a relevant surface topography to attain functionalities such as controls of wettability and adhesion with bio-organisms.

1.4.1 Surface Finishing of Stainless Steels

The surface quality of stainless steels is one of the key parameters determining the material deterioration originated from surface such as corrosion and wear.[53] Integrity of stainless steel surfaces is significant for applications in real world Figure 10 illustrates the most common surface defects that can be generated during manufacturing process. Scratches allow entrapment of reactants or contaminants that could lead to localized corrosion. Non-metallic inclusions, for example sulphides, nitrides, and silicates, are mostly formed during melting, pouring, and solidification processes. These surface inclusions can also act as preferential sites for the initiation of localized corrosion. High temperature gradients during welding can introduce heat tint films in the affected zones. Heat tint is thicker than the normal chromium oxide passive layer on stainless steel, which leads to depletion of chromium beneath the heat tint, thereby reducing the inherent corrosion resistance. In

addition, welding can create surface defects such as arc strikes and weld splatters. In order to remove surface defects and improve mechanical properties, many surface treatments on stainless steels have been developed.

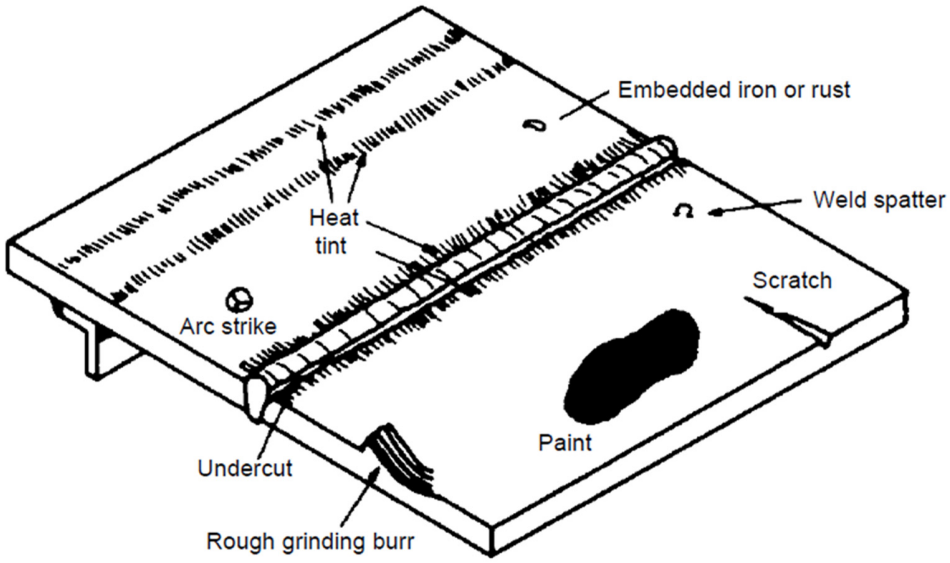

Figure 10. Surface defects arising during manufacturing process (Adapted from reference [53]).

1.4.1.1 Mechanical Surface Treatments

Mechanical methods include surface grinding,[53] blasting,[54] and shot peening.[55-56] Surface grinding and blasting are primarily used for cleaning metal surfaces. Surface grinding uses a rotating abrasive wheel, and blasting uses abrasive particles propelled by an air stream to impact on the metal surfaces. Both methods result in removal of surface contaminations as well as the naturally occurring passive layer of stainless steels, so that an additional chemical passivation step is commonly required after the mechanical methods to restore the corrosion resistance. Shot peening is a similar process to blasting, except that it relies on plastic deformation of metals rather than abrasion, which leads to lower removal rates

of metal from the surfaces. The plastic deformation induces a compressive stress in peened metal surfaces, which improves resistance to metal fatigue; shot peening is thus commonly used in applications where high cyclic fatigue is important, such as engine valve springs.

1.4.1.2 Chemical Surface Treatments

Pickling[57-58] and chemical passivation[59] are acid treatments to remove contaminants and assist formation of continuous passive film. Pickling uses aggressive acid solutions, normally consisting of a mixture of nitric acid and hydrofluoric acid, to remove existing oxide layers, particularly heat tint, from welds and the adjacent chromium depleted layer. It creates a clean stainless steel surface that enables the natural self-passivation of stainless steels. A pre-mechanical descaling to break up and disrupt the oxide layer by grinding or blasting is often performed to enhance subsequent pickling.[58] Passivation in a nitric acid solution results in removal of surface defects such as non-metallic inclusions, and promotes formation of passive film on a freshly created stainless steel surface through pickling. Chemically passivation results in chromium rich and uniform passive layer on stainless steel, thereby displaying better corrosion resistance than self-passivated stainless steels by air.

1.4.1.3 Electro-polishing

Electro-polishing, also known as electrolytic polishing is an electrochemical process that removes materials ion by ion from the metallic surface by anodic polarization in a concentrated acid solution.[60] Electro-polishing is often used as a surface finishing technique because the process can bring about smooth and bright metal surfaces due to faster rate of dissolution at peaks relative to valleys. Along with the smooth surface finish,

which lowers friction and wear, electro-polished stainless steels exhibit improved corrosion resistance due to removal of surface defects such as heat tints, burrs, and non-metallic inclusions, and establishment of chromium rich passive layer.[61] The beneficial combination of surface smoothness and improved corrosion resistance makes electro-polishing the preferred treatment for a wide range of stainless steel applications: chemical reactors, surgical tubing and tools, food processing blades, and automotive parts.

1.4.1.4 Surface Nitriding

Nitriding is a surface engineering technique that diffuses nitrogen into metal surfaces and forms nitrides to improve mechanical hardness and wear resistance.[62] Generally, nitriding stainless steel is difficult because of high activation energy for nitrogen diffusion and existence of chromium oxide film hindering nitrogen diffusion. In order to accelerate nitrogen diffusion, the conventional gas nitriding process is operated above 500 °C, which leads to formation of chromium nitride precipitation and depletion of chromium contents in matrix, thereby compromising corrosion resistance.[63-64] In contrast to the conventional nitriding process, a plasma nitriding can be carried out at relatively low temperature, normally lower than 450 °C.[65-66] This low operating temperature is beneficial because it can avoid formation of chromium nitride and thereby improving mechanical hardness without reducing corrosion resistance.

1.4.2 Structural Modification of Stainless Steel Surfaces

As discussed in previous section 1.3, surface interactions such as wettability and adhesion of bio-organisms have significant impact on performance of stainless steel applications, and are largely dependent on the surface structure. However, surface finishing techniques

on stainless steels introduced in section 1.4.1 mainly focus on achieving smooth defect-free surfaces with uniform and chromium-rich passive layer to augment wear and corrosion resistances. Despite the significant potential advantages of surface structure-modified stainless steel, few studies have been reported on creating well-defined microscale and/or nanoscale topographies on stainless steel. Such methods are presented in below.

1.4.2.1 Laser Ablation

Laser ablation is a process of removing materials from a solid surface by irradiating it with a laser beam. When the laser beam is irradiated, material is heated and evaporates or sublimates. Most common application of the laser ablation is laser drilling which uses pulsed lasers to remove material with delicate manner. Recently, researchers used ultrashort femtosecond pulsed laser ablation with spatial patterning on stainless steels to create micro/nanostructures, and demonstrated super-hydrophobicity (Figure 11)[67-69] and reduced adhesion of platelets of the surfaces.[69] Laser ablation allows precise control of surface topography from nano- to microscale structure, but the method is cost inefficient and difficult to scale up.

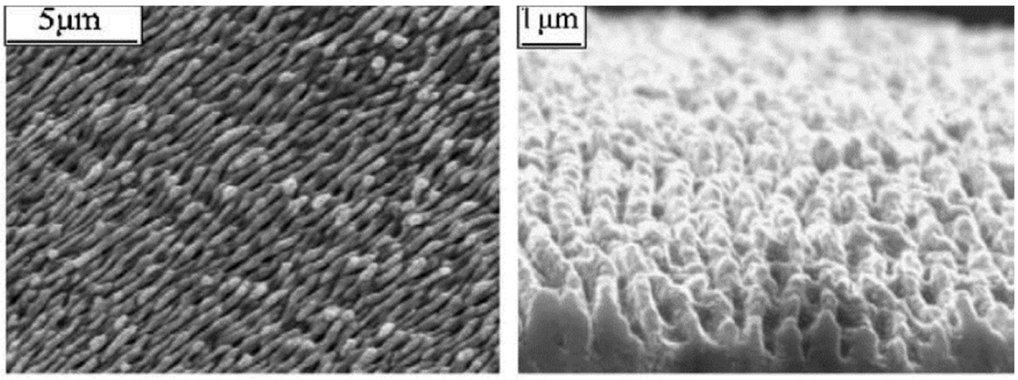

Figure 11. Femtosecond laser ablation on stainless steel surfaces (Adapted from Reference [67]).

1.4.2.2 Chemical Etching

Chemical etching is a process using chemical solution, the etchant, to react/remove unwanted parts of materials. Because chemical etching is simple and economical, it was extensively used during microelectronic device fabrication until 1980s.[70] Recently, chemical etching has been used to impart surface roughness on stainless steels, where grain boundary atoms are more susceptible to etching than atoms inside the grains, so that surface topography can be revealed.[71] Hydrofluoric acid,[72] mixtures of strong acids,[73] and ferric chloride solution[71] can be used to etch and generate surface structures on stainless steels. Subsequent fluorocarbon deposition on the chemically etched stainless steel surfaces results in super-hydrophobic behavior.[71-73] While the chemical etching method provides easy fabrication of surface topography, it is relatively difficult to systematically control the surface structure. In addition, damage on passive layers and formation of flaky deposits on the stainless steel surfaces during the chemical etching process may compromise corrosion and wear resistance. After the etch process, additional passivation step by nitric acid or other oxidizing agents is usually required to reconstruct the passive layer and restore corrosion resistance (Figure 12).[71-72]

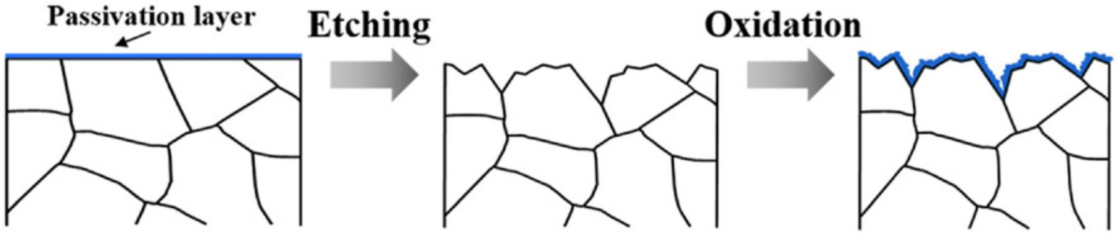

Figure 12. Chemical etching and re-passivation on stainless steels (Adapted from Reference [71])

1.4.2.3 Electrochemical Etching

Electrochemical etching is a process that involves the use of an electrolyte solution, anode, and cathode, and power source.[74] The metal to be etched is polarized in the anodic direction to etch or oxidize the metal surface. Similar to the chemical etch processes, electrochemical etching can be used to define individual grains on stainless steels by preferentially attacking grain boundaries. Grain boundary etching by electrochemical or chemical process is a commonly used technique in metallurgy to analyse size distributions and orientations of individual grains.[75] In addition to the metallurgical application, electrochemical etching can be used as a surface modification process for stainless steels. Stover et al. utilized electrochemical etching on stainless steel drug eluting stent to increase its surface area and drug loading capacity (Figure 13).[76] The electrochemical etch process readily allows for variations in applied potential and current density, thus enabling systematic control of relative etch rates at grain boundaries and grain matrices to a much greater degree than with chemical etching.[77]

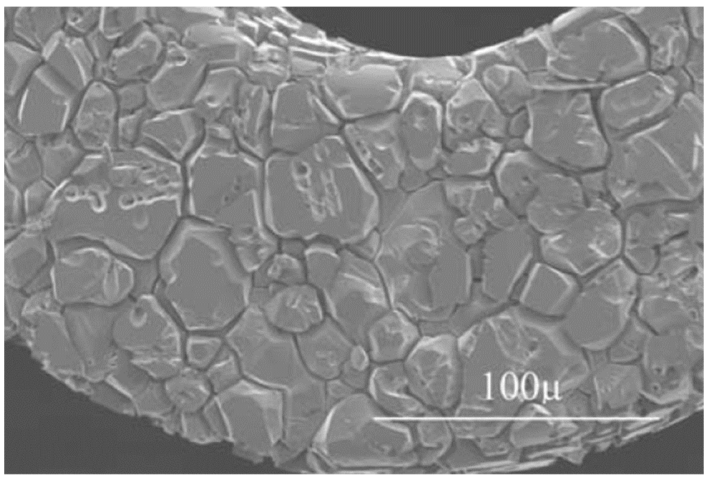

Figure 13. SEM image of electrochemically etched stainless steel stent (Adapted from Reference [76]).

1.5 Thesis Objectives and Organization

The goal of this thesis is to modify stainless steel surfaces to attain advanced functionalities, including liquid repellency, improved localized corrosion resistance, and anti-fouling property. Compared to other techniques, the electrochemical etching process provides many benefits: it is affordable, fairly scalable (especially compared to laser processes), and fine tuning of the structure is feasible by controlling electrochemical parameters such as potential and current density. There are no literature reports on utilization of the electrochemical etching to achieve the functionalities. This thesis focuses on structural and chemical modification of stainless steel surfaces by using electrochemical etching, and design stainless steel surfaces that display advanced functionalities.

Among many different types of stainless steels, austenitic stainless steel 316L was selected as starting material because of its applicability. Stainless steel 316 is one of the most commonly used austenitic stainless steels, and is primarily composed of 16-18% chromium, 10-14% nickel, and 2-3% molybdenum. The molybdenum in stainless steel 316 improves corrosion resistance making the stainless steel 316 used in food processing, chemical storage and transport, textile dying equipment, cladding of nuclear fuel, oil refining equipment, and maritime industry. Stainless steel 316L represents extra-low carbon contents of the alloy with less than 0.03% that reduces sensitization by grain boundary chromium carbide precipitation at high temperature. Therefore, stainless steel 316L is used in high temperature industrial equipment as well as in paper and pulp industry. In addition, stainless steel 316L is a preferred grade for medical devices including body implants, surgical tools, and stents, due to its biocompatibility. Therefore, stainless steel

316L is the most relevant and beneficial material when the functionalities (liquid repellency, improved corrosion resistance in seawater, antifouling) are added.

Chapter 2 focuses on control of surface structure of stainless steel 316L by using electrochemical etching to create micro/nanoscale hierarchical structures and achieve super-hydrophobic surfaces. Chapter 3 investigates the corrosion behavior of the electrochemically etched stainless steel 316L. Corrosion resistance is the primary benefit of stainless steels to have wide applications. Therefore, ensuring or improving corrosion resistance of the surface modified stainless steel 316L is essential for practical applications. Chapter 4 studies the effects of nanoscale topography on stainless steel 316L on bacterial adhesion for biomedical implant application. Chapter 5 explores a patterned copper surface with wettability contrast, which can offer potential applications such as diagnostic devices and microfluidic platforms. Copper is relatively cheap and amenable to modify the surface. Taking advantage of the maturity of copper surface modification, a simple method is presented to construct hydrophobic/super-hydrophobic patterned copper surface for droplet manipulation as a proof of concept. Chapter 6 summarizes the conclusions of this thesis along with recommendations for future research.

CHAPTER 2.

WETTABILITY CONTROL ON STAINLESS STEEL SURFACE

Reproduced from W. T. Choi, K. Oh, P. M. Singh, V. Breedveld, and D. W. Hess,

Journal of Materials Science, 2016, 51(11) pp. 5196-5206

2.1 Introduction

2.1.1 Advantages of Liquid Repellent Stainless Steel Surfaces

Stainless steels (SSs) are iron-based metal alloys with at least 10.5% chromium content by mass that display improved corrosion resistance compared to ordinary carbon steels. The exact composition of SSs varies depending upon the desired specific application; different SS compositions lead to variations in corrosion resistance, hardness, and mechanical stability. The most widely used SSs are those in the 300 series with the primary components of iron, chromium, and nickel. In this study, stainless steel 316 (SS316) is used, with nominal additive composition of 18% chromium, 10% nickel, and 2-3% molybdenum.[78] Because of the combination of corrosion resistance and mechanical stability, SSs in general –and SS316 in particular- are widely used in industries in which fluid exposure occurs, such as petrochemical, power generation, marine, food, and construction industries.[4] Control of wettability is of great practical relevance in these application areas. For example, liquid repellency in SS pipes can lead to more efficient fluid transport through hydrodynamic drag reduction, and to more effective drainage and cleaning of storage tanks. In power generation and desalination industries, enhanced heat transfer efficiency during drop-wise condensation of water vapor can save energy.[79] Finally, water repellency can

improve the corrosion resistance of SSs, thereby prolonging the lifetime of construction materials.[14]

2.1.2 Methods to Achieve Super-hydrophobic Stainless Steel Surfaces

Although water repellency of SS would offer significant advantages, relatively few studies have been reported on this critical topic in comparison to other substrates. To establish water repellency, a combination of surface chemistry with low surface energy and surface roughness with proper length scales is required.[80] Methods that have been reported to fabricate water repellent SS surfaces include laser ablation,[67-68] surface coating,[81-84] electrodeposition,[85] electro-less deposition,[86-87] and chemical etching.[72] Surface roughness can be created with high fidelity and excellent mechanical stability by laser ablation techniques, but the process is difficult to scale up and costly. SS surface roughness can also be created by application of a coating that has inherent roughness, for example in the form of embedded particles, but this approach can generate intrinsic stress that degrades the mechanical stability of the surface and interface, while adhesion of the particles/coating is an additional concern. Electro or electro-less deposition methods to induce roughness on SS also raise concerns about adhesion and mechanical stability at the interface between the deposited materials and SS due to intrinsic and thermal stresses. Lastly, liquid repellent SS surfaces created by chemical etching often show flaky features that may lack the necessary mechanical stability for wide applicability. Therefore, a process for the generation of liquid repellent SS surfaces that display high mechanical stability using a scalable, cost efficient method would be beneficial in numerous applications.

2.1.3 Electrochemical Etching to Control of Surface Structure

One approach to achieve the necessary roughness while maintaining the inherent structure and thus mechanical properties of super-hydrophobic SS surfaces, is the intentional enhancement of the intrinsic grain structure via selective grain boundary etching. Grain boundary etching, or inter-granular corrosion, describes a situation where boundaries of crystallites in a material are etched selectively relative to their grain matrices.[17, 88] That is, under certain conditions, etching or oxidation of metals at grain boundaries occurs more rapidly than etching or oxidation reactions of metal grain matrices. The difference in etch rate between the grain boundary and grain matrix originates from the presence of structural defects or variations in the alloy composition at the grain boundaries, which have higher interfacial energy and relatively weak bonding, resulting in enhanced etch rates. Selective etching accentuates intrinsic grain structures and thereby can create roughness; if this roughness is of the proper length scale, water repellent surfaces can result. A major advantage of this approach is that the structures are an integral part of the SS substrate, so that relatively high mechanical stability of such structures should be realized relative to structures generated from deposition or addition of particles.

Few studies have focused on the surface modification of stainless steel surfaces through electrochemical grain boundary etching to enhance their performance in specific applications. One study used electrochemical grain boundary etching of stainless steel stent surfaces to provide large surface areas for drug coating,[76] but no surface wetting properties were reported. In this study we present for the first time a method for the design of water repellent SS surfaces through controlled, selective electrochemical grain boundary etching. Variation in applied external potential in the electrochemical cell yields changes in the

selectivity of grain boundary versus bulk grain etch rates, which in turn leads to changes in surface topography. Surface structure and chemistry of the electrochemically etched SS316L were investigated with scanning electron microscopy (SEM) and x-ray photoelectron spectroscopy (XPS); a particular focus of this work is the relationship between applied potential and the resulting surface structure. In addition, water wetting behavior of these surfaces is correlated with surface topography. Based on the relationship between applied potential and surface structure, we designed hierarchically enhanced intrinsic grain structures on the SS316L surface through two-step electrochemical etching. Deposition of a fluorocarbon film onto the etched surfaces further improved water repellency by establishing hydrophobic surface chemistry in addition to the favorable surface topography.

2.2 Experimental

2.2.1 Materials and Sample Preparation

Nitric acid (HNO_3, 70%) was purchased from Fisher Scientific. SS316L plates (20 cm x 30 cm x 0.05 cm) were purchased from Maudlin Products and cut into samples with two different sizes (2.5 cm x 1.5 cm x 0.05 cm and 2.5 cm x 2.5 cm x 0.05 cm) using a waterjet cutter; these samples served as working electrode and counter electrode, respectively. Prior to etching, the samples were cleaned by ultra-sonication sequentially in acetone, methanol, and isopropyl alcohol, and subsequently dried in air at ambient temperature. Electrical connections of the electrodes to SS wire were established by spot welding. Subsequently, the working electrode specimen was masked with insulating tape (Electroplating Tape 470, 3M), leaving an exposed area of 0.13 cm^2 for electrochemical etching. On the counter electrode, SS wire was coated with insulating varnish (GC Electronics 10-9002A) to prevent contact with the electrolyte. Glass staining jar (9 cm x 5 cm x 3 cm) purchased from Ted Pella was served as electrochemical cell. Detailed electrochemical cell configurations are shown in Figure 14.

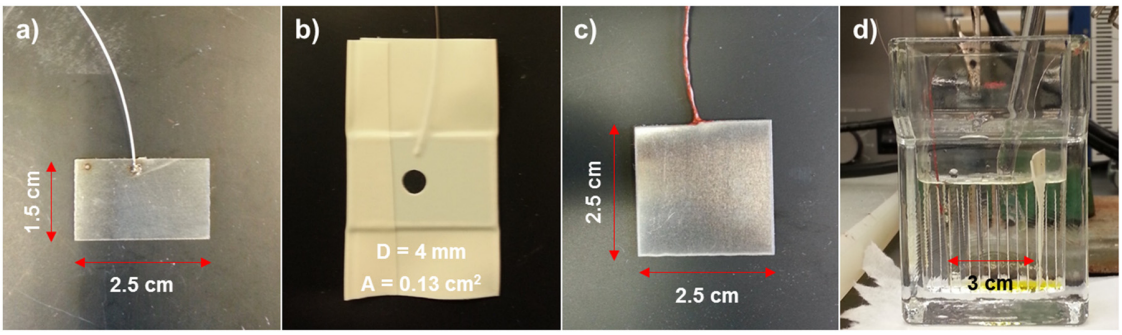

Figure 14. Sample preparation of SS316L electrodes. (a) Wire welding on working electrode, (b) Masking on working electrode with the active area, (c) Counter electrode, d) Electrochemical cell with three electrode system.

2.2.2 Potentiostatic Electrochemical Etching

Dilute nitric acid was used as the electrolyte: 24 mL of HNO_3 (70%) was mixed with 15 mL of deionized water. A three electrode system was used in these experiments. A saturated calomel electrode (SCE) was used as a reference. The working and counter electrodes faced each other with a separation distance of 3 cm, and the reference electrode was placed near the working electrode. (Figure 14d). A potentiostat (Gamry Reference 600) was used to perform electrochemical etching; an initial delay of 300 s at open circuit conditions was instituted prior to electrochemical etching. Potentiostatic electrochemical etching was carried out at anodic potentials between 1.1 V and 2.4 V (vs. SCE) for 300 s and resulting current densities varied from 1 mA/cm^2 (1.1 V) to 1797 mA/cm^2 (2.4 V) (Figure 15). Overpotential is a potential difference between equilibrium potential and potential at which electrochemical reaction occurs. Overpotential is a driving force of electrochemical reaction, which can be controlled by applied potential, and current density represents the rate of electrochemical reaction.

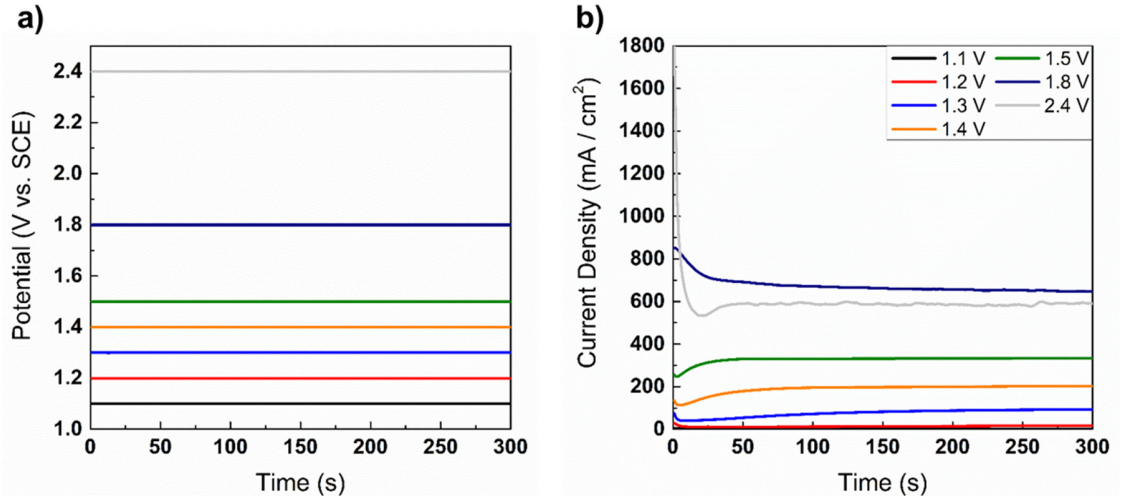

Figure 15. Potentiostatic electrochemical etching behavior. (a) Potential-time (V-s) potentiostatic polarization, (b) Current-time (A-s) curves for electrochemical etching of SS316L at constant potential and temperature.

In a two-step potentiostatic electrochemical etching process, the first step was performed at an anodic potential of 1.3 V (vs. SCE) for 300 s, and the second step was conducted at an anodic potential of 1.8 V (vs. SCE) for 10 s. After the first step of electrochemical etching, the SS316L sample was removed from the electrochemical cell and rinsed with de-ionized water and the electrolyte was replaced with fresh electrolyte. The SS316L sample was re-installed into the electrochemical cell to conduct the second step of potentiostatic electrochemical etching at 1.8 V (vs. SCE) for 10 s. After etching, the samples were rinsed with de-ionized water, acetone, methanol, and isopropyl alcohol, and dried under ambient conditions prior to surface characterization. The “as-received” control sample was subjected to the sequential cleaning process, but was not etched in the electrochemical cell.

2.2.3 Modification of Surface Chemistry

After structure generation on SS316L samples, the samples were placed in a parallel plate rf (13.56MHz) vacuum plasma reactor, with 6 inch diameter circular stainless steel electrodes, with a distance between the electrodes of 1 inch.[89] Fluorocarbon film deposition was performed at 110 ℃, 120 W, and 1 torr pressure using a mixture of pentafluoroethane (Praxair) and Argon at 20 SCCM and 75 SCCM, respectively. Deposition times of 5 s and 40 s resulted in highly cross-linked fluorocarbon layers covalently bonded to the SS316L surface with thicknesses of 23 (±1) and 149 (±1) nm, respectively.

2.2.4 Characterization

The surface morphology of etched SS316L samples was characterized by scanning electron microscopy (Hitachi SEM SU8010, Japan) at 3 kV acceleration potential. A goniometer (Ramé-Hart 290) was used to measure contact angles. Static contact angles were obtained by dispensing 4 μL of deionized water (DI-water) onto sample surfaces; images were captured with a CCD camera and analyzed with Ramé-Hart software. In order to measure the advancing contact angle, 1 μL of DI-water was initially placed on the surface, and the droplet volume increased in 0.08 μL increments. Receding contact angles were measured by decreasing the droplet volume in 0.08 μL increments. To measure roll-off behavior, 4 μL DI-water droplets were placed on the SS316L samples, and the base of the goniometer tilted at a rate of 1 º/s. The thickness of plasma-deposited fluorocarbon films was measured on Si wafers that were placed next to the SS316 samples using ellipsometry (M-2000 ellipsometer, J. A. Woollam Co. Inc.). In order to study the composition of SS316L surfaces, X-ray photoelectron spectroscopy (XPS) analyses were conducted using a

Thermo Fisher Scientific K-Alpha XPS with a 400 μm micro-focused monochromatic Al Kα X-ray source.

2.3 Results and Discussion

2.3.1 Effect of Anodic Potential on Stainless Steel Surface Structure

Figure 16 shows low magnification scanning electron microscope (SEM) images of the morphology of SS316L surfaces that were electrochemically etched at different potentials. The surface of SS316L without electrochemical etching shows residual roughness features that were created during the manufacture of SS316L plates (Figure 16a). At 1.1 V applied potential, narrow grain boundaries became visible (Figure 16b). When the specimen was electrochemically etched at 1.2 V (Figure 16c), the etched grain boundaries widths increased, but flat top grain surfaces were maintained. As the applied potential increased to 1.3 V, the distance between grains increased and the grain surfaces started to show dissolution (Figure 16d). Further increases in potential (1.4 V, 1.5 V) led to rounded grains due to significant etching of the grain edges and surfaces (Figure 16e, f). Finally, when the potential was >1.8 V, no identifiable grain structures were observed at this magnification (Figure 16g, h).

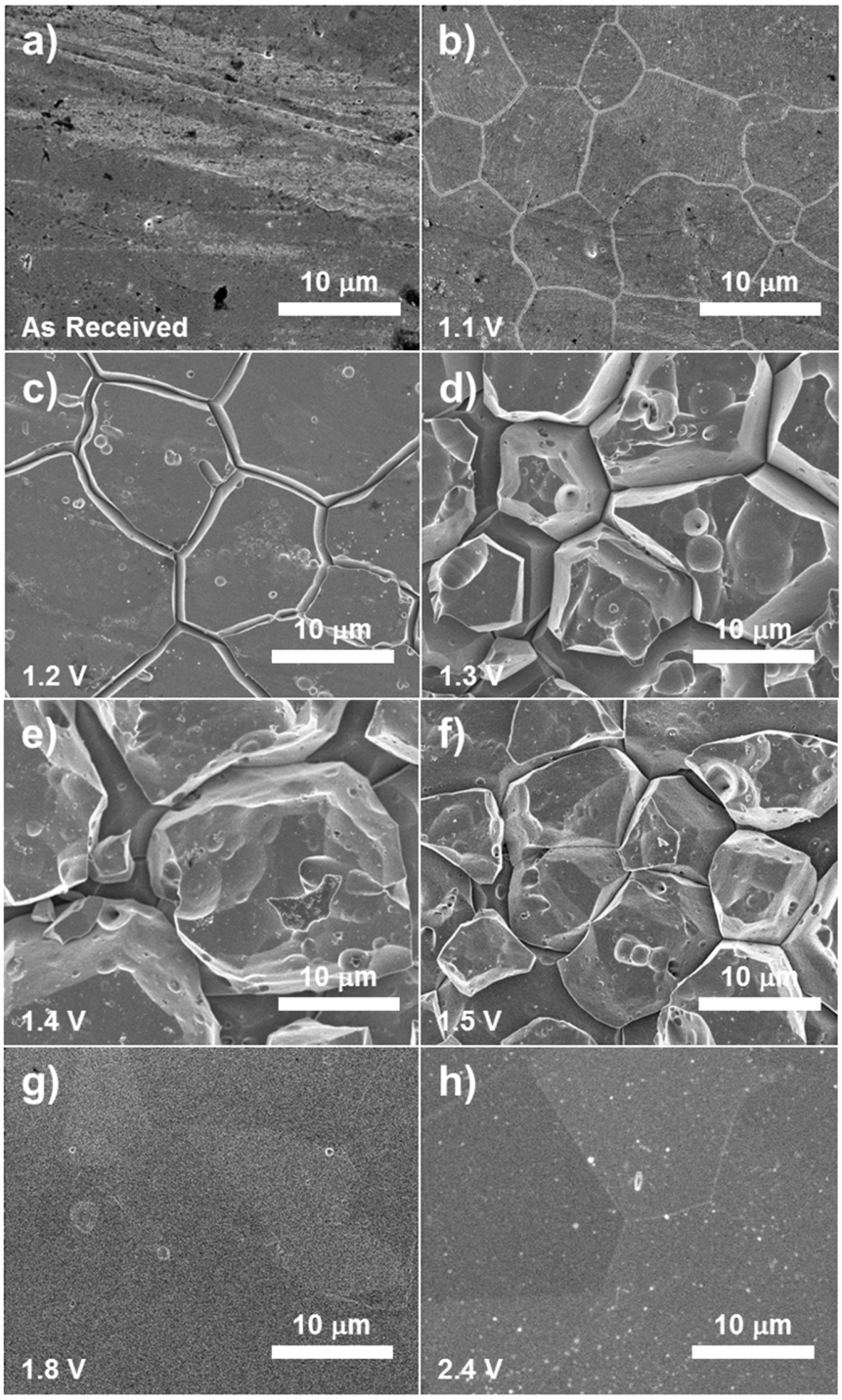

Figure 16. Low magnification SEM images of SS316L electrochemically etched at different potentials for 300 s: (a) As-received SS316L, (b) electrochemically etched SS316L with a potential of 1.1 V, (c) 1.2 V, (d) 1.3 V, (e) 1.4 V, (f) 1.5 V, (g) 1.8 V, (h) 2.4 V vs. SCE. The scale bar corresponds to 10 μm.

High resolution images in Figure 17 show the evolution of nanoscale structure generated in addition to changes in grain shapes as the anodic potential was altered. Surfaces of SS316L without electrochemical treatment showed no particular structure but roughness from the manufacturing process was clearly visible (Figure 17a). When a potential of 1.1 V was applied, selective grain boundary etching occurred, but initial features that existed due to mechanical processing of SS316L were not completely removed (Figure 17b). It is clear from Figure 17c that when the SS316L sample was etched with an anodic potential of 1.2 V, the initial roughness was eliminated and flat grain surfaces were observed. As the potential increased further (1.3 V - 1.5 V), electrochemical etching of grain surfaces was extensive, which resulted in rounded grain shapes and the evolution of nanoscale roughness on top of the grains (Figure 17d - f). Further increase in the potential (1.8 V) yielded a surface with only sponge-like nanoscale structure but no grain boundary etching (Figure 17g). Finally, at a potential of 2.4 V, a smooth surface, which corresponds to electro-polishing behavior (Figure 17h) resulted. These low and high resolution SEM images clearly show that different surface structures on SS316L can be achieved by controlling the anodic potential in the electrochemical system.

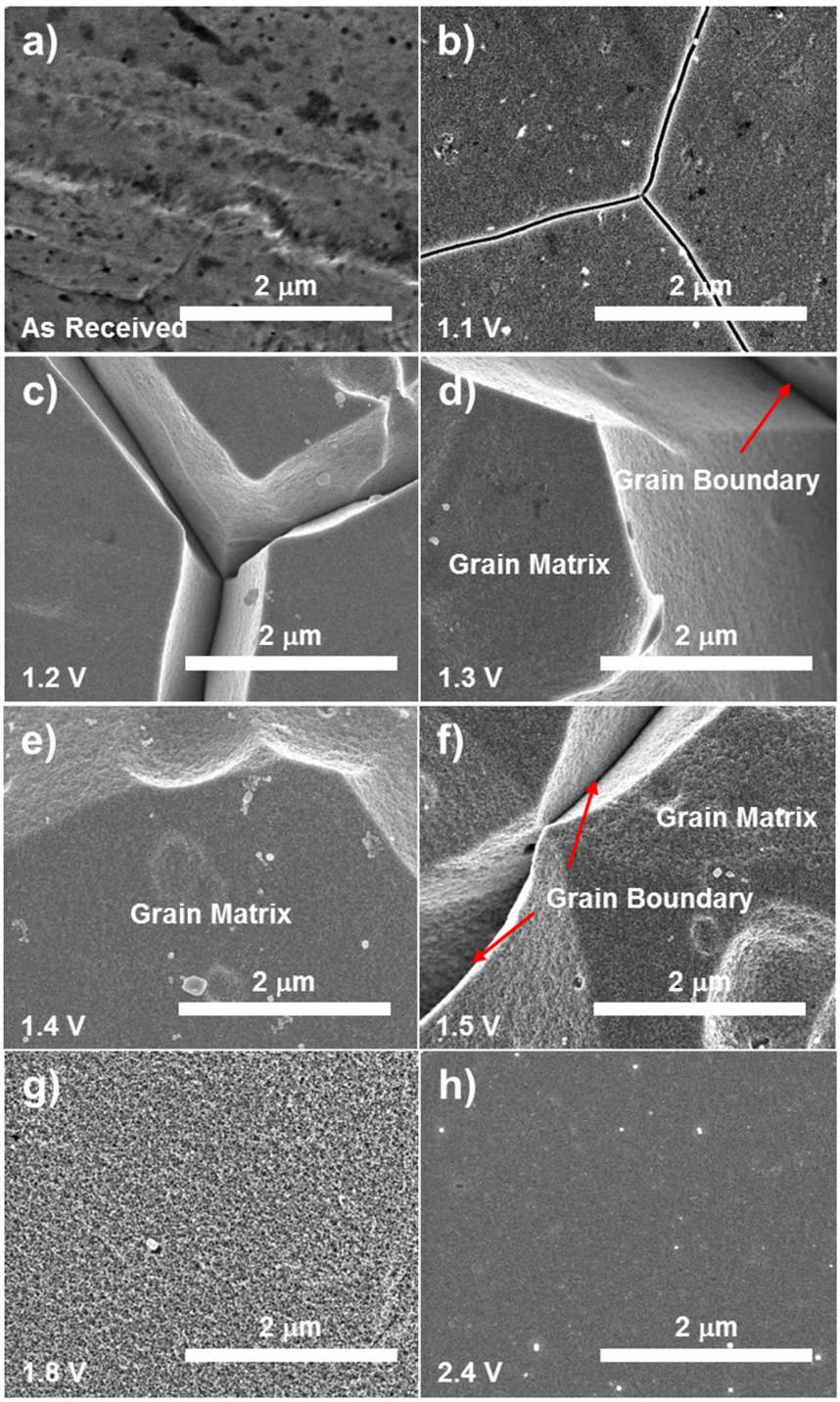

Figure 17. High magnification SEM images of SS316L electrochemically etched at different potentials for 300 s: (a) As-received SS316L, (b) electrochemically etched SS316L with a potential of 1.1 V, (c) 1.2 V, (d) 1.3 V, (e) 1.4 V, (f) 1.5 V, (g) 1.8 V, (h) 2.4 V vs. SCE. The scale bar corresponds to 2 μm.

Electrochemical etching at different applied potentials for the same time period (300 s) results in different levels of total charge transported to the sample, because currents also vary. In order to better define the effect of applied potential on grain boundary etching behavior, additional electrochemical etching studies were performed on SS316L samples at different applied potentials, while maintaining constant total charge transport (Figure 18).

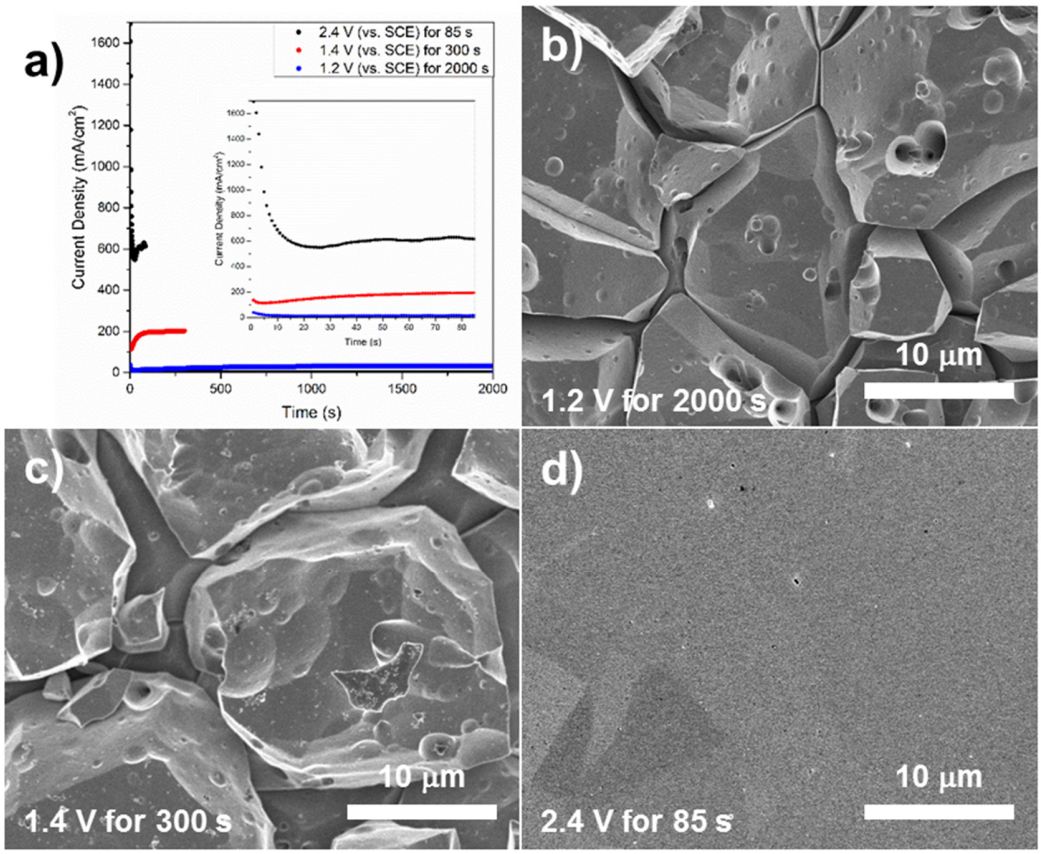

Figure 18. Effect of anodic potential on grain boundary etching while maintaining constant total charge. (a) Current-time (A-s) curves for electrochemical etching of SS316L at constant potential and temperature with different etch time. Inset graph shows current density-time curves at the beginning of the etch process (0 – 85 s), (b)-(d) SEM images of SS316L electrochemically etched at different potentials for different etch time: (b) 1.2 V for 2000 s, (c) 1.4 V for 300 s, (d) 2.4 V for 85 s.

Three SS316L samples were electrochemically etched at 1.2 V, 1.4 V, and 2.4 V for 2000 s, 300 s, and 85 s, respectively. Integration of the area under the current-time (A-s) curves for each SS316: sample yielded a total charge of 7.22 C, 7.38 C, and 7.22 C, respectively (Figure 18a). The SS316L sample electrochemically etched at 1.4 V showed more rounded grain shapes than did the SS316L sample electrochemically etched at 1.2 V (Figure 18b-c). In addition, electrochemical etching of SS316L at 2.4 V for 85 s led to electro-polishing (Figure 18d). These results demonstrate that the applied potential in the voltage range of 1.1 V – 2.4 V is a critical variable for the control of grain boundary etching behavior and that the structural variations in Figure 16 and Figure 17 cannot be attributed to differences in total charge.

In order to gain more insight into the effect of anodic potential on etched structure, we define the grain boundary etch selectivity, *S*,

$$S = \frac{(R_B)}{(R_M)} \quad (1 \leq S \leq \infty) \tag{5}$$

where *R* represents the etch rate of SS316 (working electrode) per unit area. The subscripts, *B* and *M*, represent the grain boundary and the grain matrix, respectively. If we consider the case where electrochemical etching only takes place at grain boundaries, R_M goes to zero, which results in high selectivity as *S* diverges to infinity. In contrast, when there is no distinction in the rate of SS etched per unit area between grain boundary and grain matrix, $R_B = R_M$, and *S* equals one, which represents lack of selectivity towards grain boundary etching.

Consider now several different applied potentials: 1) 1.2 V, 2) 1.4 V, and 3) 2.4 V (Figure 19). When the applied potential is low (1.2 V), only a small current flows through the electrochemical circuit. In this case, the current density generated at the active grain boundary is larger than the one generated at the less-active grain face, and the grain boundary etches faster than the grain matrix, resulting in high etch selectivity.[90] When the applied potential is increased to 1.4 V, a larger current flows and the difference in current density between grain boundary and grain matrix is reduced, which yields lower selectivity and rounded grains. A further increase in applied potential (2.4 V) leads to sufficiently high current that the difference in current density between grain boundary and grain matrix is negligible. No etch selectivity is therefore realized, and the surface is electro-polished.

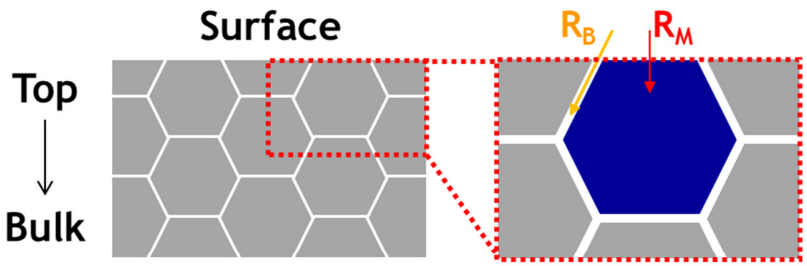

Potential	Etch Rate	Selectivity	Etch Type
1.2V	$R_M << R_B$	$S_{1.2V} > S_{1.4V}$	Selective
1.4V	$R_M < R_B$		Semi-Selective
2.4V	$R_M \fallingdotseq R_B$	$S_{2.4V} \fallingdotseq 1$	Electro-polishing

Figure 19. The relative selectivity of grain boundary etching depends on applied potential

2.3.2 Effect of Anodic Potential on Stainless Steel Surface Chemistry

X-ray Photoelectron Spectroscopy (XPS) was performed to investigate the composition of SS316 surfaces. Figure 20 displays XPS spectra of four samples; the as-received control sample without electrochemical treatment, and samples that were electrochemically etched at applied potentials of 1.2 V, 1.4 V, and 2.4 V. Figure 20a shows survey XPS spectra for these samples. Considering that the carbon content of SS316L is <0.03%, the relatively large carbon content observed can be ascribed to atmospheric contamination during atmospheric exposure and sample storage.[91] XPS peaks from O, Fe, and Cr are clearly visible with different intensities for each sample. The [Cr]/[Fe] ratio was determined from the respective XPS integrated peak areas. [Cr]/[Fe] ratios of 0.44, 1.24, 0.93, and 0.95 were calculated for non-etched samples, and for samples etched at 1.2 V, 1.4 V, and 2.4 V, respectively. These results imply that electrochemical etching leads to increases in chromium content in passive surface layers formed on SS316L.[92] High resolution O1s, Fe2p, Cr2p, and Mo3d XPS spectra of the four samples are shown in Figure 20b-e. [93-94] XPS spectra of the O1s electron binding energy region include at least two de-convoluted peaks originating from O^{2-} and OH^- (Figure 20b).[93] The $[O^{2-}]/[OH^-]$ ratio increases after electrochemical etching, indicating that the passive layer formed by electrochemical etching is a dehydrated form of the original oxide layer.[93] XPS spectra of Fe2p and Cr2p demonstrate that electrochemical etching leads to an increase in Cr content at the surface of SS316L with no change in the relative Fe content (Figure 20c, d). Considering that chromium(III) oxide (Cr_2O_3) is the primary moiety that establishes SS corrosion resistance,[59, 95] the increase in Cr^{3+} and O^{2-} content in SS316L after electrochemical etching is expected to enhance corrosion resistance. XPS spectra of Mo3d after electrochemical

etching indicate an increase in Mo content (Figure 20e). Since the inclusion of molybdenum (Mo) in SS enhances stabilization of the passive film,[9] the enhancement of Mo content at the SS316L surface should offer further corrosion resistance benefits. These results demonstrate that surface chemistry and structure of SS316L can be changed by electrochemical etching conditions.[92]

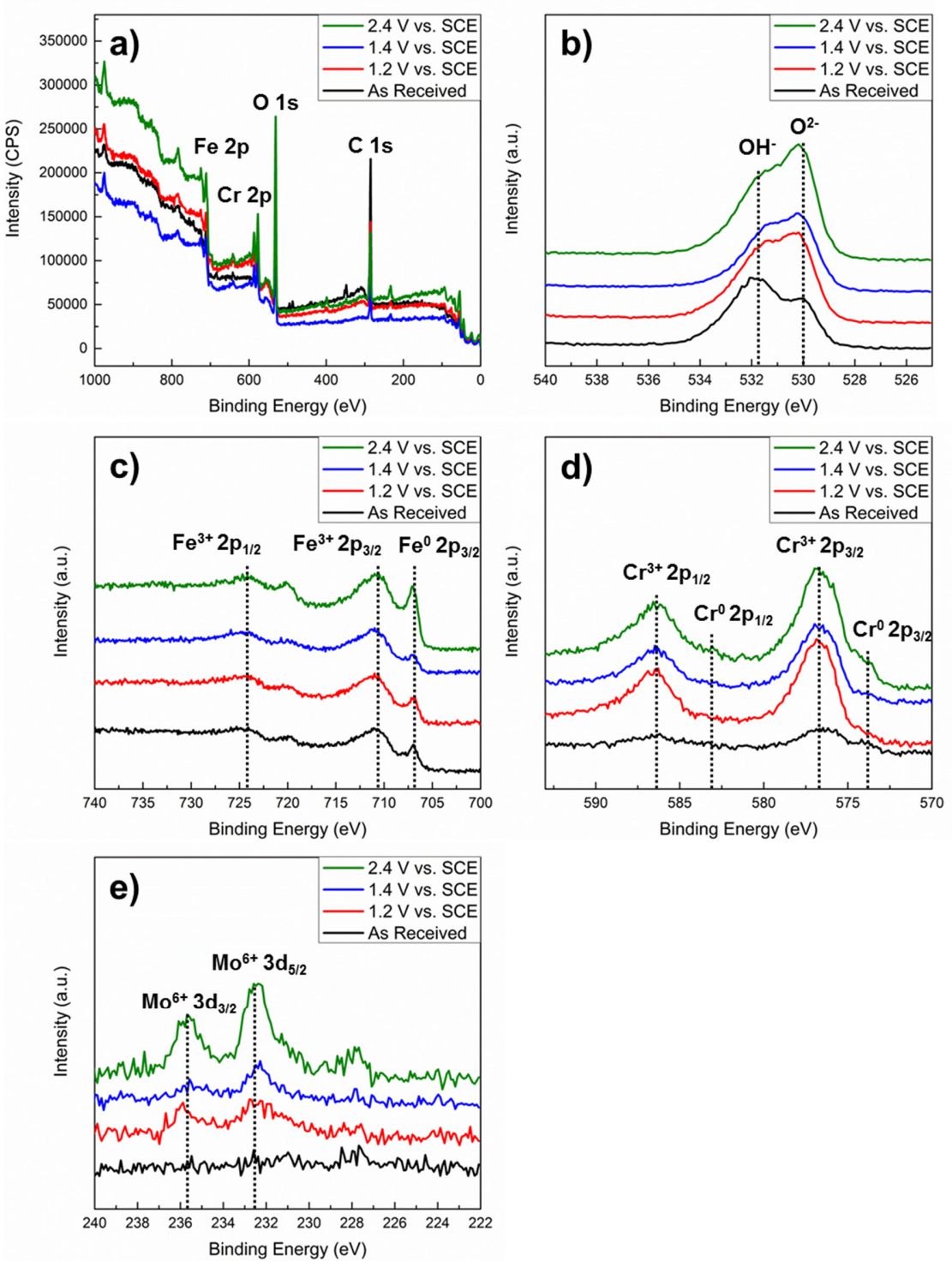

Figure 20. XPS of SS316L surfaces that were not etched or were electrochemically etched with potentials of 1.2 V, 1.4 V, and 2.4 V vs. SCE. (a) Survey spectra, (b) O1s scans, (c) Fe2p scans, (d) Cr2p scans, (e) Mo3d scans

Fluorocarbon plasma deposition was performed to coat SS316L samples in order to ensure identical surface chemistry among the samples, which enables isolation of the effects of surface topography on wetting properties without the need to account for surface chemistry variations. In addition, fluorocarbon films enhance the water repellency of all samples, while covalent bonding of the fluorocarbon film to SS316L provides a mechanically stable coating.[72, 89] A silicon wafer was placed in the reactor during deposition to allow determination of the fluorocarbon thickness; ellipsometric measurements indicated that the film thickness was 149 (±1) nm with 40 s deposition. The deposited film is composed of various fluoropolymer and hydrocarbon bonding structures.[96-97] XPS spectra of a fluorocarbon film deposited onto SS316L substrates are shown in Figure 21. The survey spectrum indicates that the major elements detected are F and C with a [F]/[C] ratio of 1.05, and a peak at 835 eV corresponds to F KLL Auger electron; Fe and Cr were below the detection limit as expected since the fluorocarbon film thickness was greater than the sample depth of XPS (<10nm) (Figure 21a). High resolution XPS spectra of C1s and F1s show detailed information on bonding structures of the fluorocarbon layer (Figure 21b, c).

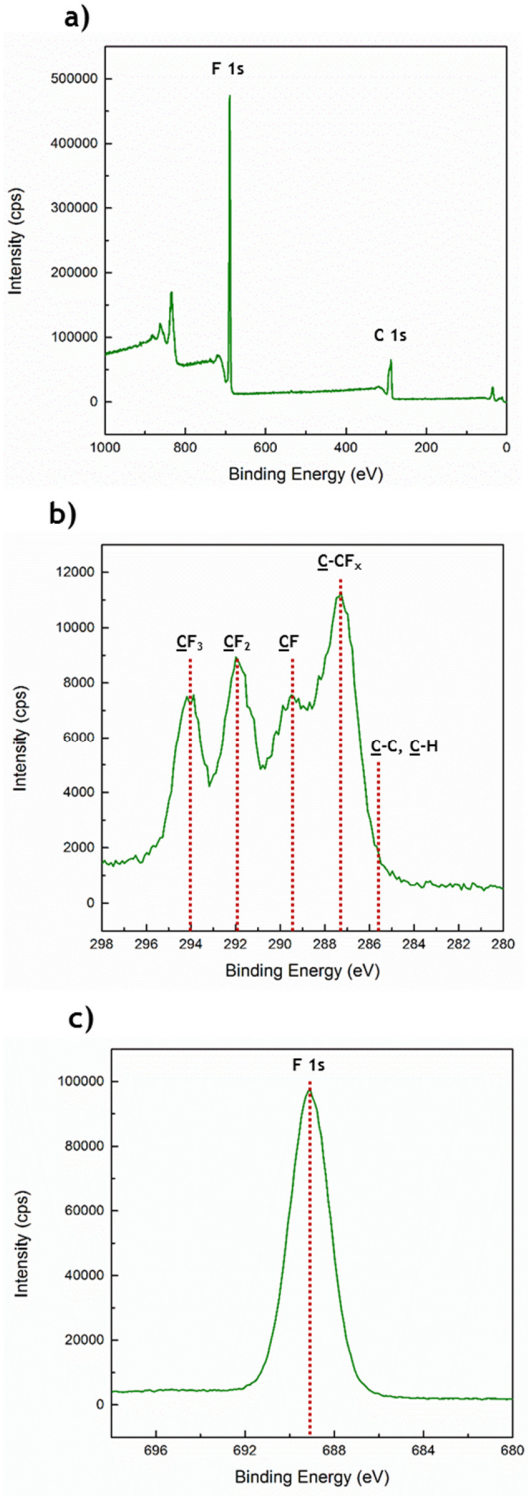

Figure 21. XPS spectra of fluorocarbon films deposited onto SS316L samples. (a) Survey spectrum, (b) C1s scan, (c) F1s scan.

2.3.3 Effect of Anodic Potential on Wetting Behavior

Water wetting behavior of the unmodified and modified SS substrates was characterized by contact angle measurements. As shown in Figure 22a, surface modification of SS316L through electrochemical etching and fluorocarbon plasma deposition leads to significant changes in surface wettability, with an increase in roughness and coating formation leading to higher water contact angles. Figure 22b shows static and advancing contact angles for SS316L samples that were electrochemically etched at different potentials. The static contact angle increased from 87.9 ° ± 4.7 for as-received SS316L to 135.8 ° ± 2.7 for SS316L that was electrochemically etched at 1.4 V. Further increases in the applied potential led to a decrease in water contact angle; the sample electrochemically etched at 2.4 V showed a static contact angle of 78.6 ° ± 4.7. Advancing contact angles show a similar trend, but with slightly higher contact angles compared to the static contact angles. However, droplets on all samples without fluorocarbon coating were pinned at contact lines and did not show changes in contact lines as the volume decreased. As a result, no receding contact angles could be measured and all samples were “sticky”, even when static contact angles were >120°, which indicates repellency. When SS316L was electrochemically etched, a sticky hydrophobic surface was generated due to strong adhesion between water droplets and the electrochemically etched SS316L surface.[89, 98-99]

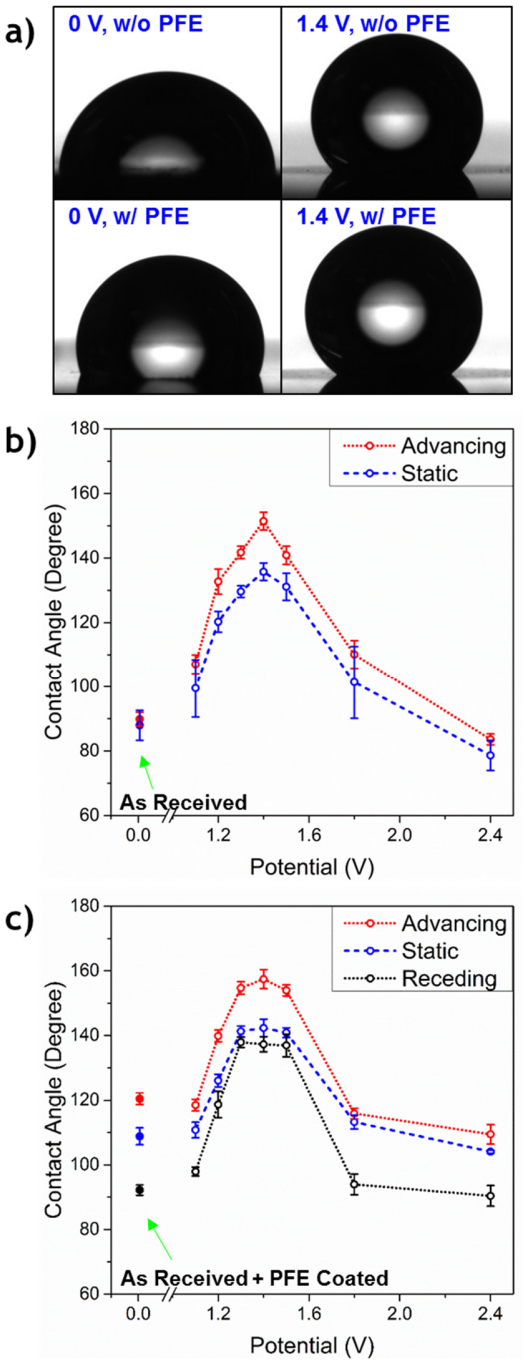

Figure 22. Effect of potential on water wetting behavior of SS316L surfaces: (a) Images of static contact angles of DI-water on un-etched and etched (1.4 V) SS316L samples with and without fluorocarbon deposition, (b) Advancing and static contact angles of DI-water on SSS316L samples electrochemically etched with different applied potentials before fluorocarbon deposition (c) Advancing, receding, and static contact angles of DI-water on SS316L samples electrochemically etched at different applied potentials after fluorocarbon deposition

In order to examine only the effect of surface structure on wetting behavior in more detail, contact angle measurements were carried out on SS316L samples coated with fluorocarbon (149 nm) (Figure 22c). The control sample with fluorocarbon deposition but no electrochemical treatment showed a static contact angle of 108.9 ° ± 2.6.[89] When the applied potential increased to 1.4 V, the static contact angle increased to 142.4 ° ± 2.7. Further increases in potential resulted in a decrease in the static contact angle to 104.1 ° ± 0.5 for the electro-polished sample. These observations indicate that electrochemical etching enhances surface roughness until the applied potential of 1.4 V is reached; this increased roughness leads to an increase in water contact angles. Further increases in applied potential smoothed the existing surfaces, and yielded a concomitant decrease in water contact angles. As anticipated, the smooth, electro-polished sample has the lowest contact angle; in fact, the static contact value in this case is the same as that for a silicon wafer coated with the same fluorocarbon layer. In addition, the sample electrochemically etched at an applied potential of 1.4 V followed by fluorocarbon deposition showed a contact angle hysteresis of 20.2 °. That is, the combination of electrochemical etching at 1.4 V and fluorocarbon deposition leads to a water repellent SS316L surface. Figure 23 shows high magnification SEM images of SS316L surfaces that were electrochemically etched at different potentials (1.8 V and 2.4 V) with and without fluorocarbon deposition. While application of an anodic potential of 1.8 V resulted in sponge-like structure on top of the SS316L surface (Figure 23a), a potential of 2.4 V led to a smooth surface (Figure 23b). Deposition of a fluorocarbon film resulted in agglomerated nanoscale features on 1.8 V electrochemically etched SS316L sample (Figure 23c), but no identifiable nanoscale features on 2.4 V electrochemically etched SS316L sample at this size scale (Figure 23d),

which yielded slight differences in water contact angles between these two samples (Figure 22).

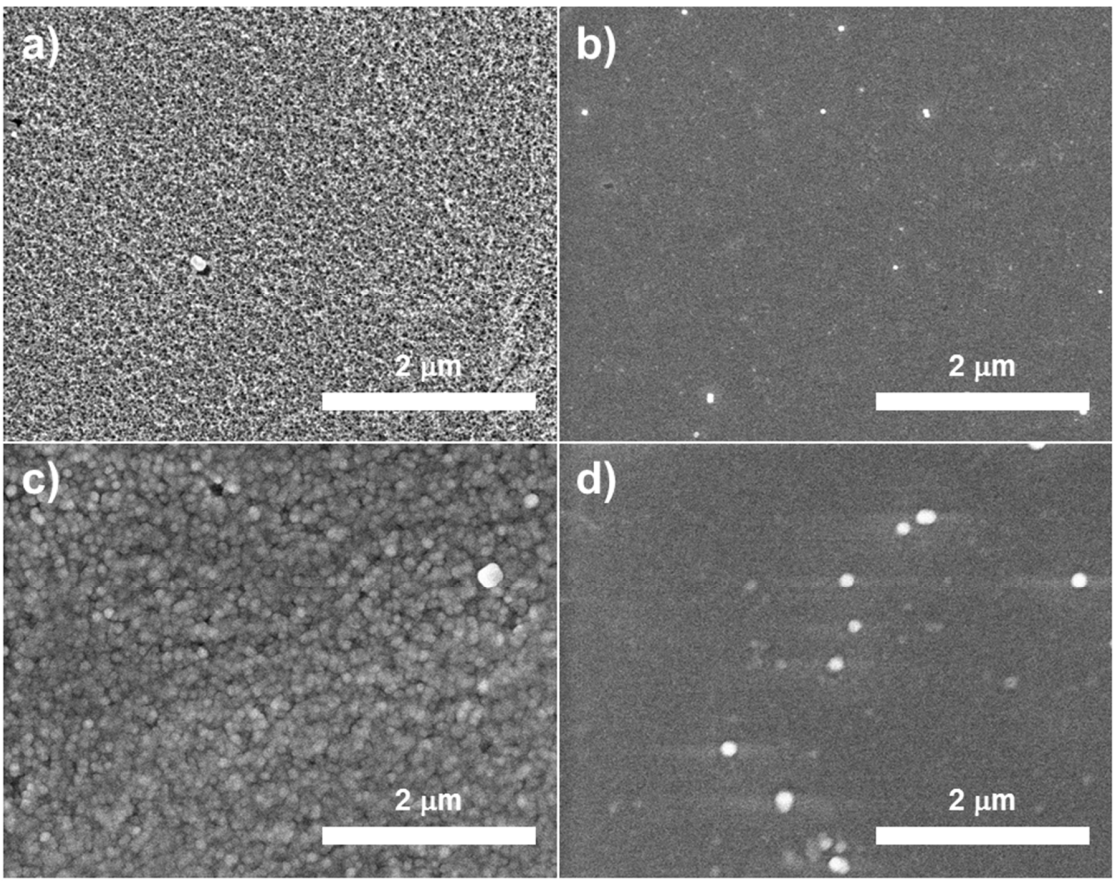

Figure 23. SEM images of SS316L electrochemically etched at different potentials for 300s: (a) electrochemically etched at potential of 1.8 V without fluorocarbon deposition, (b) electrochemically etched at a potential of 2.4 V without fluorocarbon depsosition, (c) electrochemically etched at a potential of 1.8 V with fluorocarbon deposition, (d) electrochemically etched at a potential of 2.4 V with fluorocarbon deposition.

2.3.4 Hierarchical Intrinsic Grain Structure on SS316 and Superhydrophobicity

It is well-known that hierarchical structure plays a pivotal role in creating super-hydrophobic surfaces.[37, 100] In order to accentuate both nano- and micro-scale roughness on SS316L, a two-step potentiostatic electrochemical etching at 1.3 V for 300 s (Step 1) and 1.8 V for 10 s (Step 2) was conducted (Figure 24).

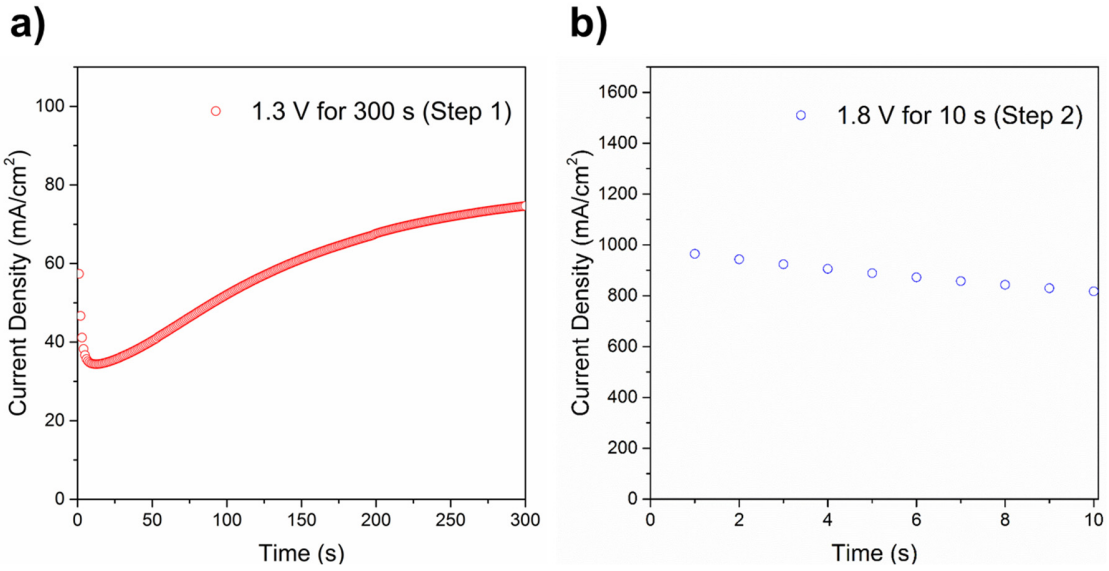

Figure 24. Two-step potentiostatic electrochemical etching behavior. (a) Current density-time (mA/cm2 - s) curve at the applied potential of 1.3 V for 300 s (Step 1), (b) Current density-time (mA/cm2 - s) curve at the applied potential of 1.8 V for 10 s (Step 2)

Figure 25 show low and high magnification SEM images of the morphology of two-step processed SS316L. The two-step processed SS316L substrate showed similar microscale roughness (Figure 25a) to that of SS316L electrochemically etched at 1.3 V (Figure 16d). However, the two-step electrochemical etching gave rise to the evolution of sponge-like nanoscale roughness on top of the SS316L grains (Figure 25b) while electrochemical etching at an anodic potential of 1.3 V resulted in relatively flat grain surfaces (Figure 17d).

The two-step processed SS316L with hierarchical roughness showed a remarkably high static water contact angle of 137.5 ° ± 5.0 even without fluorocarbon deposition. However, the contact angle hysteresis of DI-water was 33.4 ° (advancing and receding contact angles of 153.3 ° ± 3.3 and 119.9 ° ± 3.8, resp.) and a 4 µL DI-water droplet placed on the two step processed SS316L surface did not roll off even when the goniometer stage was tilted to 90 °. This indicates that the hierarchical structure created on SS316L through the two-step electrochemical etching imparts moderate water repellency. Fluorocarbon plasma deposition (23 nm) onto the hierarchical intrinsic grain structure further enhanced water repellency. The two-step processed SS316L sample with fluorocarbon deposition resulted in a high static water contact angle of 163.9 ° ± 1.2 and roll-off of 4 µL droplets at a tilt angle of 10.7 ° ± 2.9 (Figure 25c). The contact angle hysteresis decreased to 6.9 ° with advancing and receding contact angles of 168.3 ° ± 1.6 and 161.4 ° ± 1.6, respectively (Table 2). That is, the combination of the two-step electrochemical etching and fluorocarbon deposition resulted in a highly water repellent SS316L surface.

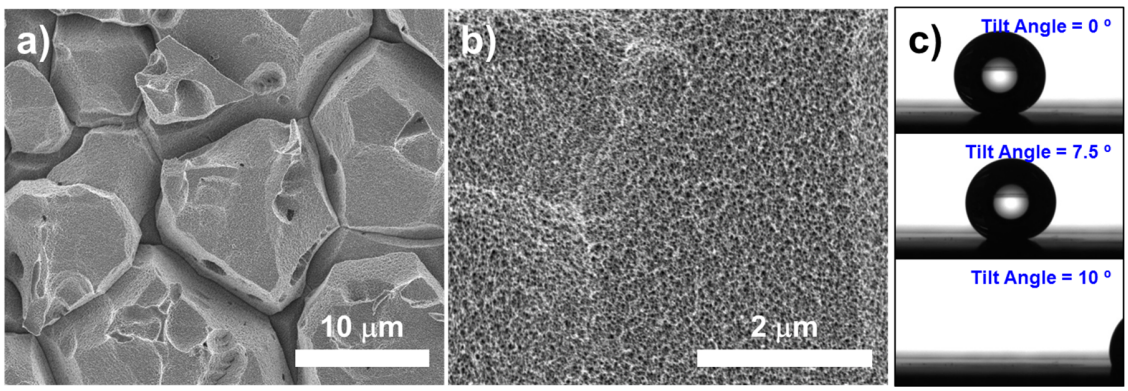

Figure 25. Hierarchical intrinsic grain structures on SS316: and wetting behavior: (a) low magnification SEM image, (b) high magnification SEM image, (c) roll-off behavior of 4 µL DI-water droplet on the hierarchically structured SS316L with fluorocarbon deposition.

Table 2. Summary of wetting behavior of DI-water on the two-step processed SS316L with and without fluorocarbon deposition

	Two-step Electrochemical Etching (w/o Fluorocarbon Deposition)	**Two-step Electrochemical Etching (w/ Fluorocarbon Deposition, 5 s)**
Static Contact Angle (º)	137.5 ± 5.0	163.9 ± 1.2
Contact Angle Hysteresis (º)	33.4	6.9
Roll-off Angle, 4 μL DI-Water (º)	Sticky	10.7 ± 1.8

2.4 Conclusions

A simple method to control water wetting behavior on SS316L surfaces has been demonstrated. The evolution of roughness on SS316 surfaces via modification of intrinsic grain structures was achieved by electrochemical etching; this structure variation led to alteration of the wetting behavior. Variation of the applied anodic potential changed the etch selectivity between grains and grain boundaries and thus the resulting surface structure. A low (1.2 – 1.3 V) applied potential yielded highly selective etching, and a higher (1.4 V – 1.5 V) applied potential resulted in low selectivity of grains relative to grain boundaries during etching; further increases in applied potential (1.8 V) resulted in a surface with only sponge-like nanoscale roughness. Finally, the applied potential of 2.4 V led to a smooth electro-polished surface. Topographies of SS316L substrates etched at different applied potentials were consistent with a direct relationship between applied potential and etch selectivity. In addition, an increase in Cr concentration on SS316L surfaces was observed upon electrochemical etching, which is expected to enhance the corrosion resistance. Based upon the relationship between applied anodic potential and surface topography, we designed a process to achieve nano/microscale hierarchical intrinsic grain structures on SS316L substrates. Water wetting behavior demonstrated that the hierarchically structured SS316L surface showed a high static contact angle of 137.5 ° ± 5.0, even without chemical surface modification. Deposition of a fluorocarbon film onto the hierarchically structured surface further increased the water contact angle to 163.9 ° ± 1.2. An additional difference in these samples is that samples with fluorocarbon coating have roll-off angles of (10.7 ° ± 2.9), leading to roll-off super-hydrophobic SS316L surfaces. A two-step process of electrochemical etching followed by fluorocarbon film

deposition provides a simple method to create water repellent stainless steel surfaces that will likely display mechanical stability and corrosion resistance.

CHAPTER 3.

IMPROVED LOCALIZED CORROSION RESISTANCE OF STAINLESS STEEL

Material from this chapter has been accepted for publication in

W. T. Choi, K. Oh, P. M. Singh, V. Breedveld, and D. W. Hess,

Hydrophobicity and Improved Localized Corrosion Resistance of Grain Boundary Etched Stainless Steel in Chloride-containing Environment,

Journal of the Electrochemical Society (2017)

3.1 Introduction

3.1.1 Localized Corrosion of Stainless Steels in Chloride-containing Environment

Metal corrosion is a naturally occurring phenomenon commonly defined as the deterioration of a metal triggered by a chemical reaction with its environment.[13-14] Due to the ubiquitous use of metals in infrastructure, production and manufacturing, transportation, and utilities, corrosion results in compromised safety and recurring repair costs.[14] One of the most commonly employed approaches to control corrosion is the use of corrosion resistant alloys.[14] Stainless steels (SSs), which are defined as steel alloys containing at least 10.5% chromium content by mass, are the most frequently used materials in aqueous environments because of their enhanced corrosion resistance relative to carbon steels.[78] Chromium participates in the formation of a stable passive film on SSs

that protects the bulk metal against corrosion.[4] However, SSs still suffer from localized corrosion when exposed to chloride-containing aqueous environments, including seawater[101-102] and bleach plants associated with pulp and paper industries.[103]

Localized corrosion phenomena such as pitting and crevice corrosion are accelerated forms of corrosion at discrete sites that result from local breakdown of passive films in corrosive environments.[18-19] Chloride ions are relatively small anions with a high diffusivity that can participate in localized breakdown of the passive films. Corrosion sites created by chloride attack exhibit higher electrochemical activity than the surrounding passivated areas, which initiates local dissolution of the underlying bulk metal.[20, 104] The phenomenon is autocatalytic, because localized production of metal cations induces electro-migration of chloride anions from the bulk electrolyte towards the corrosion sites in order to maintain charge neutrality; furthermore, hydrolysis of the metal cations in water can increase acidity, which further accelerates the rate of localized corrosion.[19] Initiation of localized pitting corrosion on SSs is associated with the presence of surface inhomogeneities such as MnS inclusions, which can lower the activation energy for passive film dissolution.[19-20, 105-106]

3.1.2 Methods to Prevent Localized Corrosion of Stainless Steels

Strategies to improve the localized corrosion resistance of SSs include enrichment of Cr and Mo at the SS surfaces and removal of surface inhomogeneities.[95] These SS surface treatments include mechanical polishing,[59, 107] passivation,[59, 95, 108-109] and electro-polishing.[60, 78, 107, 110] Mechanical polishing results in Cr-rich SS surfaces.[59] Surface passivation of SS using a nitric acid solution removes surface inhomogeneities and enhances the formation of a Cr-rich passive film.[95] Electro-polishing is a technique to

control the surface finish of a metal by anodic electrochemical dissolution to yield a smooth metal surface. Electro-polishing removes surface inhomogeneities from the SS surface and simultaneously forms Cr- and Mo-rich passive films. Electro-polished SS surfaces show higher localized corrosion resistance than mechanically polished and passivated SS surfaces.[110] Chromium oxide/hydroxide (Cr_2O_3/$Cr(OH)_3$) in the passive film hinders movement of cations into the electrolyte and thereby delays local breakdown of the passive film.[59] The Mo component also stabilizes the passive film.[111] In contrast, MnS inclusions are preferred sites for pit corrosion initiation.[20, 102, 105-106, 112-113]

3.1.3 Topographical Enhancement to Prevent Marine Fouling

Fouling by marine organisms on submerged SS surfaces increases the probability of localized corrosion on SS surfaces due to metabolic activity of the bio-organisms.[114-116] Traditionally, coatings of antifouling materials have been employed to solve these problems, but antifouling agents can kill and destroy marine organisms and thus cause environmental concerns.[117] Recently, many studies have been devoted to the development of non-toxic strategies to prevent biofouling by mimicking surface topographies of marine species that naturally resist biofouling such as sharks,[39, 118] shells,[52, 119-120] and crabs.[51, 119] The combination of microscale topography and surface hydrophobicity is known to effectively reduce the fouling of marine organisms.[50, 121] The SS surface treatments described above enhance localized corrosion resistance but generate smooth, hydrophilic surfaces. Therefore, it is of great interest to develop micro-structured, hydrophobic SS surfaces with resistance against localized corrosion for maritime applications.

3.1.4 Present Work based on Grain Boundary Etched Stainless Steels

Grain boundary etching is a common metallographic technique used to delineate the grain structure of metals and metal alloys, thereby allowing analysis of size and orientation of grains.[75] Its application to modify SS surfaces for specific performance enhancement instead of metallography is rare: one reports applies grain boundary etching to a drug-eluting SS stent surface to increase the surface area and, as a result, the drug loading.[76] Recently, we demonstrated that potentiostatic polarization in a nitric acid solution can be used to create/control surface structures on stainless steel 316L (SS316L), which enabled tunable water wettability.[77] The grain structure of SS316L surfaces was accentuated by selective grain boundary etching and the resulting roughness yielded a hydrophobic surface. This etching process provided the appropriate length scales of surface roughness for excellent wetting control. In the current study, we report the localized corrosion behavior of the hydrophobic, grain boundary etched SS316L and compare the results to as-received SS316L, as well as electro-polished SS316L, which is known to possess improved localized corrosion resistance, albeit with hydrophilic properties.

We investigated the corrosion behavior of these three different SS316L surfaces through potentiodynamic polarization in a neutral 0.6 M sodium chloride solution, which mimics a seawater environment.[122] Potentiodynamic polarization was performed up to potentials corresponding to the onset of localized corrosion. Water contact angle measurements were used to determine the water wettability of the SS316L surfaces. Surface structures of the different SS316L samples were analyzed by scanning electron microscopy (SEM). Chemical composition of the SS316L surfaces was obtained by X-ray photoelectron spectroscopy (XPS), which supplied insight into the relationship between changes in

surface chemistry and corrosion behavior in 0.6 M sodium chloride solution induced by both grain boundary etching and electro-polishing.

3.2 Experimental

3.2.1 Materials

Nitric acid (ACS reagent, 70%) was purchased from Sigma Aldrich. Sodium chloride (ACS reagent, ≥ 99.0 %) was purchased from J. T. Baker. Both chemicals were used without further purification. SS316L plates ($30 \times 20 \times 0.05$ cm^3) were purchased from Maudlin Products; chemical compositions of the SS316L plates were obtained by X-ray fluorescence (XRF, Oxford Instruments X-MET 8000) and are compared with the material test report provided by Maudlin Products in Table 3; the compositions are in good agreement. A platinum foil ($2.5 \times 2.5 \times 0.0025$ cm^3, 99.9%) was purchased from Alfa Aesar. Insulating tape (Electroplating Tape 470) was purchased from 3M.

Table 3. Chemical composition of the stainless steel 316L, wt%; remaining content is Fe

	Cr	Ni	Mo	Mn	Cu
XRF	16.78 (±1.07)	9.94 (±0.68)	2.09 (±0.13)	1.34 (±0.11)	0.29 (±0.10)
Maudlin Products	16.54	10.17	2.10	1.41	0.29
	C	Si	S	P	N
XRF	-	-	-	-	-
Maudlin Products	0.021	0.510	0.001	0.032	0.020

3.2.2 Sample Preparation: Potentiostatic Polarization

Two different sizes (2.5 × 1.5 × 0.05 cm^3 and 2.5 × 2.5 × 0.05 cm^3) of SS316L samples were cut from the as-received sheets using a water jet cutter. These two samples served as working and counter electrodes, respectively, for the potentiostatic polarization. Prior to potentiostatic polarization treatments, the SS316L substrates were washed with acetone, methanol, and isopropyl alcohol to remove surface organic contaminants, and the samples were air-dried at ambient temperature. Stainless steel wires were attached to the electrodes via spot welding to establish electrical connections. Insulating tape was employed to mask the working electrode, leaving an active area (0.13 cm^2) exposed for electrochemical treatments. Nitric acid (48% by weight) was used as the electrolyte. A saturated calomel electrode (SCE) served as the reference electrode in the three-electrode system. All potential values reported in this paper are relative to SCE. The distance between working and counter electrodes was maintained at 3 cm, and reference electrode was placed near the working electrode. A potentiostat (Gamry Reference 600) was used to perform the potentiostatic polarizations. After initial delays of 300 s at open circuit conditions, potentiostatic polarization tests were performed at anodic potentials of 1.3 V and 2.4 V for 300 s at room temperature; the two potentials yielded grain boundary etched and electro-polished SS316L surfaces, respectively.[77] After the potentiostatic polarizations, the SS316L samples were removed from the electrochemical cell, rinsed with deionized water, and dried at room temperature for one day prior to characterization. Details about the experimental configuration for potentiostatic polarization can be seen in Figure 14.[77]

3.2.3 Corrosion Behavior: Potentiodynamic Polarization

Corrosion resistance of the three SS316L samples was tested using potentiodynamic polarization in 0.6 M sodium chloride solution in an open jar with natural aeration. The as-received, grain boundary etched, and electro-polished SS316L samples were used as working electrodes, while platinum foil and the SCE served as counter and reference electrodes, respectively. Mechanical polishing of SS316L with 600 grit sandpaper is a known method to remove surface inhomogeneities of samples, thereby reducing sample to sample variation. However, mechanical polishing is a post-processing step that must be conducted on individual parts and affects the dimensions in a poorly controlled manner, which limits the applicability of mechanical polishing as surface finishing step in ultimate applications where corrosion resistance is critical. Therefore, we selected commercially available as-received SS316L as a reference point to compare corrosion behavior. After an initial delay of 1800 s at open circuit conditions, potentials were ramped in the anodic direction with a scan rate of 0.2 mV/s. Scans were performed from the open circuit potentials to the potential where the SS316L samples showed stable localized corrosion behavior, as indicated by a sudden increase in current density by more than two orders of magnitude.[13] All potentiodynamic polarization experiments were conducted at room temperature. After potentiodynamic polarization, the SS316L samples were removed from the electrochemical cell, rinsed with deionized water, and dried at room temperature prior to surface morphology characterization.

3.2.4 SS316L Surface Characterization

Surface morphologies of the SS316L samples were characterized by SEM (Hitachi SEM SU8010, Japan) at 3 kV acceleration potential and optical microscopy (OM, Olympus LEXT 3D Material Confocal Microscope). A goniometer (Ramé-Hart 290) was used to measure water contact angles. Water contact angles were obtained by dispensing 4 μL deionized water droplets onto the SS316L samples at room temperature; images of droplets were captured with a CCD camera and analyzed via the goniometer software. Chemical composition of the SS316L samples was determined by XPS using a Thermo Fisher Scientific K-Alpha XPS with a 400 μm micro-focused monochromatic Al Kα X-ray source.

3.3 Results and Discussion

3.3.1 Surface Modification of SS316L

As shown in Figure 26, the surface structure of SS316L was modified by potentiostatic polarization. An applied anodic potential of 1.3 V results in a grain boundary etched SS316L surface with accentuated 5-20 μm intrinsic grain structures (Figure 26b), while 2.4 V leads to a smooth electro-polished SS316L surface (Figure 26c). The roughness features that are evident on the as-received SS316 (Figure 26a) were created during the sheet manufacturing processes. Grain boundaries are preferential etching sites under certain potential conditions.[17, 88] In this system, highly selective grain boundary etching is achieved at an applied potential of 1.3 V, which accentuates the intrinsic grain structures on the SS316L surface. Potentiostatic polarization at an anodic potential of 2.4 V shows little to no selectivity towards grain boundary etching, thereby generating an electro-polished SS316L surface. The effects of modifying the SS316L surfaces via potentiostatic polarization on corrosion behavior in 0.6 M sodium chloride solution and on wettability are discussed in the following sections.

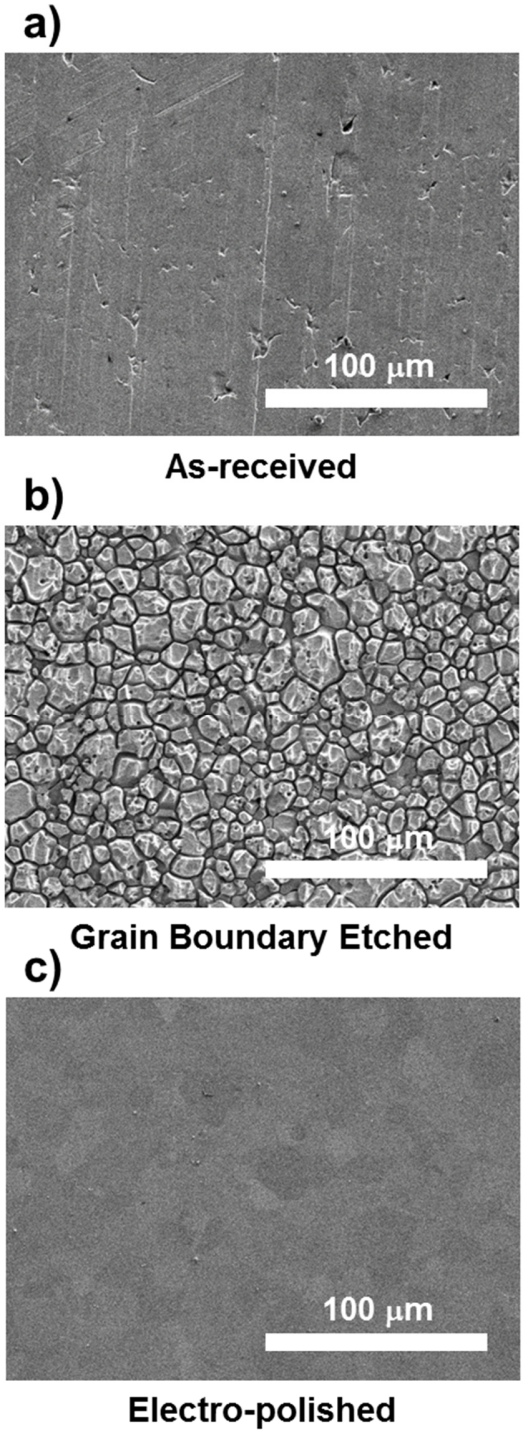

Figure 26. SEM images of SS316L samples: (a) As-received SS316L, (b) Grain boundary etched SS316L, (c) Electro-polished SS316L.

3.3.2 Corrosion Behavior of SS316 Surfaces

Figure 27 shows anodic potentiodynamic polarization curves of as-received, grain boundary etched, and electro-polished SS316L samples. These curves display onset points of SS316L sample dissolution, passivity, and rapid increases in current density due to localized corrosion.[13, 123] Since the SS316L samples were polarized in the anodic direction from open circuit conditions, the starting point of each curve represents the onset of SS316L dissolution and the corresponding potential is the so-called open circuit potential (E_{OC}). Passivity is defined as corrosion resistance due to formation of thin oxide films under oxidizing conditions and is indicated by the presence of a steep slope in Figure 27, i.e. large changes in potential for small increments in current density.[92, 123] The sharp increase in current density at high potential (i.e. flat section of the graph) represents the onset of localized corrosion, and the potential at which this occurs is referred to as the breakdown potential (E_{BD}).[13] In order to capture the stochastic nature of localized corrosion,[124-125] eight samples were prepared for each SS316L surface and potentiodynamic polarization measurements were performed on all samples (Figure 27a, b, c). Representative potentiodynamic polarization curves for each substrate are displayed in Figure 27d to facilitate direct comparison of polarization curves (E_{OC} and E_{BD} values) for as-received, 1.3 V and 2.4 V samples. Specifically, the curves in Figure 27d were selected from Figure 27a, b, and c, as having E_{OC} and E_{BD} values closest to the population average of the eight recorded curves. The average values of E_{BD} and E_{OC} and their standard deviations are summarized in Figure 27e and f. The as-received SS316L samples exhibit spikes in current density in potential ranges from open circuit potentials to 0.2 V, while sharp increases in current density were observed in the potential range 0.32 V to 0.86 V;

these increases represent metastable localized corrosion and stable localized corrosion, respectively (Figure 27a).[123] In the potentiodynamic polarization curves of grain boundary etched and electro-polished SS316L samples, no characteristic metastable localized corrosion was observed; passivity was observed at potentials up to 0.9 V. Beyond the passivity region, stable localized corrosion occurred for the grain boundary etched and the electro-polished SS316L samples in fairly narrow potential ranges: 0.96 to 1.05 V for grain boundary etched, and 0.99 to 1.07 V for electro-polished samples (Figure 27b, c). The lack of metastable localized corrosion and the high E_{BD} values with a narrow distribution indicate superior localized corrosion resistance compared to the as-received SS316L sample (Figure 27e). In addition, the E_{OC} values for the grain boundary etched and electro-polished SS316L samples were higher than for the as-received SS316L sample, which can be attributed to a higher rate of cathodic reaction on electrochemically treated SS316L samples (Figure 27f). The corrosion behavior of SS316L mechanically ground with 600 grit paper was also tested in 0.6 M sodium chloride solution. Results demonstrate that the breakdown potential occurred in the range of that of as-received SS316L samples (Figure 28a). In addition, we prepared mechanically ground and grain boundary etched SS316L samples and tested the corrosion behavior, which was consistent with potentiodynamic polarization curves of grain boundary etched SS316L without the mechanical grinding pretreatment (Figure 28b). We also tested cyclic polarization of SS316L samples.

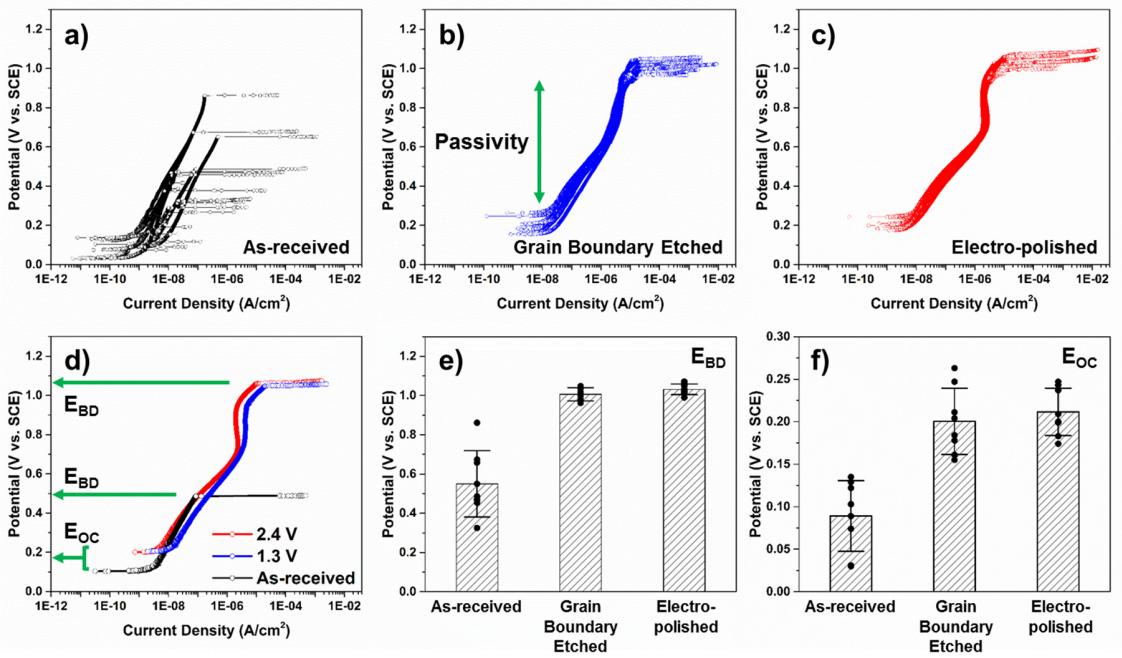

Figure 27. Corrosion behavior of SS316L samples in 0.6 M NaCl solution. Potentiodynamic polarization curves for eight samples each of (a) As-received SS316L, (b) Grain boundary etched SS316L, (c) Electro-polished SS316L. (d) Direct comparison of representative potentiodynamic polarization curves for each SS316L sample. (e) Summary of E_{BD} values for all three SS316L sample types; columns and error bars represent averages and standard deviations of the E_{BD} values, respectively. Scattered dots represent the spread of E_{BD} values for each curve. (f) Summary of E_{OC} values for all SS316L samples; columns and the error bars represent averages and standard deviations of the E_{OC} values, respectively. Scattered dots represent the spread of E_{OC} values for each sample type.

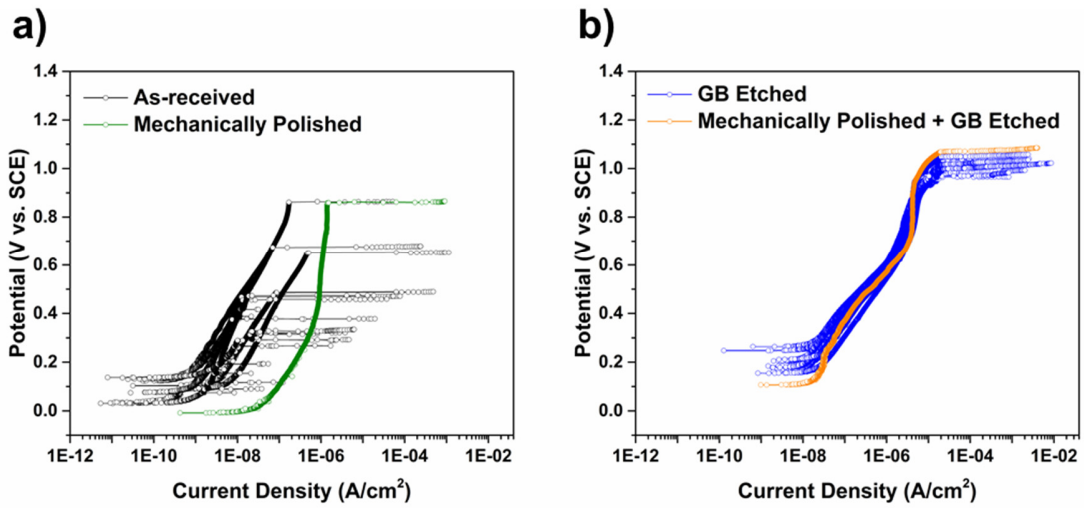

Figure 28. Corrosion behavior of SS316L samples in 0.6 M NaCl solution. Potentiodynamic polarization curves of (a) As-received SS316L and mechanically ground SS316L with 600 grit paper, (b) Grain boundary etched SS316L and mechanically ground and then grain boundary etched SS316L samples.

The morphology of localized corrosion sites on SS316L samples after potentiodynamic polarization was also investigated using SEM (Figure 29). The as-received SS316L samples showed formation of mouth pits with lacy pits around the mouth pit peripheries (Figure 29a).[126] The grain boundary etched and electro-polished SS316L samples showed localized corrosion in the form pitting and crevice corrosion (Figure 29b, c). Pitting corrosion is known to arise at open surfaces of the passivated metals, while crevice corrosion occurs in confined spaces where access to bulk electrolyte is limited.[18-20] Cavities formed inside the active area (see experimental details) of grain boundary etched and electro-polished SS316L surfaces represent pitting corrosion (Figure 29b1, 2, and 29c1, 2), while cavities along the periphery of the active area are indicative of crevice corrosion (Figure 29b3, c3). We hypothesize that the confined space between masking tape and SS316L surfaces along the periphery of the active area can act as an initiation site for

crevice corrosion by limiting access of bulk electrolyte to the space. In addition, depth profiles of pits created on the three kinds of SS316L samples were measured (Figure 30). The pit generated on as-received SS316L was relatively narrow and deep compared to the pits on grain boundary etched and electro-polished SS316L samples. Further study is necessary to investigate the relationship between surface modification and types and morphology of localized corrosion.

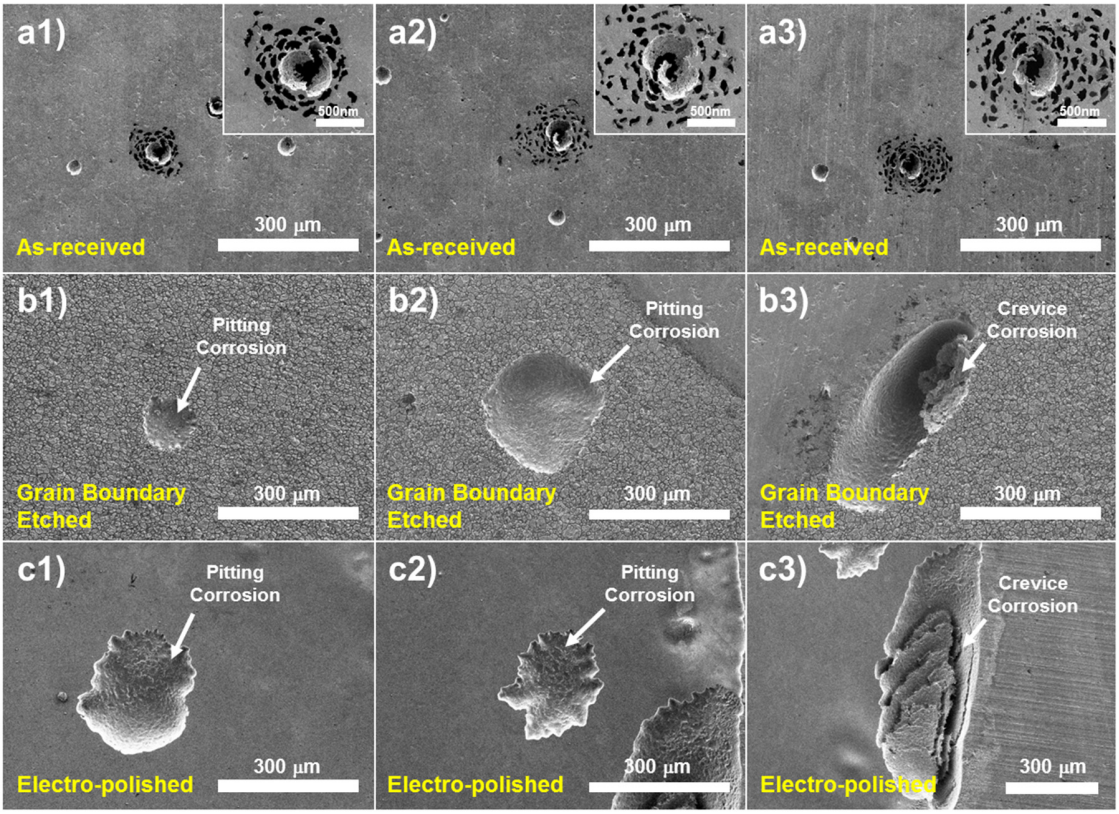

Figure 29. Morphology of localized corrosion on SS316L samples after potentiodynamic polarization: (a) Pitting corrosion on as-received SS316L samples; insets represent magnified images. (b) Pitting and crevice corrosion on grain boundary etched SS316L samples. (c) Pitting and crevice corrosion on electro-polished SS316L samples.

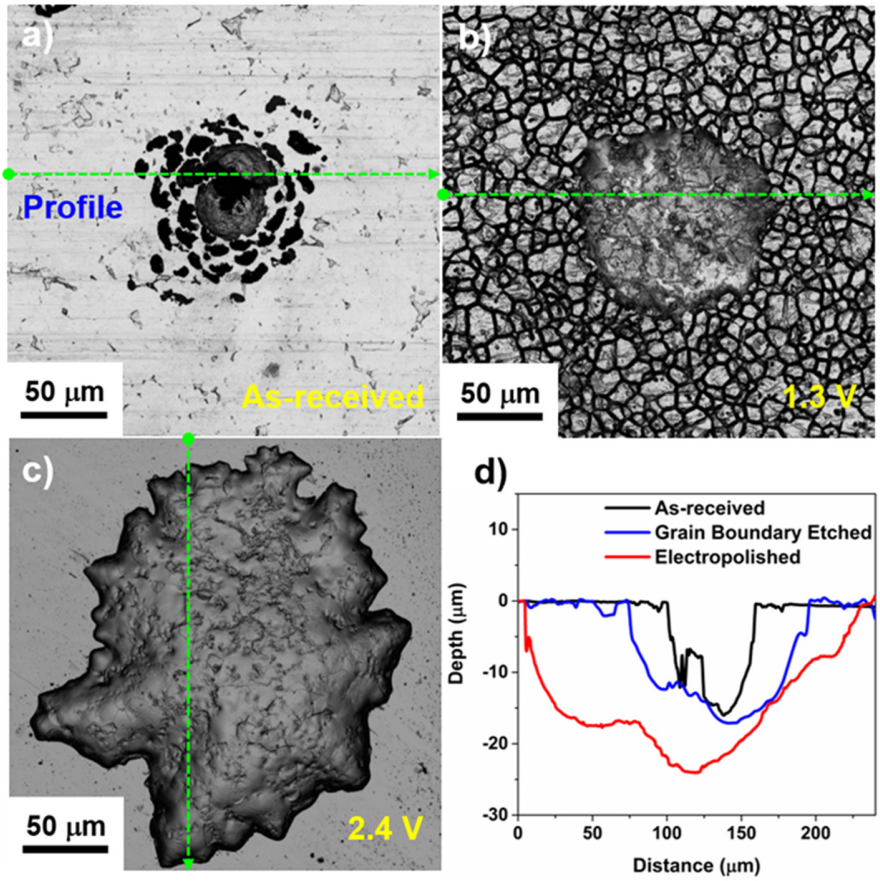

Figure 30. Morphology and pitting corrosion on SS316L samples after potentiodynamic polarization: (a) Pitting corrosion on as-received SS316L sample, (b) Pitting corrosion on grain boundary etched SS316L sample, (c) Pitting corrosion on electro-polished SS316L sample, (d) Depth profiling of each pit.

3.3.3 Chemical Composition of SS316 Surfaces

The chemical composition of passive films on SS316L surfaces plays a pivotal role in corrosion behavior. Figure 31 shows XPS spectra of as-received, grain boundary etched, and electro-polished SS316 surfaces. Potentiostatic polarization of SS316L samples in nitric acid solution leads to increases in Cr and Mo content in the passive films. (Figure 31a, b).

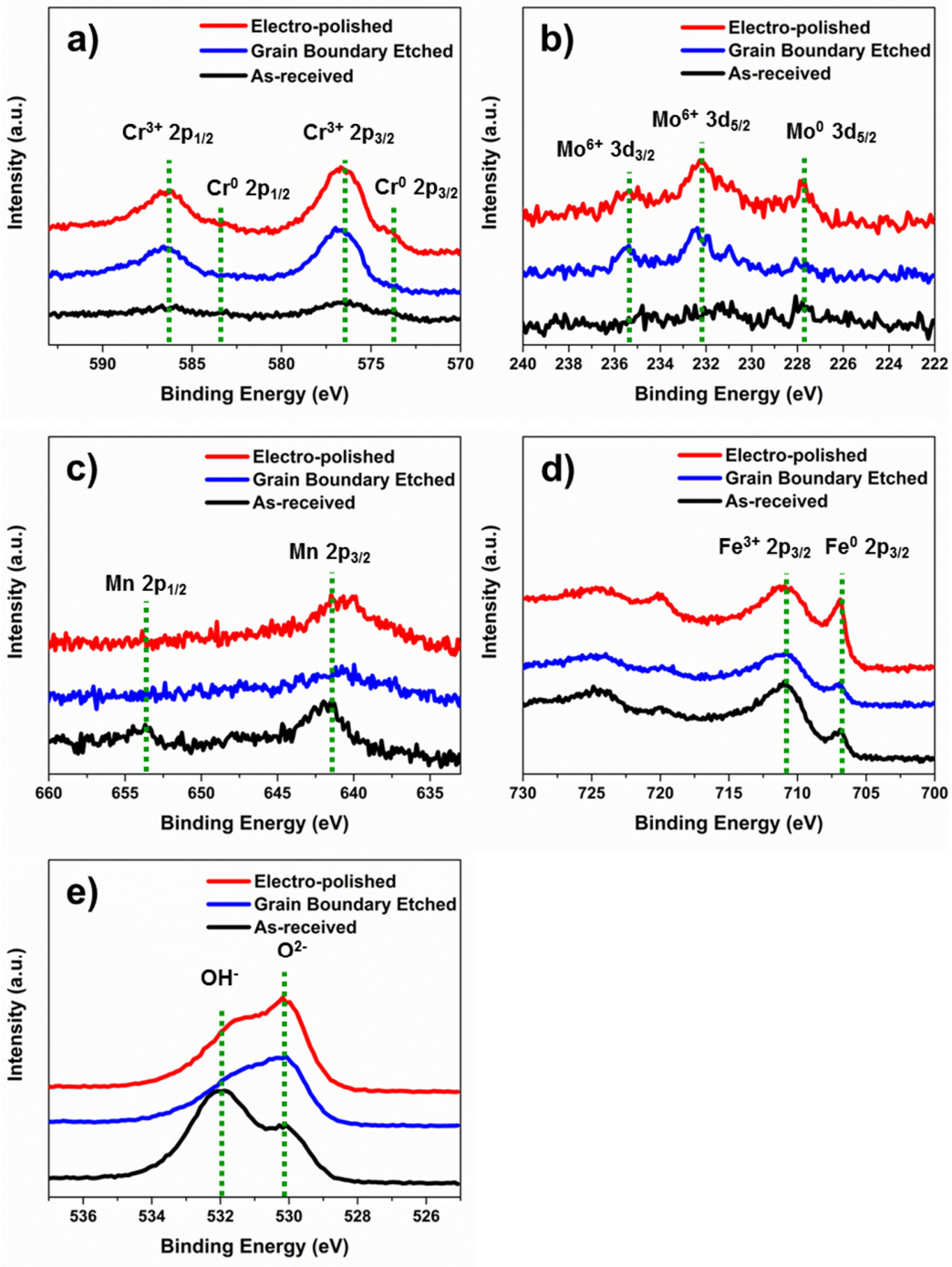

Figure 31. XPS spectra of SS316L samples. (a) Cr2p scans; (b) Mo3d scans; (c) Mn2p scans; (d) Fe2p scans; e. O1s scans.

After potentiostatic polarization, the Mn content in the passive films decreases slightly (Figure 31c). In contrast, no definitive changes in Fe content were observed in the passive films of SS316L samples after potentiostatic polarization (Figure 31d). O1s XPS spectra show that the passive films on surface-modified SS316L samples possess more oxide than hydroxide components (Figure 31e). Enrichment of Cr and Mo and the removal of Mn at SS surfaces are known to improve the localized corrosion resistance of SSs.[20, 59, 111] Therefore, the improved corrosion resistance of the grain boundary etched and electro-polished SS316L samples in 0.6 M sodium chloride solution can be attributed to the formation of superior passive films during potentiostatic polarization.

3.3.4 Wetting Behavior of SS316 surfaces

Figure 32 shows the water wetting behavior of as-received, grain boundary etched, and electro-polished SS316L samples. The static contact angle of 4 μL deionized water droplets on the as-received SS316L is 87.3 ± 4.5 º, while the grain boundary etched and the electro-polished SS316L samples show static contact angles of 135.7 ± 2.6 º and 81.0 ± 4.2 º, respectively. The increased water contact angle on the grain boundary etched SS316 surface can be attributed to the evolved microscale intrinsic grain structures which allow air to be trapped beneath the water droplet, thereby significantly enhancing the observed contact angle.[29-30] The electro-polished SS316L surface lacks microscale roughness and thus showed a similar water contact angle as the as-received SS316L surface. The grain boundary etched SS316L displayed hydrophobicity and microscale structure, which can prevent bio-fouling, thereby further reducing the probability of localized corrosion initiation in a maritime environment.[39, 50, 114-116, 121] Preliminary investigations have indeed shown that the surface topography on SS316L achieved by potentiostatic polarization can

significantly reduce the adhesion of bacteria compared to the surfaces of as-received and electro-polished SS316L. An in-depth study of the correlation between SS316L surface topography and biofouling is required.

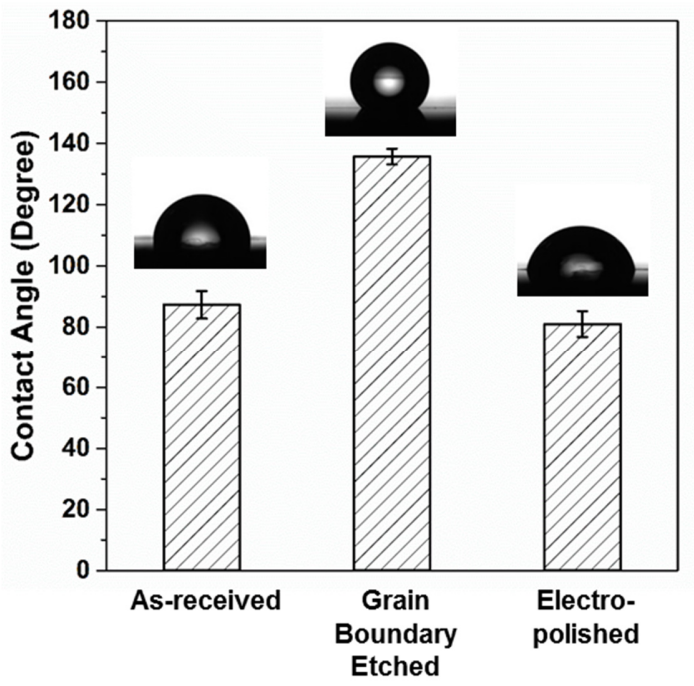

Figure 32. Water contact angles of as-received, grain boundary etched, and electro-polished SS316L samples.

3.4 Conclusion

Grain boundary etching has long been used in metallurgy as a metallographic method to reveal grain structure. Here we have shown that the process can also be used to simultaneously enhance wetting and corrosion properties of stainless steel. Specifically, we demonstrated a simple method to improve the localized corrosion resistance of SS316L surfaces in 0.6 M sodium chloride solution, while simultaneously achieving microscale topography and hydrophobicity. Grain boundary etched SS316 surfaces were created by potentiostatic polarization at the anodic potential of 1.3 V in nitric acid solution, leading to superior localized corrosion resistance with a narrow distribution of high breakdown potentials ranging from 0.96 to 1.05 V. On the other hand, as-received SS316L samples show relatively poor localized corrosion resistance with a wide range of low breakdown potential values from 0.32 to 0.86 V. This enhanced localized corrosion resistance of the grain boundary etched SS316L can be attributed to the formation of Cr- and Mo-rich passive film of SS316L during the potentiostatic polarization surface treatment. The corrosion resistance of the etched samples is similar to electropolished substrates, the current benchmark, but the grain boundary etched SS316L also display microscale topography at the appropriate roughness length scale to yield a hydrophobic surface with a water contact angle of 135.7 ± 2.6^{o}. In contrast, electropolished SS316L is hydrophilic. The combination of microscale topography and hydrophobicity on grain boundary etched SS316L offers the potential to prevent biofouling in maritime environment and thus further deter the occurrence of localized corrosion.

CHAPTER 4.

INHIBITION OF BACTERIAL ADHESION ON STAINLESS STEEL SURFACE

4.1 Introduction

4.1.1 Importance of A Study on Bacterial Adhesion on A Surface

Bacterial adhesion to diverse types of materials is a critical initial step that causes many health complications in a wide range of applications including medical implants and surgical tools,[127] water purification systems,[128] and industrial processes.[129] For example, the formation of biofilms in pipes used in a myriad of industrial processes can bring about serious problems such as impeding heat transfer across the pipe surface as well as increasing fluid drag or corrosion rate, which result in energy dissipation and production losses.[130-131] Pathogenic bacterial adhesion on surfaces used in food manufacture or at home can contaminate the food products, which is causative of infectious disease. In particular, bacterial adhesion and growth on medical device surfaces lead to serious surgical and/or implant infection problems, which can be life-threatening and will incur substantial healthcare costs. Surgical tools in hospitals including scalpels, drips, implants and catheters, are common sources exposed to pathogenic bacteria and subsequent infection. Dentists have also indicated that contamination not only on dental implants and surgical tools but also on clinical water lines for cooling and rinsing oral tissues can be serious infection sources. [132-133]

Considering the potential damage in industry and human health induced from bacterial adhesion, it is critical to understand bacterial behavior on the most commonly used material surfaces. Furthermore, the development of functional surfaces to inhibit bacterial adhesion and growth is of great importance for prevention of pathogenesis originating from foreign body infections. A systematic understanding of bacterial adhesion on a commonly-used surface such as stainless steel will generate insight into the more general design of bacteria-resistant surfaces. The current understanding of bacterial adhesion mechanisms is summarized in the next section.

4.1.2 Proposed Mechanisms of Bacterial Adhesion on a Surface

Bacterial adhesion on a surface is a complex process that is affected by various factors including the environmental conditions (i.e., temperature, pH, and fluid flow),[134-135] the bacterial types, and the material surface characteristics including chemical composition, charge, hydrophobicity, and surface texture.[135-137] There are several terms used to describe the interaction between bacterial cells and surfaces. In general, 'adhesion' means the sticking of a cell to a substrate, and 'cohesion' indicates cell-to-cell attachment. Adhesion is usually regarded as the initial adsorption or the general accumulation of an organism on a surface, while attachment is considered to be the consolidation of the interface between a cell and a surface mediated by the formation of extracellular polymeric substances (EPS).[138] Many researchers have described the process of accumulation of bacterial cells on a surface in three stages: 1) adhesion, 2) attachment via EPS formation, and 3) colonization induced from bacterial growth and subsequent biofilm formation.

Upon contacting surfaces, bacterial adhesion can occur according to the following steps. Initial adsorption step occurs very rapidly within 1 min and is reversible, which is believed to involve the long-ranged non-specific interactions such as hydrodynamic and electrostatic interactions.[139-141] During this short time period, the adhesive force between bacteria and surfaces increases rapidly. Following adhesion step is considered as irreversible and occurs on a time scale of several hours. Several observations suggest that the bacterial adhesion is mainly decided by physicochemical effects, not biological effects, including the loss of interfacial water, structural changes in surface molecules, and repositioning of the cell body to maximize adhesion to the surface. Therefore, the surface characteristic is very important to establish the affinity of bacterial cells. The van der Waals interactions between the hydrophobic region of the outer cell wall and the surface is involved in this adhesion process.[142-144] The irreversible attachment is also facilitated by the EPS production, which anchors cells to surfaces.[145]

From an overall physicochemical point of view, it is believed that bacterial adhesion and attachment are mediated by long-ranged nonspecific interactions such as van der Waals forces, electrostatic forces, acid-base interactions, and Brownian motion forces.[136, 146] Bacterial cells can be freely suspended in bulk fluids before adhering to surfaces while experiencing different environments.[135] The motile bacterial cells apart from the surface only experience the bulk fluid, whereas the cells at a near-surface liquid can experience hydrodynamic effects of the surface. Meanwhile, bacteria in a near-surface constrained region can feel both the hydrodynamic and physicochemical effects of the surface.[147] Therefore, as soon as bacterial cells reach a surface, they will be attracted or repelled depending on the net force of the different non-specific interactions described above.[148]

However, despite a large number of studies on the interaction of bacteria with surfaces, current understanding is still incomplete due to the wide variety of cells and materials with different properties. Therefore, interdisciplinary active collaboration between biologists, chemists, materials scientists, and engineers are required to identify the properties of surfaces that interact with microorganisms, understand the bacterial behavior on the surfaces, and establish generic protocols to develop and modify surface characteristics for inhibition of bacterial adhesion and growth.

4.1.3 Strategies to Inhibit Bacterial Adhesion

Bacteria can adhere to a wide variety of different materials including glass, aluminum, stainless steel, various organic polymers, and fluorinated materials such as Teflon.[149-150] Many studies have been devoted to understand the correlation between bacterial adhesion and surface properties as well as to develop functional surfaces inhibiting bacterial adhesion. [38, 135] Two basic strategies exist to reduce bacterial adhesion on the surface: chemical and physical approaches.

The commonly used chemical strategy is to apply surface coatings with anti-microbial agents such as silver, copper, or quaternary ammonium compounds.[38, 151] The coated surfaces slowly release anti-microbial materials, which kill adhered bacteria.[152] The bactericide-releasing coating approach is effective to reduce bacterial adhesion, but there are considerable drawbacks including the possibility of the emergence of drug resistant pathogens, toxicity to mammalian cells, de-lamination, and loss of antibacterial functionality when the coating agents are exhausted.[151, 153] Self-assembled monolayers (SAMs) of alkanethiolates on a gold surface demonstrated excellent inhibition of *E.coli*

bacterial adhesion, but the platforms also provided resistance to nonspecific adhesion including proteins, viral and mammalian cell adhesion.[137] Another coating approach is to use a polymer brush; poly ethylene glycol (PEG) is the representative example for this approach. The surface-grafted PEG chains exhibit relatively weak adhesive forces to bacteria compared to that on substrate surfaces and induce steric hindrance to bacteria, thereby impeding access to the surfaces, and preventing bacteria adhesion and colonization.[38, 154-157] Thermo-responsive polymers have also been utilized to release adhered bacteria.[38] Poly(N-isopropylacrylamide) (PNIPAM) is one of the most studied thermo-responsive polymers, which displays a lower critical solubility temperature (LCST) in water of 32 °C. At a temperature below the LCST, PNIPAM is water-soluble and has an extended coil conformation. Above the LCST, the polymer becomes water-insoluble and changes its conformation to a collapsed form. This phase transition behavior is triggered by temperature changes which enable release of adhered bacteria via reversible shrinking and swelling of PNIPAM coated on the surface upon heating and cooling.[158-159] However, grafting methods for polymer chains have significant limitations such as dependency of substrate chemical composition on surface grafting and susceptibility to thermal or hydrolytic degradation.[160]

Physical strategies are based on the design of surface structure, which has been inspired by natural species such as sharks and plant leaves that display antifouling and/or antibacterial effects. The most representative surface structure-induced artificial anti-bacterial surfaces include SharkletTM technology[161] and slippery liquid-infused porous surfaces.[162] Advances in nanometer-scale fabrication and characterization of diverse surfaces have allowed a number of intensive studies on the interactions between cells and substrates.

Recently, the effect of nanoscale topography of a surface on bacterial adhesion has been highlighted since mammalian cells have to compete with bacteria in many environments, but current knowledge in this area is still developing. Recent trends in the field of nano-structured surfaces for inhibiting bacterial adhesion are summarized in the next section.

4.1.4 Nano-Technologies to Inhibit Bacterial Adhesion, Attachment, and Growth

While nanotechnology is well established for many electronic, optoelectronic, and sensor applications, the development of biomedical applications of nano-structured surfaces is still in the early stages[163-164]; the advanced nanotechnology has been recently contributing to develop functional surfaces to decrease infection. Some recent studies have confirmed that nano-featured surface topographies can effectively prevent initial bacterial adhesion. The previous studies, where the focus is on demonstration that nano-textured surfaces can significantly reduce bacterial adhesion and growth while selectively promoting interactions with desired mammalian cells and presenting bio-compatibility, are described below. Soft lithography techniques such as nano-imprinting methods facilitate the creation of nano-topographies on polymers and metals. For example, nano-structured polydimethylsiloxane (PDMS), fabricated by an anodized titanium oxide (ATO) templating method, significantly inhibited the growth of bacterial cells (*S. aureus* and *E.coli*) but remained non-toxic to fibroblasts and endothelial cells without the use of antibiotics. Nano-textured poly(methyl methacrylate) (PMMA) films exhibited antibacterial characteristics due to low adhesion of bacteria on structured surfaces.[165] Wu et al. have also demonstrated that diverse types of Au nanostructures on a tungsten surface (i.e., nanopillars, nanorings, nanonugets), fabricated by a templated electrodeposition method, exhibited excellent antibacterial properties.[166]

Moraru reported that alumina surfaces with nanoscale topography can significantly reduce microbial adhesion and biofilm formation by creation of nano-porous anodized aluminum oxide (AAO) surfaces via a two-step anodization process in concentrated acid.[167] Surface-bacteria interaction forces were estimated using the extended Derjaguin Landau Verwey-Overbeek (XDLVO) theory. Results indicate that the reduction of bacterial adhesion of the nano-porous surface originates from synergetic repulsion due to electrostatic forces and effective surface free energy. Based on this calculation, the authors found that the most effective pore diameter for inhibiting bacterial adhesion on an alumina surface is 15 to 25 nm, which is in a good agreement with their experimental results.[168]

The net force between bacterial cell and a nano-featured surface is believed to be repulsive based on the XDLVO model, thereby reducing adhesion of diverse bacterial cells. There are additional mechanisms proposed to explain the antibacterial effect on nano-structured surfaces. For instance, the competition between cell membrane elasticity and the capillarity of the nano-protrusion features of the surface can enhance engulfment because of increased deformation and stress on cell membranes.[169]

This effect is further increased with longer and more pronounced surface nano-spikes, which rupture the cell membrane and penetrate into attached bacterial cell, ultimately resulting in bacterial death (bactericidal effect).[170] Liu and coworkers suggested that the nanoscale roughness on a surface could contribute to increased total protein adsorption due to the increased surface area, which may affect bacterial adhesion.[44]

4.1.5 Methods to Characterize Bacterial Adhesion on a Surface

In-vitro studies of the process, characteristics, and mechanism of bacterial adhesion to materials can offer insight into how to achieve basic preventive strategies and the development of functional surfaces. The *in-vitro* experimental methods for bacterial attachment study are summarized in the review paper written by Yuehuei and coworkers.[171] These methods include the selection of bacteria, sample surface preparation, conducting bacterial adhesion or biofilm formation experiments, and characterization methods to examine attached bacteria and biofilms. Many direct and indirect methods for counting attached bacteria on a surface have been also published.[172-175] Typical techniques employed include direct counting methods[173] such as imaging with transmitted light microscopy, epifluorescence microscopy, and scanning electron microscopy (SEM), as well as indirect methods[174-175] such as counting colony forming units, radiolabeling, spectrophotometry for stained bacteria, adenosine triphosphate (ATP) marker, and nucleic acid probes.

Below I briefly summarize the colony forming unit (CFU) counting method and SEM observations that we have mainly employed in this study (Figure 33). CFU plate counting is the most commonly used method for counting viable bacterial cells attached to a surface. There are the two basic approaches for the CFU counting method.[176] The first method is to mix a measured volume of the sample (1 ml) with the appropriate molten agar medium (10 ml) in a sterile petri dish. This is called the pour plate. Another method is the surface spread method. In this approach, serial 10-fold dilutions of the original sample are prepared. Then, 100 µl of the diluted solution in series are pipetted onto the surface of each of three replicated agar plates. The drop is spread over the entire surface using an inoculation loop or a flamed glass spreader. All plates are incubated at 37 °C for overnight in either the pour

plate method or surface spread method. Then, the colonies are counted and the bacterial density in the original solution is back-calculated from the dilution factors. Our studies used the surface spread CFU counting method after detaching adhered cells from the samples. Scanning electron microscopy (SEM) is one of the direct methods to monitor the morphology of adhered bacterial cells on a surface. It is a well-established basic method not only to observe the cells but also the morphology of the material surface, which allows establishment of relationships between cell behavior and the surface characteristics. Many studies have elucidated the anti-bacterial characteristics of the nano-textured surface through SEM observation.[164, 167-168]

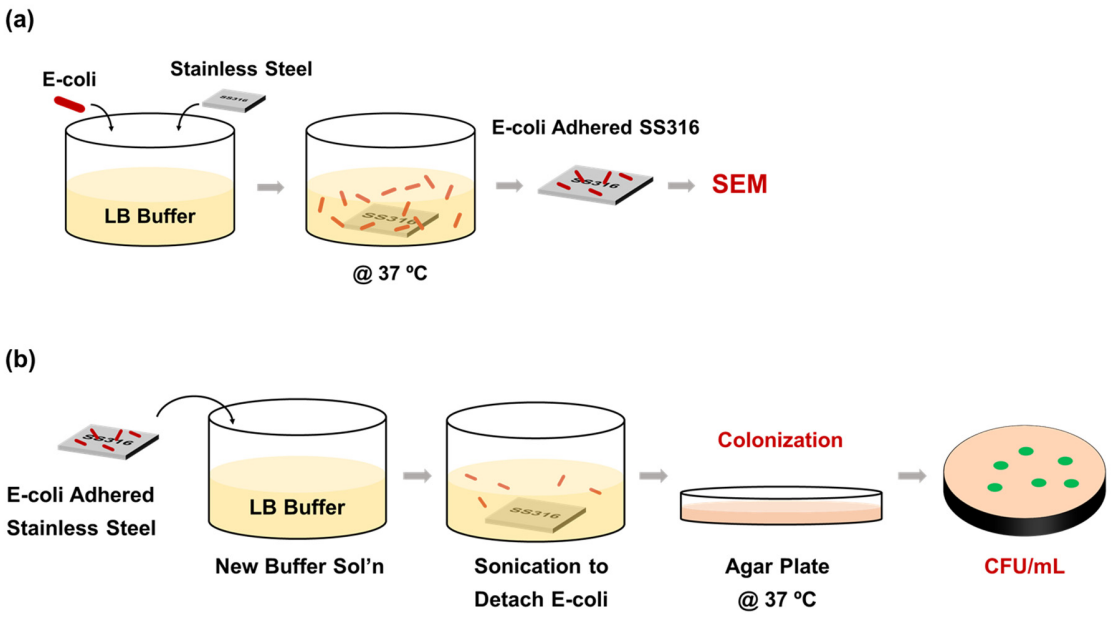

Figure 33. Analysis of bacterial adhesion on SS316L surface. (a) Observation of bacterial adhesion on SS316L surface via SEM, (b) Quantification of surface-adhered bacteria by counting colony forming unit.

4.1.6 Present work based on Nano-textured SS316L Surface

Motivated by the previous studies on development of functional surfaces to prevent bacterial adhesion, the aim of this work is to create nanostructures on a stainless steel 316L (SS316L) surface to address bacterial adhesion. SS316L is the most widely used type of stainless steel for orthopedic, cardiovascular, and craniofacial applications due to its biocompatibility, corrosion resistance, mechanical strength, and formability.[14, 177-178] Recently, it was reported that the nano-featured SS316L created through severe shot peening presented a remarkable decrease in the adhesion and growth of Gram-positive bacteria (*S. aureus* and *S. epidermidis*) while maintaining osteoblast adhesion and proliferation.[14] However, the severe shot peeing on stainless steels may destruct passive layers, and thereby weaken corrosion resistance of the stainless steels. Considering the extensive use of stainless steel 316L in biomedical devices and implants, it is of a great relevance to attain anti-bacterial functionality while ensuring excellent corrosion resistance at the same time. In the previous chapter, we demonstrated the superior corrosion resistance of electrochemically etched stainless steel 316L.

With this in mind, the present *in vitro* study reports the effect of nanostructured stainless steel 316L surfaces, fabricated by electrochemical etching, on the adhesion of a model microbial organism and mammalian cell. The as-received (AR-), nano-textured (NT-), and electro-polished (EP-) SS316L samples were prepared and surface morphology characterized by SEM and atomic force microscopy (AFM); chemical compositions were determined by XPS. Gram-negative bacteria show more resistance to antibodies or antibiotics because of the impenetrable cell membrane as compared with Gram-positive bacterial cells. Furthermore, most of the pathogenic bacteria including *Acinetobacter*,

Pseudomonas, *E. coli* belong to Gram-negative group. Therefore, *E. coli* has been used as a model Gram-negative bacterium in the present study, which is also well-known as the predominant pathogens responsible for foreign body infections. Antibacterial properties of the NT-SS316L surface have been identified by counting CFU of the adhered *Escherichia coli* (*E. Coli*) and monitoring the bacterial adhesion behavior by SEM. To confirm cytotoxicity to the mammalian cells, we investigated adhesion and growth of fibroblast cells (NIH-3T3) on SS316L surfaces. Fibroblasts are connective tissue cells that play a crucial role in wound healing and one of the most common cells used in *in vitro* biomaterial testing.

4.2 Experimental

4.2.1 Materials

Nitric acid (ACS reagent, 70%) and SS316L plates (30 × 20 × 0.05 cm^3) were purchased from Sigma Aldrich and Maudlin Products, respectively. Insulating tape (Electroplating tape 470) was purchased from 3M. Organic solvents, acetone (99.5%), methanol (99.8%), and isopropanol (99.5%), were purchased from VWR International.

4.2.2 Sample Preparation

Two different sizes (2.5 × 1.5 × 0.05 cm^3 and 2.5 × 2.5 × 0.05 cm^3) of SS316L samples were prepared by using a water jet cutter. These two samples served as working and counter electrodes, respectively. Prior to electrochemical surface modification, the samples were rinsed with acetone, methanol, and isopropanol to remove organic contaminants, and subsequently air-dried at ambient temperature. Electrical connections of SS wire onto the SS316L samples were established by spot welding. The working electrode was masked with insulating tape leaving an active area of 0.19 cm^2 for electrochemical surface modification. Diluted nitric acid solution (48% by weight) was used as the electrolyte. A three electrode system was used with a saturated calomel electrode (SCE) serving as the reference electrode. The separation distance between working and counter electrodes was maintained at 3 cm, and reference electrode was placed near the working electrode. A potentiostat (Gamry Reference 600) was used to perform electrochemical surface modification. After initial delays of 60 s under open circuit conditions, potentiostatic polarizations were conducted at anodic potentials of 2.2 V (vs. SCE) for 60 s and 2.6 V (vs. SCE) for 240 s at room temperature (Figure 34), which generated NT- and EP- SS316L

surfaces, respectively. After potentiostatic electrochemical surface modification, the SS316L samples were removed from the electrochemical cell, washed with deionized water, and dried at room temperature for one day prior to further characterization and bacterial adhesion tests.

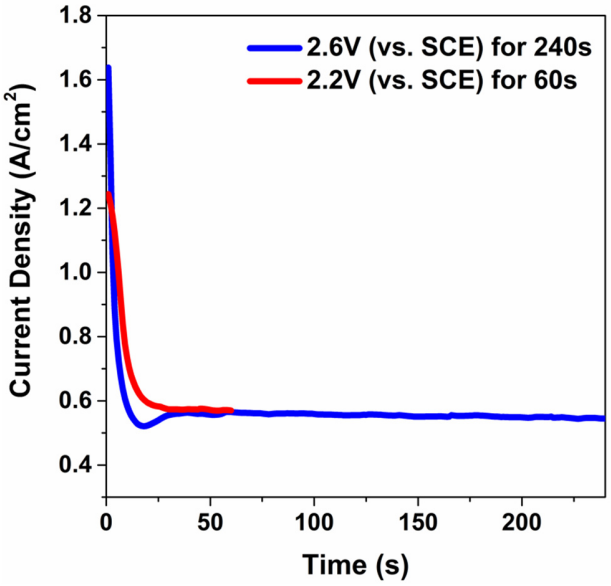

Figure 34. Electrochemical surface modification on SS316L samples. Potentiostatic polarization at anodic potentials of 2.2 V (vs. SCE) and 2.6 V (vs. SCE).

4.2.3 SS316L Surface Characterization

Surface morphologies of SS316L samples were characterized by SEM (Hitach SEM SU8010, Japan) at 3kV acceleration potential, and topographical information was acquired by AFM (Veeco Dimension 3100). Chemical compositions of SS316L surfaces were analyzed by XPS (Thermo Fisher Scientific K-Alpha XPS) with a 400 μm micro focused monochormatic Al Kα X-ray source.

4.2.4 Bacterial Cultures and Assays

E. coli was used in this study as a model microorganism for bacterial adhesion assays. All sterile SS316 samples were transferred into 6-well cell culture plates, treated at the prepared bacterial solutions with a constant bacterial concentration (at optical density (O.D.) ≈ 0.3) in lysogency broth (LB) media (10 g of trypton, 5 g of yeast extract and 10 g of NaCl in 1 L of deionized water) and cultured for either 12 or 24 h in an incubator (37 °C, humidified, 5% CO_2). For those samples, the medium was exchanged with 5 ml of sterilie fresh LB media every 12 hrs. Subsequently, sample were rinsed three times with phosphate-buffered saline (PBS) and transferred into a 50 ml tube with 10 ml of PBS. Following this, each sample was sonicated for 7 min and voltexed for 20 s to release bacteria remainingon the sample surface into the solution. A series of diluted solutions of bacteria in PBS were then spread onto LB agar plates (either 1 mL/agar or 0.1 mL/agar). Bacteria colonies were counted after 24 hr of incubation at 37 °C. All experiments were performed in triplicate with three samples; mean values were calculated.

4.2.5 Fibroblast Cell Cultures and Assays

Mouse fibroblast, NIH-3T3 (ATCC), was cultured in Dulbecco's Modified Eagle Medium (DMEM, ATCC) supplemented with 10 % fetal bovine serum (FBS, Sigma-Aldrich) and 1 % penicillin/streptomysin (P/S, Gibco). The cleaned and sterilized SS316L samples were placed individually into the wells of a 6-well plate. The cells were seeded onto the samples at a density of 100,000 cells/ml per substrate and were placed in an incubator fro 24 hr at 37 °C with humidified 5% CO_2 atmosphere. After 24 hr of incubation, the samples were washed three-times with PBS. Cell metabolic activity was determined using a quantitative

colorimetric conversion assay of 3-[4,5-dimethylthiazol-2-yl]-2, 5-diphenyl tetrazolium bromide (MTT) after exposure for 24 hr. Cells were incubated with MTT solution for 3 hr and washed with PBS. The formazan product was solubilized in dimethyl sulphoxide (DMSO) (Figure 35). After reaction solutions were plated and their optical density at 570 nm and 630 nm determined with a microplate-reader (Bio-TEK Instruments, INC). Cell-free medium was included as a control.

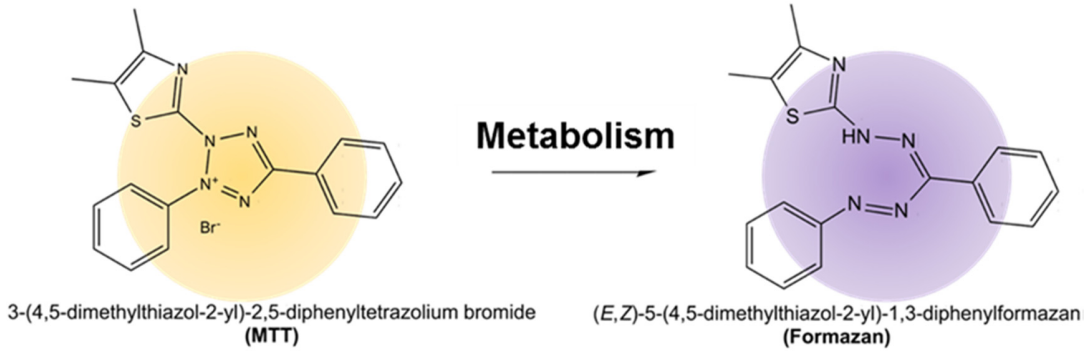

Figure 35. MTT reduction in live cells by mitochondrial reductase

The morphology of viable NIH-3T3 cells adhered on the NT-SS316L surface was investigated by SEM after 24 h of incubation. After PBS washing the samples were fixed with 4 % of paraformaldehyde for 4 h at 4 °C, and then treated with a series of ethanol concentrations in deionized water (i.e. 50, 70, 90, and 100 %) for sample dehydration. Finally, the SEM samples were treated with a chemical drying agent, hexamethyldisilizane (HMDS), in a series of concentrations with ethanol (30, 60, and 100% for 20 min, respectively) and fully dried in a fume hood overnight.

4.3 Results and Discussion

4.3.1 Surface Structure of Electrochemically Modified SS316L Surfaces

The morphology of AR-, NT-, and EP-SS316L surfaces were characterized by SEM and AFM. The AR-SS316L represents a commercially available SS316L substrate that serves as a standard control, while EP-SS316L served as an additional control surface since it displays a relatively flat and defect-free surface. This study focuses on the NT-SS316L sample to probe the effect of nano-roughness on bacterial adhesion for comparison to the two control samples. To compare and analyze the surface structures of the three different SS316L samples, three-dimensional topography profiles and top surface morphologies were obtained by AFM and SEM, respectively (Figure 36).

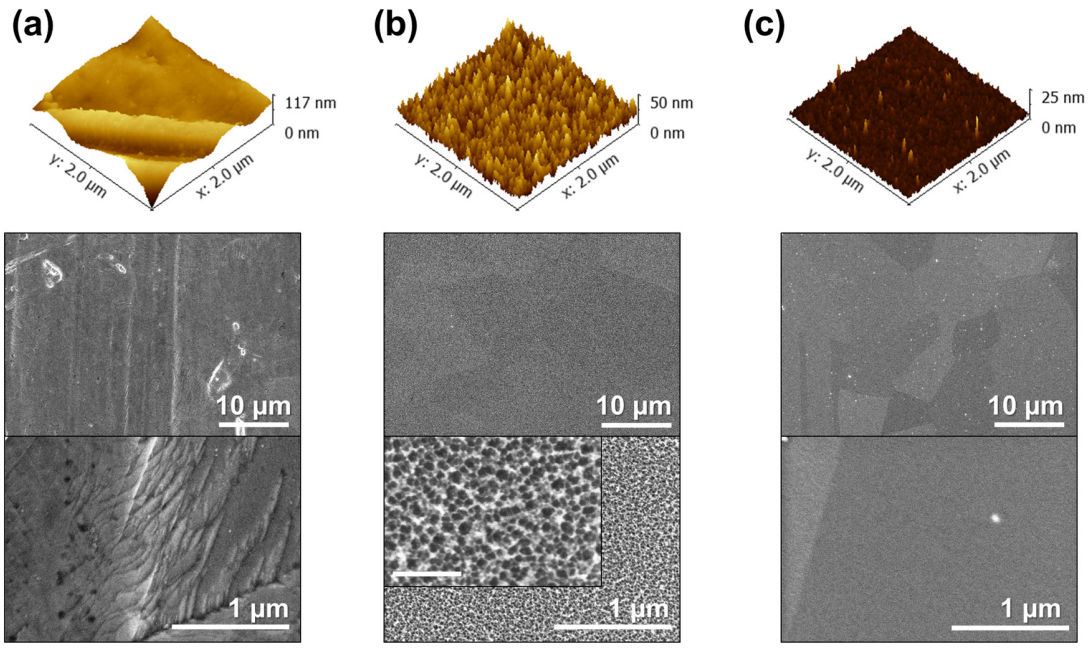

Figure 36. Three dimensional AFM topography profiles (top) and SEM images of (a) AR-SS316L, (b) NT-SS316L, and (c) EP-SS316L surfaces. The scale bar of the inset SEM image is 200 nm.

NT- and EP-SS316L surfaces were obtained by electrochemical etching at applied potentials of 2.2 V (vs. SCE) and 2.6 V (vs. SCE), respectively. The AR-SS316L surface displays typical defects and micrometer-scale surface features, characteristic of formation during the manufacturing process. In contrast, EP-SS316L presents a relatively flat surface with a root mean square (RMS) roughness ~1.2 nm. The NT-SS316L surface exhibits nanometer-scale pores and protrusions. The dimensions of surface nanostructures are significant with respect to inducing a repulsive force to bacteria on the surface; it has been demonstrated that pore sizes around 20 nm can effectively repel bacteria by inhibiting adhesion to the surface.[167-168] The NT-SS316L surface etched at 2.2 V (vs. SCE) displays pore sizes of around 20 ~ 25 nm, which is believed to be effective for inhibiting bacterial adhesion. Along with the desired pore sizes, the NT-SS316L surface possesses sharp nano-protrusions as confirmed by AFM, which can induce mechanical stress to bacterial cell membranes, thereby deterring bacterial adhesion. Therefore, with the beneficial combination of desired pore size and surface nano-spikes, the NT-SS316L sample is expected to display antibacterial performance; results will be discussed in section 4.3.3.

4.3.2 Surface Chemistry of the Electrochemically Modified SS316L

In terms of applicability of SS316L in the biomedical arena, corrosion resistance is an essential characteristic which is largely affected by the chemical composition of SS316L passive films. Figure 37 displays XPS spectra of AR-, NT-, and EP-SS316L samples. In survey spectra of the SS316L samples, peaks designating Fe, Cr, O, and C are clearly visible (Figure 37a). Fe and Cr are primary elements of the SS316L, and increases in Cr content on NT- and EP-SS316L surfaces are evident. O content can be mainly ascribed to oxide and hydroxide films on the SS316L surfaces. Considering the low C content

(<0.03%) in SS316L, the C detected at SS316L surfaces can be attributed to adventitious carbon from air exposure during handling and storage. High-resolution XPS spectra of Cr2p confirm the increases in Cr content on both NT- and EP-SS316L surfaces compared to AR-SS316L (Figure 37b). Furthermore, Mo content increases while Mn content decreases slightly on SS316L surfaces after electrochemical surface modification (Figure 37c, d). In contrast, no detectable changes were observed in Fe content (Figure 37e). O1s XPS spectra indicate that the electrochemically surface modified SS316L samples have more oxide than hydroxide content (Figure 37f). Chromium oxide (Cr_2O_3) is the primary cause of corrosion resistance of stainless steels, and Mo content at the surface stabilize the chromium oxide passive layer.[59, 110] Mn components can be act as corrosion initiation sites.[20] Therefore, the results demonstrate that changes in surface chemistry upon the electrochemical surface modifications are beneficial for corrosion resistance.

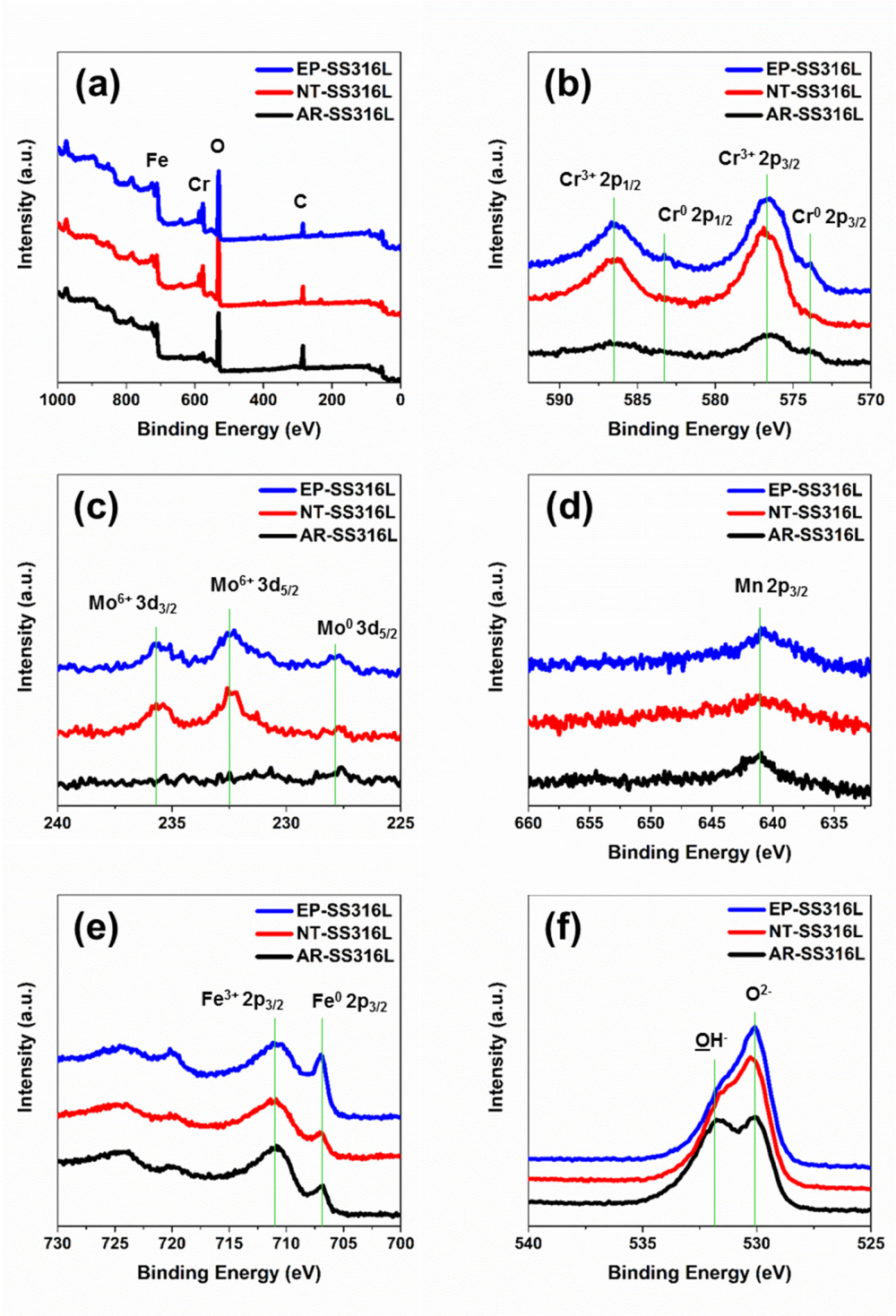

Figure 37. XPS spectra of AR-, NT-, and EP-SS316L surfaces. (a) Survey spectra, (b) Cr2p scans, (c) Mos3d scans, (d) Mn2p scans, (e) Fe2p scans, (f) O1s scans.

4.3.3 Bacterial Adhesion on SS316L Surfaces

E. coli is one of the most extensively used model microorganisms for the study of surface colonization; for this reason, it was employed in this study. The adhesion and growth of *E.coli* by CFU counting and SEM were monitored in order to assess the efficiency of NT-SS316L surfaces to reduce bacterial adhesion relative to AR- and EP-SS316L surfaces (Figure 38). Bacterial adhesion on the three SS316L surfaces was evaluated through bacterial cultures at times up to 48 hrs. To quantify the number of *E.coli* adhered to each SS316L surface, the CFU of the adhered cells was counted using the spread plate method after resuspension of the cells into fresh media and plating them under static conditions (in LB agar gel at 37 °C for 24h, see the details in the Experimental). The CFU obtained from each SS316L sample indicates the number of adhered and live *E.coli* cells on that surface. Initially adhered live *E.coli* cells on the three different SS316L surfaces were compared after 12 h of bacterial culture (Figure 38a). The initial adhesion of *E.coli* on the NT-SS316L surface was markedly smaller compared to the AR- and EP-SS316L surfaces. After 24 h and 48h of *E.coli* cultures, the NT-SS316L surface maintained the low level of E.coli adhesion, whereas a significant increase in *E.coli* adhesion was observed on the AR-SS316L surface (Figure 38). SEM images of the SS316L samples after 24 h culture of *E.coli* (Figure 38b-d) were obtained for comparison with the CFU results. Again, the relatively small amount of *E.coli* adhered to the NT-SS316L was clearly distinguishable from AR- and EP-SS316L surfaces, which is in good agreement with CFU counting results. Clearly, the NT-SS316L surface successfully inhibits bacterial adhesion and growth on the NT-SS316L surface relative to the AR- and EP-SS316L surfaces.

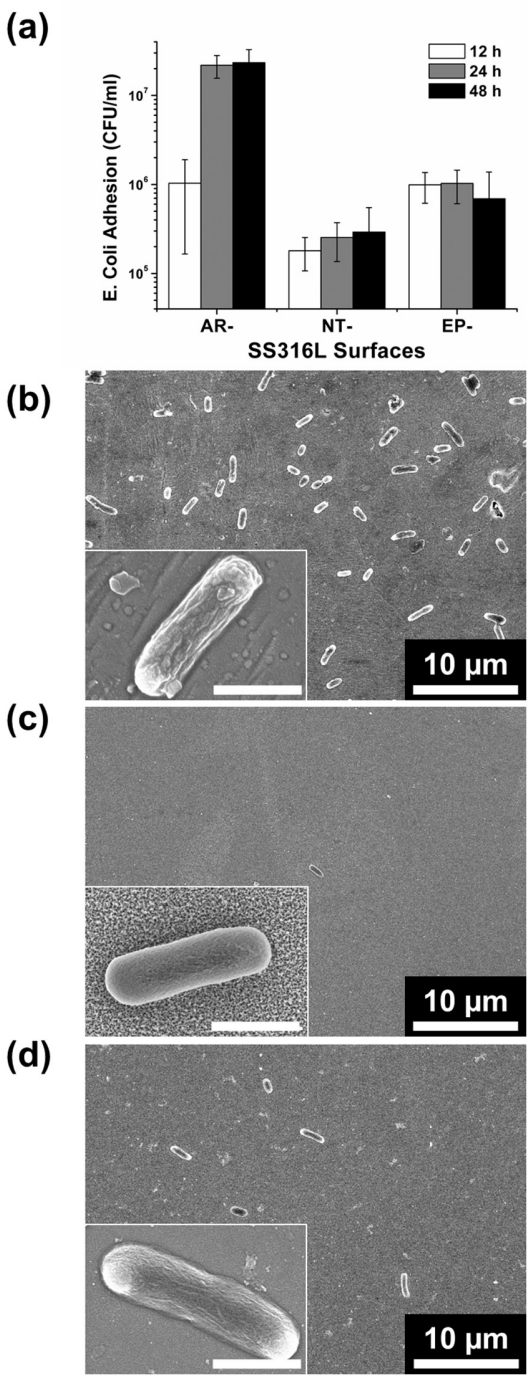

Figure 38. Bacterial adhesion on SS316L surfaces. (a) Number of adhered *E.coli* cells on AR-, NT-, and EP-SS316L surfaces following 12 h, 24 h, and 48 h of incubation (data represent mean ± standard deviation, N=3), characterized by colony forming unit (CFU) per ml. The morphology of the *E.coli* adhered on (b) AR-, (c) NT-, and (c) EP-SS316L surfaces after 24 h cultivation. The scale bars of the inset images are 1 µm.

4.3.4 Cell Adhesion and Metabolic activity on the NT-SS316L Surface

The adhesion and proliferation of mammalian cells on anNT-SS316L surface are essential to evaluate the potential of this material for implant applications. In order to evaluate the cyto-compatibility of NT-SS316L surfaces, we monitored the morphology of fibroblast cells (NIH-3T3) attached onto NT-SS316 by SEM and conducted MTT assays for evaluation of the metabolic activity of NIH-3T3 cells. As shown in Figure 39a, the SEM images revealed that NIH-3T3 fibroblasts spread and elongated actively on the NT-SS316L surface with spindle-like and star-type shapes, which indicates the mammalian cells can attach well to the NT-SS316L surface. Furthermore, there was no difference in the fibroblast adhesion on NT-SS316L from that on the AR-SS316L surface, which is a commercially available material for human implants (Figure 39b). In addition, the metabolic activity of NIH-3T3 cells confirmed by MTT assay was not altered by the surface characteristics of SS316L samples (Figure 39c). All SS316L samples show excellent biocompatibility and active metabolism similar to what is observed in the PS culture dish. These results imply that the NT-SS316L materials developed in this study are very promising candidates for biomedical applications, since they offer biosafety to the mammalian cells but effectively and efficiently inhibit the adhesion and growth of bacterial cells.

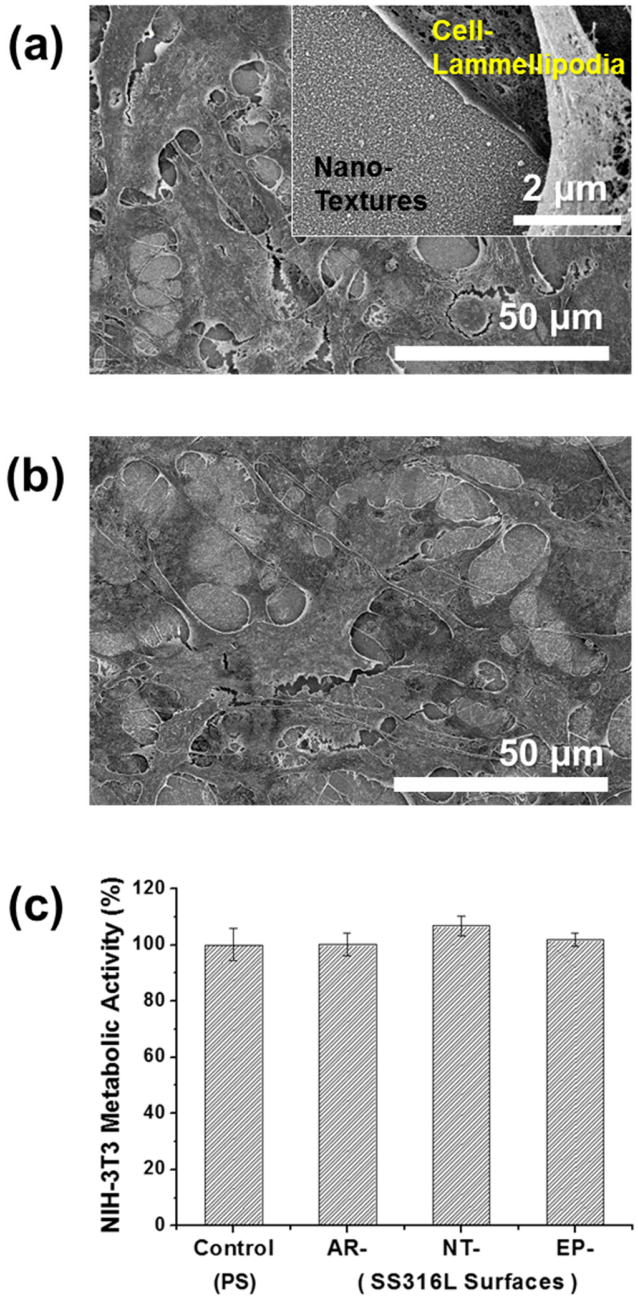

Figure 39. SEM images of NIH-3T3 cells cultured on (a) NT-SS316L and (b) AR-SS316L for 24 h. The inset image represents the active interaction with cells and the nano-textured surface. (c) Metabolic activity of NIH-3T3 fibroblast cells cultured on three different SS316L surfaces compared to the control on the PS culture dish.

4.4 Conclusions

Bacterial adhesion to metallic surfaces can cause serious patient implant infections along with substantial increases in healthcare costs. In this study, we demonstrated that nano-textured SS316L surfaces can successfully inhibit bacterial adhesion but do not exhibit toxicity to mammalian cells. Electrochemical etching has been used to create nanometer-scale surface roughness on stainless steel 316L (SS316L), which is the alloy typically used in medical devices and orthopedic implants. The initial adhesion and growth of a Gram-negative model microorganism, *Escherichia coli* (*E. coli*), on the as-received, nano-textured, and polished SS316 surfaces were investigated by counting CFU and SEM imaging for up to 48 hrs of bacteria cultivation. A significant reduction of adhered *E. coli* cells was observed on the nano-textured surface, whereas there is no difference in fibroblast (NIH-3T3) adhesion and metabolic activity between samples. In addition, the nano-textured SS316L presented a Cr- and Mo-rich surface as compared with as-received SS316L, which implies an improvement of corrosion resistance. The nano-textured SS316L developed in this study does not require antibiotic or chemical modifications for *E. coli* adhesion inhibition. Therefore, this nano-structured offers significant potential for medical applications, since it offers increased corrosion-resistance, nanotopography-induced inhibition of bacterial adhesion, and biocompatibility.

CHAPTER 5.

MODIFICATION OF ANOTHER METALLIC SURFACE: HYDROPHOBIC/SUPER-HYDROPHOBIC PATTERNING OF COPPER SURFACES

5.1 Introduction

Natural species often evolve exterior structures that are designed for living in certain environments. For example, the Namib Desert beetle has a hydrophilic/hydrophobic pattern that efficiently collects water by mist condensation in dry desert environments.[179] Inspired by nature, many researches have been focused on developing a patterned surface with a high wetting contrast against background which has variety of potential applications including droplet manipulation for diagnostics, microfluidic platforms, and water harvesting devices. The wettability contrast pattern can be achieved by local control of surface structure, chemistry, or both. Various methods including lithography,[180] laser irradiation,[181] plasma treatments,[182-183] inkjet printing[184] have been employed.

Copper is a widely using engineering material because of its abundance, and desired engineering properties such as ductility and high thermal/electrical conductivity.[185] Significant efforts have been devoted to modify the surface structure and chemistry of copper to create super-hydrophobic copper surfaces. The surface roughness on copper surface can be achieved by various methods including etching,[186-187] electrodeposition,[188-189], thermal oxidation,[190-191] and solution immersion.[192-197] Further modifications in surface chemistry with low surface energy materials such as Teflon,[195] alkylfluorosilane,[192-193] and

alkanoic acid[196-197] lead to the super-hydrophobic copper surfaces. Taking advantage of maturity of super-hydrophobic copper surface, we present a simple method to create hydrophobic pattern on the super-hydrophobic copper surface by using a pen. A permanent marker pen is a convenient implement used to apply ink to a surface for writing or drawing. Once the marker drawn ink is dried on the surface, it is normally waterproof and cannot be erased by water, and thereby can serve as a temporal masking layer to protect underlying surface from reactions. However, concentrated acids are commonly used in etching and electrodeposition to acquire surface roughness,[187, 198] which might damage the drawn ink patterns. Also, the ink patterns can be decomposed during the thermal oxidation process due to the high operating temperature (> 500 °C).[190-191] We utilized a relatively mild technique, immersion in an aqueous solution, to grow nanowires outside the patterned area selectively, while maintaining the stability of drawn ink patterns. After the selective nanowire growth, the ink patterns can be removed by soaking into acetone, and subsequent deposition of fluorocarbon film on the surface resulted in hydrophobic/super-hydrophobic patterned copper surface. Based on the development of the novel patterning method, we designed hydrophobic patterns (dot, line, and curves) on super-hydrophobic copper surface to demonstrate droplet transfer, merging, guiding, and storage.

5.2 Experimental

5.2.1 Materials

Copper foil (0.127mm thick, 99.9%), glacial acetic acid (ACS reagent 99.7%), sodium bicarbonate (ACS reagent 99.7%), acetone (99.5%), and ammonium persulfate (ACS reagent 98%) were purchased from VWR International. Marker pens (Sharpie ultrafine point permanent marker; black) were purchased from Office Depot.

5.2.2 Sample Preparation

Figure 40 shows schematic illustration of fabricating super-hydrophobic copper surface. Prior to the process, copper foil was cleaned in acetone and glacial acetic acid at room temperature to remove organic contaminants and native copper oxide, respectively.[199] After drying with nitrogen, a pattern was drawn on the pre-cleaned copper surface by using a marker. Then, the copper sample with a pattern on it was immersed in the aqueous solution (0.1 M sodium bicarbonate and 0.02 M ammonium persulfate) for 24 hr to grow nanowires.[200] During this process, the pattern served as a masking layer to prevent contact of the underlying copper surface to the reagent solution, thereby selectively growing nanowires outside on the exposed Cu surface. After the nanowire growth, the copper sample was withdrawn from the solution and rinsed with DI-water and dried with nitrogen gas. Then, the ink pattern on the copper sample removed using acetone, then air-dried at ambient temperature. Finally, copper sample was placed in a parallel plate rf (13.56MHz) vacuum plasma reactor, with 6 inch diameter circular stainless steel electrodes, with a distance between the electrodes of 1 inch,[89] and a thin layer of fluorocarbon was deposited onto the surface to achieve a hydrophobic/super-hydrophobic wettability pattern.

Fluorocarbon film deposition was performed at 110 °C, 120 W, and 1 torr pressure using a mixture of pentafluoroethane (Praxair) and Argon at 20 SCCM and 75 SCCM, respectively. Deposition times of 5 s resulted in highly cross-linked fluorocarbon layers covalently bonded to the nanowire grown copper surface with thicknesses of 23 (±1) nm.

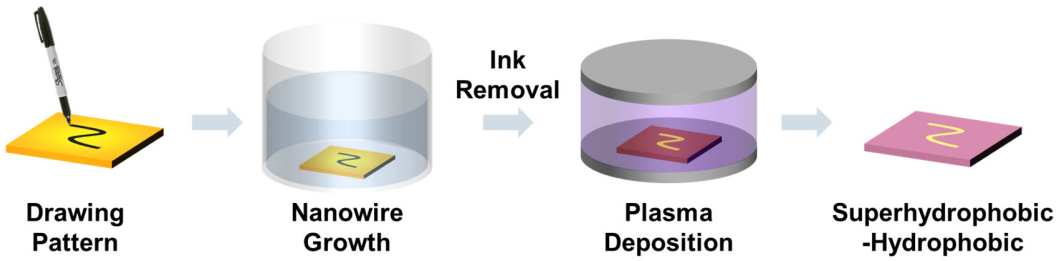

Figure 40. Schematic illustration of the process for fabrication of a hydrophobic pattern on a super-hydrophobic copper surface.

5.2.3 Characterization

The surface morphology of copper samples was characterized by scanning electron microscopy (Hitachi SEM SU8010, Japan) at 3 kV acceleration potential. A goniometer (Ramé-Hart 290) was used to measure contact angles. Static contact angles were obtained by dispensing 4 µL of DI-water onto sample surfaces; images were captured with a CCD camera and analyzed with Ramé-Hart software. The ellipsometer (M-2000 ellipsometer, J. A. Woollam Co. Inc.) was used to measure the thickness of plasma-deposited fluorocarbon films on Si wafers that were placed next to the copper samples using ellipsometry.

5.3 Results and Discussion

5.3.1 Hydrophobic/super-hydrophobic Patterned Copper Surface

Figure 41 displays an example of hydrophobic/super-hydrophobic binary wettability patterned copper surface. A variety of patterns can be easily designed on the copper surface from altering the sizes of dots, lines, and letters. Patterned region shows a relatively flat surface, and roughness features were created during the manufacturing process of the copper foil. Background regions displayed hierarchical structure composed of microscale granular structures and nanowires. Static water contact angles on the patterned and background surfaces were 110.9 ° ± 2.2 and 161.7 ° ± 2.2 with 4 μL DI-water droplets, respectively, demonstrating a successful fabrication of hydrophobic and super-hydrophobic wettability on a copper surface.

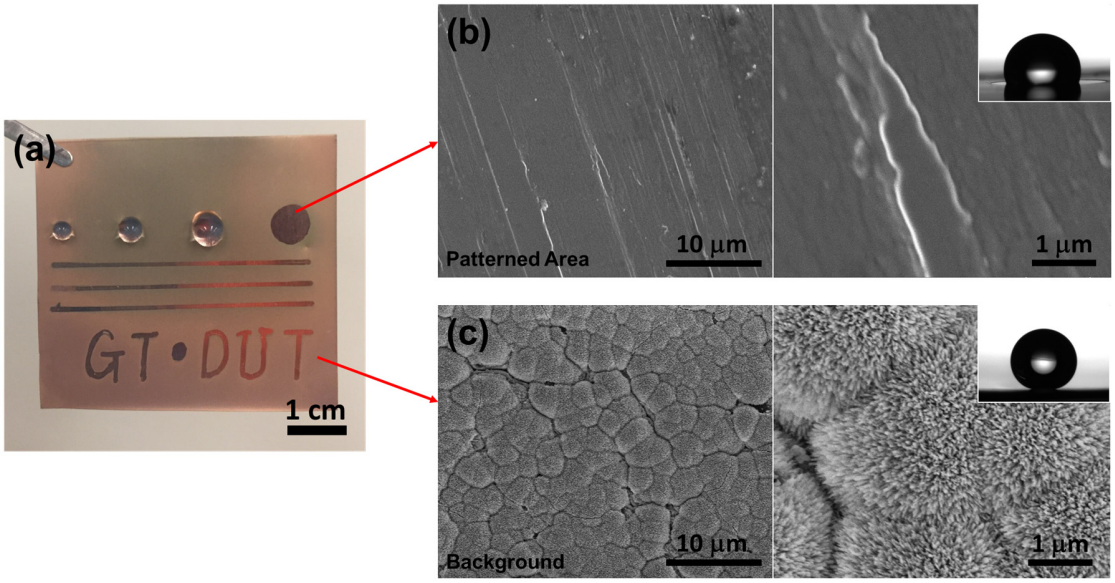

Figure 41. Diverse patterns on copper surface. (a) An optical image of wettability patterned copper surface, (b) Low and high magnification SEM images of hydrophobic patterned area, (c) Low and high magnification SEM images of super-

hydrophobic background area. Insets represent 4 μL DI-water droplet placed on each surface.

5.3.2 Droplet Manipulation

Figure 42 shows a demonstration of droplet transfer by using the dot patterned copper samples. Different sizes of dot patterned copper surfaces have different adhesive forces to water droplets.[184] Initially, 4 μL of water droplet was placed on a super-hydrophobic copper surface without a pattern. A dot patterned copper surface was inverted and aligned to a configuration that water droplet is in contact to dot pattern area (Dot 1). Then, this droplet can be picked up by lifting the patterned copper substrate. Finally, this droplet can be transferred to a larger dot patterned copper surface (Dot 2).

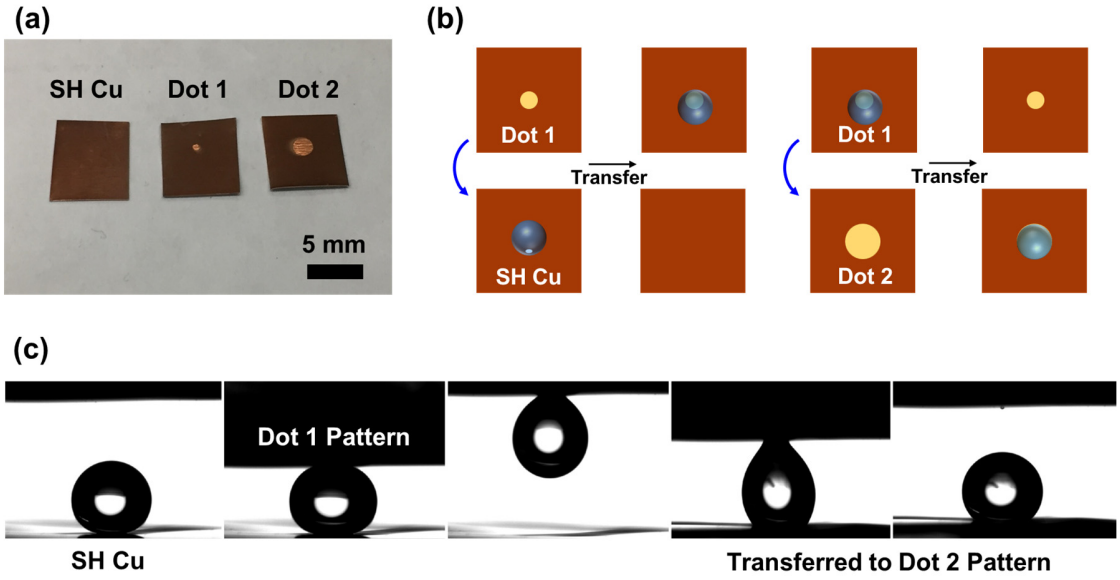

Figure 42. Dot pattern on copper surface. (a) An optical image of super-hydrophobic and dot patterned copper surfaces, (b) Scheme of droplet transport, (c) A series of snapshots of droplet transfers.

In addition, lines and curves can be imparted on copper surfaces, which can be used as the means to guide and merge droplets (Figure 43). These results demonstrate a proof of concept for this simple patterning technique. Further studies are needed to determine the applicability of this approach to the development of bioassay platforms and diagnostic devices.

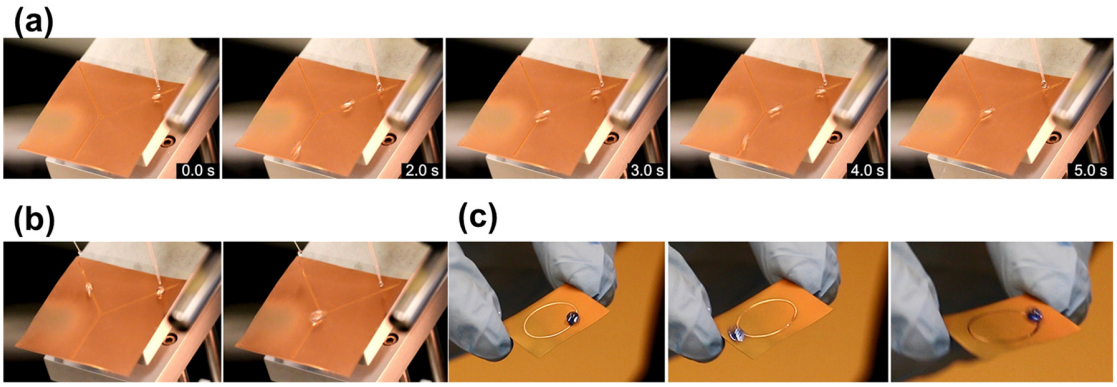

Figure 43. Line and curve patterns on copper surfaces. (a) Droplet guiding, (b) Droplet merging, (c) Droplet guiding and storage.

5.4 Conclusions

In conclusion, a simple method to fabricate a hydrophobic/super-hydrophobic pattern on copper surface was developed for droplet manipulation. A commercial marker was utilized to draw a desired pattern directly on a copper surface, which was served as a masking layer protecting underlying copper surface. The pattern drawn copper surface was immersed in an aqueous solution, and nanowire was selectively grown on outside patterned area, which was confirmed by SEM. Subsequent removal of ink pattern revealed shiny copper surface. Finally, thin film of fluorocarbon was plasma deposited onto the copper surface, which resulted in hydrophobic patterned surface and super-hydrophobic background surface with static contact angles of 110.9 ° ± 2.2 / 161.7 ° ± 2.2 with 4 μL DI-water droplets, respectively. Based upon the novel patterning technique, droplet manipulations were demonstrated on the wettability patterned copper surfaces. Hydrophobic dot patterns with different sizes imparted on super-hydrophobic copper surfaces were utilized as droplet transporting devices by picking up and releasing water droplets through different adhesion forces of different sizes of dots to the droplets. In addition, line and curve patterns were fabricated to guide, merge, and store water droplets. This facile method can be applied to the development of bioassay platforms and diagnostic devices.

CHAPTER 6. CONCLUSIONS AND FUTURE WORK

6.1 Primary Findings and Conclusions

Surface modification of SS316L from micro to nanoscale structures has been demonstrated by using electrochemical etching. Variation in the applied anodic potential during electrochemical etching alters the etch selectivity between grains and grain boundaries, thereby producing various surface structures. With low anodic potential (1.2 – 1.3 V vs. SCE), highly selective grain boundary etching occurs, which results in the evolution of intrinsic grain structures. As the applied anodic potential increases (1.4 – 1.5 V vs. SCE), grain boundary etch selectivity decreases. Further increase in the applied potential (1.8 V vs. SCE) yields a surface with only nanoscale sponge-like topography on the SS316L surface. Finally, the application of anodic potential of 2.4 V vs. SCE generates a smooth electro-polished surface. This unique relationship between applied anodic potential and surface topography allows control of water wettability on SS316L surfaces.

Achievement of hydrophobic and especially super-hydrophobic stainless steel surfaces is of great practical relevance for many applications. For instance, super-hydrophobic stainless steel pipes can transport fluids more efficiently through hydrodynamic drag reduction, and more effective drainage and cleaning of storage tanks are possible with super-hydrophobic stainless steel surfaces. A hierarchical structure that combines nanoscale and microscale surface structures plays a pivotal role in creating super-hydrophobic surfaces. Based upon the established applied potential–topography relationship, hierarchical intrinsic grain structures with both nanoscale and microscale features have been designed using a two-step electrochemical etching process. Deposition

of a fluorocarbon film onto the hierarchically structured SS316L surface results in a super-hydrophobic surface with a static water contact angle of 163.9 ° ± 1.2 and a roll-off angle of 10.7 ° ± 2.9 with 4 μL water droplets.

Corrosion resistance is a primary advantage of stainless steels, which is the basis for their extensive use. In particular, stainless steel applications in the maritime industry require superior corrosion resistance because seawater that contains 0.6 M sodium chloride and maritime bio-organisms triggers the breakdown of passive films and initiates localized corrosion which compromises mechanical stability. The corrosion resistance of electrochemically surface modified SS316L in 0.6 M sodium chloride solution has been investigated. Electrochemical etching in a nitric acid solution at an anodic potential of 1.3 V vs. SCE results in a selectively grain boundary etched SS316L surface. This modified material displays superior localized corrosion resistance in 0.6 M sodium chloride solution with a narrow distribution of high breakdown potentials (0.96 to 1.05 V vs. SCE) compared to those (0.32 to 0.86 V vs. SCE) of as-received SS316L. This enhancement can be ascribed to the formation of a superior passive film with Cr and Mo enrichment during the electrochemical etching process. In addition, the grain boundary etched SS316L surface exhibits hydrophobicity and microscale topography, which offers the potential to inhibit adhesion of and fouling by marine organisms, thereby further preventing occurrence of localized corrosion on the surface-modified SS316L.

Since SS316L has enhanced corrosion resistance and thus is commonly used as a material for implants and biomedical devices. Pathogenic bacterial adhesion to implants and biomedical devices causes serious infectious diseases. As a result, surface modifiedSS316L was investigated to assess the inhibition of bacterial adhesion. Electrochemical etching at

an anodic potential of 2.2 V vs. SCE was performed on SS316L to create nanoscale surface roughness. Subsequently, *E. coli* was cultured on SS316L surfaces. Significant reduction in *E.coli* adhesion occurs on nano-textured SS316L compared to an as-received SS316L surface, as confirmed by CFU counting and SEM imaging. The nano-topography induces a repulsive force on *E.coli* and nanostructure spikes can penetrate and/or generate stress at the cell membrane, thereby making *E.coli* adhesion on the nano-textured SS316L surface unfavorable. In addition, adhesion and metabolic activity of fibroblasts (NIH-3T3) were tested, and no inhibition of fibroblast proliferation and growth are observed with modified compared to as-received SS316L samples. Therefore, the nano-textured SS316L surfaces developed in this study can effectively reduce bacterial adhesion without antibiotic coatings and chemical modification, while maintaining biocompatibility with desired cells.

A patterned surface with a wetting contrast against background has diverse potential applications such as diagnostics, microfluidic platforms, and water harvesting devices. A simple method to fabricate a hydrophobic/super-hydrophobic pattern on copper surface by using a commercially available marker pen was devised. Directly drawn ink pattern was served as a masking layer against aqueous solution, thereby growing nanowire selectively on background region, and subsequent fluorocarbon film deposition completed hydrophobic/super-hydrophobic patterned copper surface. Various patterns can be generated including dots, lines, curves, and letters. Adhesive forces between surface and water droplets can be controlled by size and shape of patterns. Different sizes of dot patterned copper surfaces were designed to be utilized as droplet transporting devices. In addition, line and curve patterns were also fabricated to guide, merge, and store water droplets.

6.2 Future work and Recommendations

6.2.1 Oil repellent stainless steel surfaces

Substantial advances in the design of water repellent SS surfaces have been achieved in this work. However, as shown in Figure 44, SS316L surfaces with structures generated by electrochemical etching do not show oil repellency. The different wetting behavior of water and oils originates from differences in the liquid surface tensions. The surface tension of oils (γ_{LV} ~ 30 mN/m) is much lower than that of water (γ_{LV} = 72.8 mN/m). The low surface tension of the liquid facilitates liquid spreading on the solid surface. A smooth polytetrafluoroethylene (PTFE) surface, one of the most intrinsically hydrophobic materials known, displays a water contact angle of ~110 °, [201-202] while the oil contact angle is ~40°. Hence, surface chemistry alteration of the material is not sufficient to generate oil repellency. Many studies have addressed the creation of a surface that displays oil repellency. The critical factor for oil repellency on a solid surface is the formation of microscopic air pockets trapped beneath the liquid droplet; this scenario can be achieved with a specific combination of low surface energy material/chemistry and surface structures with re-entrant angles.[203-204] Figure 45 shows the formation of a solid-liquid-air composite interface on a structured surface. For the sloped structure (Figure 45a), the equilibrium contact angle is larger than 90 ° to ensure the composite interface. However, with the re-entrant structure, when the equilibrium contact angle is less than 90 °, it is possible to generate a composite interface that inhibits liquid penetration (Figure 45b). We are not aware of the generation of re-entrant structures constructed on SS surfaces. One way to achieve such structures is to electro-plate metal onto the electrochemically etched SS316L surface. The topology with sharp corners will have thicker deposited layers on the

outside corners and thinner layers of deposition in the recessed areas due to differences or non-uniformities in current distribution. That is, current flow is enhanced at sharp edges relative to recessed areas. In the electroplating industry, non-uniform deposition should be minimized. However, it may be possible to create re-entrant intrinsic grain structures by utilizing non-uniform electro-plating. If successful, this will be beneficial for many oil handling applications such as oil transporting pipes and oil-water separation operations.

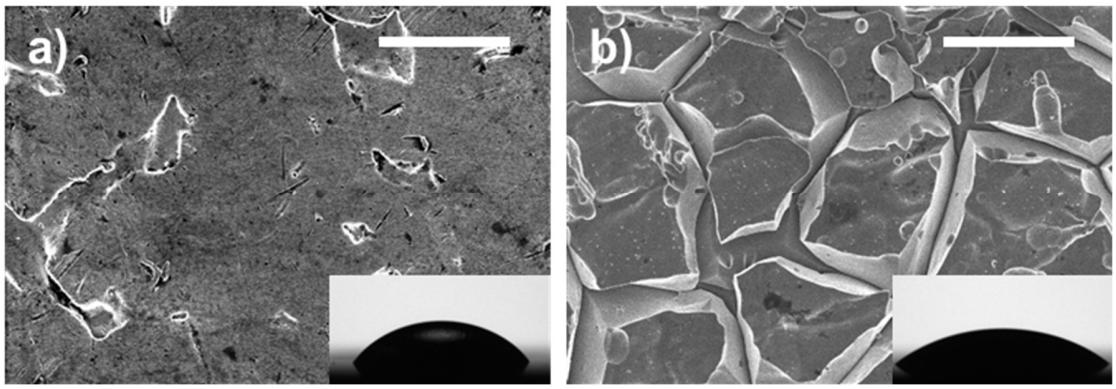

Figure 44. SEM images of SS316 electrochemically etched at different applied potentials: (a) As-received SS316L, (b) Electrochemically etched SS316L with an applied potential of 1.2 V (vs. SCE). The scale bar corresponds to 10 µm. The inset pictures show a hexadecane droplet on each surface. Both surfaces are coated with a 120 nm fluorocarbon film.

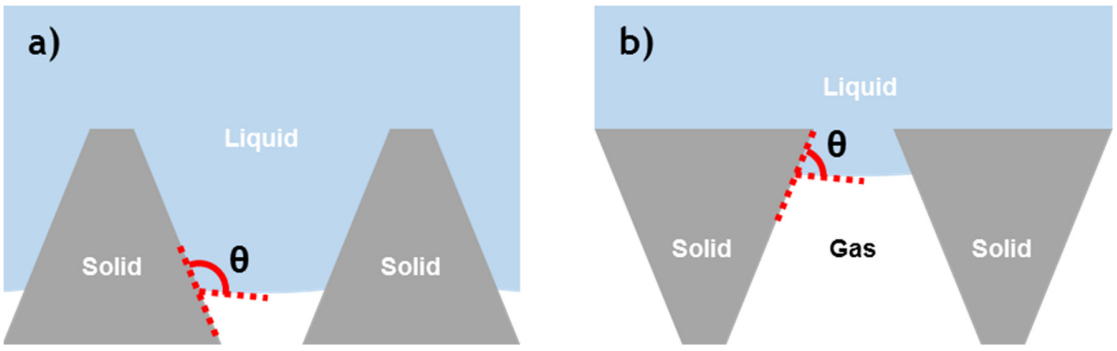

Figure 45. Formation of a solid-liquid-air composite interface on a structured surface. a) Liquid on entrant structured surface, b) Liquid on re-entrant structured surface.

6.2.2 Antifouling Effect of Surface-Modified SS316L

In chapter 3, I found that the microscale grain boundary etched SS316L surface have a superior localized corrosion resistance compared to as-received SS316L in 0.6 M NaCl solution mimicking seawater. The corrosion resistance as well as antifouling performance against diverse sizes of marine organisms ranging from algae to barnacles are significant for the SS316L applications in maritime industry. Direct investigation of the antifouling effect is required to prove the antifouling performance on the modified SS316L surface. *Amphora coffeaeformis* is a common model organism of algae for antifouling assay, which has 25 ~ 40 μm body size.[205] The adhesion of the algal cells on the surface can be detected and quantified by recording the *in vivo* chlorophyll fluorescence of the *Amphora* cells and counting them in a captured fluorescence image. In addition, barnacles cause the most serious problems as macro-fouling organisms in a wide geographical distribution. The cyprid from adult barnacles can be selected for the future investigation of marine antifouling effects on the grain boundary etched SS316L. In addition, grain sizes of SS316L can be controlled by thermal or thermomechanical treatment. Electrochemical etching on the grain size pre-controlled SS316L can evolve intrinsic grain structures with diverse sizes, which allows additional tunability of surface topography and optimization of antifouling SS316L surface against marine organisms.

6.2.3 Corrosion Resistance of Nano-textured SS316L in A Body Solution

Nano-textured SS316L can effectively reduce surface bacterial adhesion while maintaining adhesion and metabolic activity of desired bio-organisms such as fibroblasts. Corrosion of SS316L implants can degrade structural integrity and make them not functional and thereby compromise functionality, ultimately demanding replacement.[206-207] In addition, metallic particles can be released by the corrosion process, which can cause inflammatory reactions.[208] In particular, SS contains Ni; since Ni particles are carcinogenic, they could present a health concern.[209] Therefore, for biomedical applications, high corrosion resistance of the material in the human body is demanded. The human body is a highly oxygenated saline electrolyte at a pH of around 7.4 and a temperature of 37 °C. The ionic composition and protein concentration in body fluids can affect the corrosion behaviour of SS316L. For example, pitting corrosion arising from the breakdown of the passivating oxide film can be enhanced by the presence of proteins in the tissue fluid and serum.[210-211] Therefore, demonstrating corrosion resistance of nano-textured SS316L in a body solution is a necessary step to establish the applicability of nano-textured SS316L for *in vivo* biomedical applications. Furthermore, the bacterial cell lines can be extended to other pathogenic strains such as *Staphylococcus aureus* and *Psedomonas aeruginosa* for the purpose of anti-bacterial performance against diverse pathogens on the surface-modified SS316L. Human fibroblasts, osteoblasts, or endothelial cells can also be tested in order to claim the *in vivo* applicability of the developed SS316L surface.

REFERENCES

1. A non-rusting steel; Sheffield Invention especially good for rable cutlery. *New York Times* **1915,** *January 31*.

2. Global stainless steel production from 2005 to 2015. *https://www.statista.com/statistics/223028/world-stainless-steel-production/ (Accessed in Dec. 2016)*.

3. Roger A. Covert, A. H. T., Stainless steels: an introduction to their metallurgy and corrosion resistance. *Dairy, Food and Environmental Sanitation* **2000**, 506-517.

4. Cobb, H. M., The history of stainless steel. *ASM International* **2010**.

5. Stainless Steel. *https://en.wikipedia.org/wiki/Stainless_steel (Accessed Dec. 2016)*.

6. Cunat, P.-J., Alloying elements in stainless steel and other chromium-containing alloys. *Euro Inox* **2004,** (1-24).

7. Chapter 1. Introduction to stainless steels. *Alloy Digest Sourcebook: Stainless Steels, ASM International* **2000**.

8. Kosmac, A., Stainless steels at high temperaturee. *Euro Inox 18*, 1-37.

9. P. Atanda, A. F., O. Oluwole, Sensitization study of normalized 316L stainless steel. *Journal of Minerals & Materials Characterization & Engineering* **2010,** *9* (1), 13-23.

10. Classifications of stainless steel. *American Welding Society https://app.aws.org/wj/1998/11/kotecki/ (Accessed in Dec. 2016)*.

11. Stainless steels for design engineers: Chapter 6. austenitic stainless steels. *ASM International* **2008**.

12. Duplex stainless steel. *International Molybdenum Association http://www.imoa.info/molybdenum-uses/molybdenum-grade-stainless-steels/duplex-stainless-steel.php (Accessed in Dec. 2016)*.

13. Jones, D. A., Principles and prevention of corrosion. *Prentice Hall* **1996**.

14. Bagherifard, S.; Hickey, D. J.; de Luca, A. C.; Malheiro, V. N.; Markaki, A. E.; Guagliano, M.; Webster, T. J., The influence of nanostructured features on bacterial

adhesion and bone cell functions on severely shot peened 316L stainless steel. *Biomaterials* **2015,** *73*, 185-197.

15. Corrosion failures: San Francisco Bay Bridge bolt failure. *http://www.nace.org/corrosion-failures-San-Francisco-Bay-Bridge-Bolt-Failure.aspx (Accessed in Dec. 2016)*.

16. Cost of corrosion annually in the US over $1.1 trillion in 2016. *http://www.g2mtlabs.com/corrosion/cost-of-corrosion/ (Accessed in Dec. 2016)*.

17. Streicher, M. A., General and intergranular corrosion of austenitic stainless steels in acids: effect of cations in the acids and the influence of heat treatment and grain size of the steel. *Journal of The Electrochemical Society* **1959,** *106* (3), 161-180.

18. Frankel, G. S.; Sridhar, N., Understanding localized corrosion. *Materials Today* **2008,** *11* (10), 38-44.

19. Frankel, G. S., Pitting corrosion of metals: a review of the critical factors. *Journal of The Electrochemical Society* **1998,** *145* (6), 2186-2198.

20. Sato, N., Basics of corrosion chemistry. In *Green Corrosion Chemistry and Engineering*, Wiley-VCH Verlag GmbH & Co. KGaA: 2011; pp 1-32.

21. Preston, D. J.; Mafra, D. L.; Miljkovic, N.; Kong, J.; Wang, E. N., Scalable graphene coatings for enhanced condensation heat transfer. *Nano Letters* **2015,** *15* (5), 2902-2909.

22. Varanasi, K. K.; Hsu, M.; Bhate, N.; Yang, W.; Deng, T., Spatial control in the heterogeneous nucleation of water. *Applied Physics Letters* **2009,** *95* (9), 094101.

23. Cottin-Bizonne, C.; Barrat, J.-L.; Bocquet, L.; Charlaix, E., Low-friction flows of liquid at nanopatterned interfaces. *Nature Materials* **2003,** *2* (4), 237-240.

24. Bhushan, B.; Jung, Y. C., Natural and biomimetic artificial surfaces for superhydrophobicity, self-cleaning, low adhesion, and drag reduction. *Progress in Materials Science* **2011,** *56* (1), 1-108.

25. Khawaji, A. D.; Kutubkhanah, I. K.; Wie, J.-M., Advances in seawater desalination technologies. *Desalination* **2008,** *221* (1), 47-69.

26. Cho, Y.; Shim, T. S.; Yang, S., Spatially selective nucleation and growth of water droplets on hierarchically patterned polymer surfaces. *Advanced Materials* **2015,** *28* (7), 1433-1439.

27. Young, T., An essay on the cohesion of fluids. *Philosophical Transactions of the Royal Society of London* **1805,** *95*, 65-87.

28. Wenzel, R. N., Resistance of solid surfaces to wetting by water. *Industrial & Engineering Chemistry* **1936,** *28* (8), 988-994.

29. Cassie, A. B. D.; Baxter, S., Wettability of porous surfaces. *Transactions of the Faraday Society* **1944,** *40*, 546-551.

30. Cassie, A. B. D.; Baxter, S., Large Contact Angles of Plant and Animal Surfaces. *Nature* **1945,** *155*, 21.

31. de Gennes, P. G., Wetting: statics and dynamics. *Reviews of Modern Physics* **1985,** *57* (3), 827-863.

32. Furmidge, C. G. L., Studies at phase interfaces. I. The sliding of liquid drops on solid surfaces and a theory for spray retention. *Journal of Colloid Science* **1962,** *17* (4), 309-324.

33. Quéré, D., Wetting and Roughness. *Annual Review of Materials Research* **2008,** *38* (1), 71-99.

34. Chu, Z.; Seeger, S., Superamphiphobic surfaces. *Chemical Society Reviews* **2014,** *43*, 2784-2798.

35. Butt, H.-J.; Semprebon, C.; Papadopoulos, P.; Vollmer, D.; Brinkmann, M.; Ciccotti, M., Design principles for superamphiphobic surfaces. *Soft Matter* **2013,** *9* (2), 418-428.

36. Fürstner, R.; Barthlott, W.; Neinhuis, C.; Walzel, P., Wetting and self-Cleaning properties of artificial superhydrophobic surfaces. *Langmuir* **2005,** *21* (3), 956-961.

37. Barthlott, W.; Neinhuis, C., Purity of the sacred lotus, or escape from contamination in biological surfaces. *Planta* **1997,** *202* (1), 1-8.

38. Banerjee, I.; Pangule, R. C.; Kane, R. S., Antifouling Coatings: Recent Developments in the Design of Surfaces That Prevent Fouling by Proteins, Bacteria, and Marine Organisms. *Advanced Materials* **2011,** *23* (6), 690-718.

39. Magin, C. M.; Cooper, S. P.; Brennan, A. B., Non-toxic antifouling strategies. *Materials Today* **2010,** *13* (4), 36-44.

40. Higaki, Y.; Kobayashi, M.; Murakami, D.; Takahara, A., Anti-fouling behavior of polymer brush immobilized surfaces. *Polymer Journal* **2016,** *48* (4), 325-331.

41. P. Stoodley; K. Sauer; D. G. Davies; Costerton, J. W., Biofilms as complex differentiated communities. *Annual Review of Microbiology* **2002,** *56* (1), 187-209.

42. Kirschner, C. M.; Brennan, A. B., Bio-inspired antifouling strategies. *Annual Review of Materials Research* **2012,** *42* (1), 211-229.

43. Page, K.; Wilson, M.; Parkin, I. P., Antimicrobial surfaces and their potential in reducing the role of the inanimate environment in the incidence of hospital-acquired infections. *Journal of Materials Chemistry* **2009,** *19* (23), 3819-3831.

44. Liu, L.; Ercan, B.; Sun, L.; Ziemer, K. S.; Webster, T. J., Understanding the Role of Polymer Surface Nanoscale Topography on Inhibiting Bacteria Adhesion and Growth. *ACS Biomaterials Science & Engineering* **2016,** *2* (1), 122-130.

45. Jelic-Mrcelic, G.; Sliskovic, M.; Antolic, B., Biofouling communities on test panels coated with TBT and TBT-free copper based antifouling paints. *Biofouling* **2006,** *22* (5), 293-302.

46. Brady, R. M., No more Tin. What now for fouling control? *Journal of Portective Coatings and Linings* **2000,** *17* (6), 42-48.

47. Montali, A., Antibacterial coating systems. *Injury* **2006,** *37* (2), S81-S86.

48. Darouiche, R. O., Anti-Infective Efficacy of Silver-Coated Medical Prostheses. *Clinical Infectious Diseases* **1999,** *29* (6), 1371-1377.

49. Bixler, G. D.; Bhushan, B., Fluid drag reduction and efficient self-cleaning with rice leaf and butterfly wing bioinspired surfaces. *Nanoscale* **2013,** *5* (17), 7685-7710.

50. Carman, M. L.; Estes, T. G.; Feinberg, A. W.; Schumacher, J. F.; Wilkerson, W.; Wilson, L. H.; Callow, M. E.; Callow, J. A.; Brennan, A. B., Engineered antifouling microtopographies – correlating wettability with cell attachment. *Biofouling* **2006,** *22* (1), 11-21.

51. Brzozowska, A. M.; Parra-Velandia, F. J.; Quintana, R.; Xiaoying, Z.; Lee, S. S. C.; Chin-Sing, L.; Jańczewski, D.; Teo, S. L. M.; Vancso, J. G., Biomimicking micropatterned surfaces and their effect on marine biofouling. *Langmuir* **2014,** *30* (30), 9165-9175.

52. Bai, X. Q.; Xie, G. T.; Fan, H.; Peng, Z. X.; Yuan, C. Q.; Yan, X. P., Study on biomimetic preparation of shell surface microstructure for ship antifouling. *Wear* **2013,** *306* (1–2), 285-295.

53. Tuthill, A. H., Stainless steel: surface cleanliness. *Pharmaceutical Engineering* **1994,** *14* (6), 34-41.

54. Alaskari; Liptakova, T.; Fajnor, P.; Halamova, M., Mechanical surface treatments effects on corrosion of AISI 316 Ti stainless steel in chloride environments. *Journal of Engineering Research* **2014,** *2* (3), 195-210.

55. Wieser, H., Influence of shot peening on the corrosion fatigue properties of a stainless steel for surgical implants. *Materials and Corrosion* **2004,** *55* (3), 186-193.

56. Hashemi, B.; Rezaee Yazdi, M.; Azar, V., The wear and corrosion resistance of shot peened–nitrided 316L austenitic stainless steel. *Materials & Design* **2011,** *32* (6), 3287-3292.

57. Li, L.-F.; Caenen, P.; Daerden, M.; Vaes, D.; Meers, G.; Dhondt, C.; Celis, J.-P., Mechanism of single and multiple step pickling of 304 stainless steel in acid electrolytes. *Corrosion Science* **2005,** *47* (5), 1307-1324.

58. Li, L. F.; Celis, J. P., Pickling of austenitic stainless steels. *Canadian Metallurgical Quarterly* **2003,** *42* (3), 365-376.

59. Hultquist, G.; Leygraf, C., Surface Composition of a Type 316 Stainless Steel Related to Initiation of Crevice Corrosion. *Corrosion* **1980,** *36* (3), 126-129.

60. Lee, S.-J.; Lai, J.-J., The effects of electropolishing (EP) process parameters on corrosion resistance of 316L stainless steel. *Journal of Materials Processing Technology* **2003,** *140* (1–3), 206-210.

61. Andrade, L. S.; Xavier, S. C.; Rocha-Filho, R. C.; Bocchi, N.; Biaggio, S. R., Electropolishing of AISI-304 stainless steel using an oxidizing solution originally used for electrochemical coloration. *Electrochimica Acta* **2005,** *50* (13), 2623-2627.

62. Meka, S. R.; Chauhan, A.; Steiner, T.; Bischoff, E.; Ghosh, P. K.; Mittemeijer, E. J., Generating duplex microstructures by nitriding; nitriding of iron based Fe–Mn alloy. *Materials Science and Technology* **2016,** *32* (9), 883-889.

63. Sun, Y.; Bell, T., Sliding wear characteristics of low temperature plasma nitrided 316 austenitic stainless steel. *Wear* **1998,** *218* (1), 34-42.

64. Billon, B.; Hendry, A., Nitriding of stainless steel in ammonia: I phase distribution and microstructure. *Surface Engineering* **1985,** *1* (2), 125-130.

65. Liang, W., Surface modification of AISI 304 austenitic stainless steel by plasma nitriding. *Applied Surface Science* **2003,** *211* (1–4), 308-314.

66. Zhang, Z. L.; Bell, T., Structure and corrosion resistance of plasma nitrided stainless steel. *Surface Engineering* **1985,** *1* (2), 131-136.

67. Wu, B.; Zhou, M.; Li, J.; Ye, X.; Li, G.; Cai, L., Superhydrophobic surfaces fabricated by microstructuring of stainless steel using a femtosecond laser. *Applied Surface Science* **2009,** *256* (1), 61-66.

68. Kietzig, A.-M.; Hatzikiriakos, S. G.; Englezos, P., Patterned superhydrophobic metallic surfaces. *Langmuir* **2009,** *25* (8), 4821-4827.

69. Moradi, S.; Hadjesfandiari, N.; Toosi, S. F.; Kizhakkedathu, J. N.; Hatzikiriakos, S. G., Effect of extreme wettability on platelet adhesion on metallic implants: from

superhydrophilicity to superhydrophobicity. *ACS Applied Materials & Interfaces* **2016,** *8* (27), 17631-17641.

70. Ranade, R. M.; Ang, S. S.; Brown, W. D., Reactive ion etching of thin gold films. *Journal of The Electrochemical Society* **1993,** *140* (12), 3676-3678.

71. Park, B.; Hwang, W., A facile fabrication method for corrosion-resistant micro/nanostructures on stainless steel surfaces with tunable wettability. *Scripta Materialia* **2016,** *113*, 118-121.

72. Li, L.; Breedveld, V.; Hess, D. W., Creation of superhydrophobic stainless steel surfaces by acid treatments and hydrophobic film deposition. *ACS Applied Materials & Interfaces* **2012,** *4* (9), 4549-4556.

73. Yu, Z.; Yu, Y.; Li, Y.; Song, S.; Huo, S.; Han, X., Preparation and characterization of super-hydrophobic surfaces on aluminum and stainless steel substrates. *Surface Review and Letters* **2010,** *17* (3), 375-381.

74. Ibe, J. P.; Bey, P. P.; Brandow, S. L.; Brizzolara, R. A.; Burnham, N. A.; DiLella, D. P.; Lee, K. P.; Marrian, C. R. K.; Colton, R. J., On the electrochemical etching of tips for scanning tunneling microscopy. *Journal of Vacuum Science & Technology A* **1990,** *8* (4), 3570-3575.

75. Bell, F. C.; Sonon, D. E., Improved metallographic etching techniques for stainless steel and for stainless steel to carbon steel weldments. *Metallography* **1976,** *9* (2), 91-107.

76. Stöver, M.; Renke-Gluszko, M.; Schratzenstaller, T.; Will, J.; Klink, N.; Behnisch, B.; Kastrati, A.; Wessely, R.; Hausleiter, J.; Schömig, A.; Wintermantel, E., Microstructuring of stainless steel implants by electrochemical etching. *Journal of Materials Science* **2006,** *41* (17), 5569-5575.

77. Choi, W. T.; Oh, K.; Singh, P. M.; Breedveld, V.; Hess, D. W., Wettability control of stainless steel surfaces via evolution of intrinsic grain structures. *Journal of Materials Science* **2016,** *51* (11), 5196-5206.

78. Sutow, E. J., The influence of electropolishing on the corrosion resistance of 316L stainless steel. *Journal of Biomedical Materials Research* **1980,** *14* (5), 587-595.

79. Bani Kananeh, A.; Rausch, M. H.; Fröba, A. P.; Leipertz, A., Experimental study of dropwise condensation on plasma-ion implanted stainless steel tubes. *International Journal of Heat and Mass Transfer* **2006,** *49* (25–26), 5018-5026.

80. Bellanger, H.; Darmanin, T.; Taffin de Givenchy, E.; Guittard, F., Chemical and physical pathways for the preparation of superoleophobic surfaces and related wetting theories. *Chemical Reviews* **2014,** *114* (5), 2694-2716.

81. Feng, L.; Zhang, Z.; Mai, Z.; Ma, Y.; Liu, B.; Jiang, L.; Zhu, D., A super-hydrophobic and super-oleophilic coating mesh film for the separation of oil and water. *Angewandte Chemie International Edition* **2004,** *43* (15), 2012-2014.

82. Valipour Motlagh, N.; Birjandi, F. C.; Sargolzaei, J.; Shahtahmassebi, N., Durable, superhydrophobic, superoleophobic and corrosion resistant coating on the stainless steel surface using a scalable method. *Applied Surface Science* **2013,** *283*, 636-647.

83. Yang, H.; Pi, P.; Cai, Z.-Q.; Wen, X.; Wang, X.; Cheng, J.; Yang, Z.-r., Facile preparation of super-hydrophobic and super-oleophilic silica film on stainless steel mesh via sol–gel process. *Applied Surface Science* **2010,** *256* (13), 4095-4102.

84. Santos, O.; Nylander, T.; Rosmaninho, R.; Rizzo, G.; Yiantsios, S.; Andritsos, N.; Karabelas, A.; Müller-Steinhagen, H.; Melo, L.; Boulangé-Petermann, L.; Gabet, C.; Braem, A.; Trägårdh, C.; Paulsson, M., Modified stainless steel surfaces targeted to reduce fouling—surface characterization. *Journal of Food Engineering* **2004,** *64* (1), 63-79.

85. Liang, J.; Li, D.; Wang, D.; Liu, K.; Chen, L., Preparation of stable superhydrophobic film on stainless steel substrate by a combined approach using electrodeposition and fluorinated modification. *Applied Surface Science* **2014,** *293*, 265-270.

86. Chen, L. J.; Chen, M.; Zhou, H. D.; Chen, J. M., Preparation of super-hydrophobic surface on stainless steel. *Applied Surface Science* **2008,** *255* (5, Part 2), 3459-3462.

87. Chen, L. J.; Zhao, J. W., Preparation of Cu-coated stainless steel surfaces for superhydrophobic investigation. *Journal of Dispersion Science and Technology* **2010,** *31* (9), 1245-1248.

88. Armijo, J. S., Intergranular corrosion of nonsensitized austenitic stainless steels. *Corrosion* **1968,** *24* (1), 24-30.

89. Balu, B.; Breedveld, V.; Hess, D. W., Fabrication of "Roll-off" and "Sticky" superhydrophobic cellulose surfaces via plasma processing. *Langmuir* **2008,** *24* (9), 4785-4790.

90. Hoar, T. P.; Mears, D. C.; Rothwell, G. P., The relationships between anodic passivity, brightening and pitting. *Corrosion Science* **1965,** *5* (4), 279-289.

91. Li, Z.; Wang, Y.; Kozbial, A.; Shenoy, G.; Zhou, F.; McGinley, R.; Ireland, P.; Morganstein, B.; Kunkel, A.; Surwade, S. P.; Li, L.; Liu, H., Effect of airborne contaminants on the wettability of supported graphene and graphite. *Nature Materials* **2013,** *12* (10), 925-931.

92. Nobuyoshi Hara, K. H., Yu Sugawara, Izumi Muto, Improvement of pitting corrosion resistance of type 316L stainless steel by potentiostatic removal of surface MnS inclusions. *International Journal of Corrosion* **2012,** *2012*, 1-6.

93. Hanawa, T.; Hiromoto, S.; Yamamoto, A.; Kuroda, D.; Asami, K., XPS characterization of the surface oxide film 316L stainless steel samples that were located in quasi-biological environments. *Materials Transactions* **2002,** *43* (12), 3088-3092.

94. Asami, K.; Hashimoto, K., The X-ray photo-electron spectra ofseveral oxides of iron and chromium. *Corrosion Science* **1977,** *17* (7), 559-570.

95. Noh, J. S.; Laycock, N. J.; Gao, W.; Wells, D. B., Effects of nitric acid passivation on the pitting resistance of 316 stainless steel. *Corrosion Science* **2000,** *42* (12), 2069-2084.

96. Vaswani, S.; Koskinen, J.; Hess, D. W., Surface modification of paper and cellulose by plasma-assisted deposition of fluorocarbon films. *Surface and Coatings Technology* **2005,** *195* (2–3), 121-129.

97. Agraharam, S.; Hess, D. W.; Kohl, P. A.; Bidstrup Allen, S. A., Plasma chemistry in fluorocarbon film deposition from pentafluoroethane/argon mixtures. *Journal of Vacuum Science and Technology A* **1999,** *17* (6), 3265-3271.

98. Youngblood, J. P.; McCarthy, T. J., Ultrahydrophobic polymer surfaces prepared by simultaneous ablation of polypropylene and sputtering of poly(tetrafluoroethylene) using radio frequency plasma. *Macromolecules* **1999,** *32* (20), 6800-6806.

99. Gao, L.; McCarthy, T. J., Contact angle hysteresis explained. *Langmuir* **2006,** *22* (14), 6234-6237.

100. Feng, L.; Li, S.; Li, Y.; Li, H.; Zhang, L.; Zhai, J.; Song, Y.; Liu, B.; Jiang, L.; Zhu, D., Super-hydrophobic surfaces: from natural to artificial. *Advanced Materials* **2002,** *14* (24), 1857-1860.

101. Schwenk, W., Theory of stainless steel pitting. *Corrosion* **1964,** *20* (4), 129t-137t.

102. Ma, F.-Y., Corrosive effects of chlorides on metals. *INTECH Open Access Publisher* **2012**.

103. Stampella, R. S.; Albani, O. A.; Ruiz, E. R., Advances in corrosion and protection performance of high-alloy austenitic stainless steels in the actual and simulated bleaching media of the paper industry. *Corrosion Science* **1993,** *35* (1), 289-295.

104. Hoar, T. P.; Jacob, W. R., Breakdown of passivity of stainless steel by halide ions. *Nature* **1967,** *216*, 1299-1301.

105. Eklund, G. S., Initiation of pitting at sulfide inclusions in stainless steel. *Journal of The Electrochemical Society* **1974,** *121* (4), 467-473.

106. Wranglen, G., Pitting and sulphide inclusions in steel. *Corrosion Science* **1974,** *14* (5), 331-349.

107. Lage, R.; Møller, P.; Fallesen, H. E., The effect of surface treatment and topography on corrosion behavior of EN 1.4404 stainless steel. *Materials and Corrosion* **2015,** *66* (10), 1060-1067.

108. Crolet, J. L., Reply to "The effect of chromium enrichment in the film formed by surface treatments on the corrosion resistance of type 430 stainless steel": By T. Hong, T. Ogushi and M. Nagumo, Corros.Sci. 38, 881 (1996). *Corrosion Science* **1997,** *39* (6), 1137-1139.

109. Hong, T.; Ogushi, T.; Nagumo, M., The effect of chromium enrichment in the film formed by surface treatments on the corrosion resistance of type 430 stainless steel. *Corrosion Science* **1996,** *38* (6), 881-888.

110. Ghanavati, S.; Shishesaz, M. R.; Farzam, M.; Danaee, I., Effects of surface treatment on corrosion resistance of 304L and 316L stainless steel implants in Hank's solution. *Iranian Journal of Oil & Gas Science and Technology* **2016,** *5* (1), 65-72.

111. Jinlong, L.; Tongxiang, L.; Chen, W., Surface enriched molybdenum enhancing the corrosion resistance of 316L stainless steel. *Materials Letters* **2016,** *171*, 38-41.

112. Smialowski, M.; Szklarska-Smialowska, Z.; Rychcik, M.; Szummer, A., Effect of sulphide inclusions in a commercial stainless steel on the nucleation of corrosion pits. *Corrosion Science* **1969,** *9* (2), 123-125.

113. Baker, M. A.; Castle, J. E., The initiation of pitting corrosion at MnS inclusions. *Corrosion Science* **1993,** *34* (4), 667-682.

114. Dexter, S. C.; Zhang, H.-J.; Chandrasekaran, P., Biofouling effects on corrosion of stainless alloys in seawater. In *Mycotoxins, Wood Decay, Plant Stress, Biocorrosion, and General Biodeterioration*, Llewellyn, G. C.; Dashek, W. V.; O'Rear, C. E., Eds. Springer US: Boston, MA, 1994; pp 553-571.

115. de Messano, L. V. R.; Sathler, L.; Reznik, L. Y.; Coutinho, R., The effect of biofouling on localized corrosion of the stainless steels N08904 and UNS S32760. *International Biodeterioration & Biodegradation* **2009,** *63* (5), 607-614.

116. Dexter, S. C.; Gao, G. Y., Effect of seawater biofilms on corrosion potential and oxygen reduction of stainless steel. *Corrosion* **1988,** *44* (10), 717-723.

117. Dafforn, K. A.; Lewis, J. A.; Johnston, E. L., Antifouling strategies: History and regulation, ecological impacts and mitigation. *Marine Pollution Bulletin* **2011,** *62* (3), 453-465.

118. Callow, J. A.; Callow, M. E., Trends in the development of environmentally friendly fouling-resistant marine coatings. *Nature Communications* **2011,** *2*, 244.

119. Bers, A. V.; Wahl, M., The influence of natural surface microtopographies on fouling. *Biofouling* **2004,** *20* (1), 43-51.

120. Bers, A. V.; Díaz, E. R.; da Gama, B. A. P.; Vieira-Silva, F.; Dobretsov, S.; Valdivia, N.; Thiel, M.; Scardino, A. J.; McQuaid, C. D.; Sudgen, H. E.; Thomason, J. C.; Wahl, M., Relevance of mytilid shell microtopographies for fouling defence – a global comparison. *Biofouling* **2010,** *26* (3), 367-377.

121. Pu, X.; Li, G.; Huang, H., Preparation, anti-biofouling and drag-reduction properties of a biomimetic shark skin surface. *Biology Open* **2016,** *5* (4), 389-396.

122. Roy Chester, T. D. J., Marine geochemistry. *Wiley-Blackwell* **2012**.

123. Yi, Y.; Cho, P.; Al Zaabi, A.; Addad, Y.; Jang, C., Potentiodynamic polarization behaviour of AISI type 316 stainless steel in NaCl solution. *Corrosion Science* **2013,** *74*, 92-97.

124. Shibata, T.; Takeyama, T., Stochastic theory of pitting corrosion. *Corrosion* **1977,** *33* (7), 243-251.

125. Shibata, T., Stochastic studies of passivity breakdown. *Corrosion Science* **1990,** *31*, 413-423.

126. Ernst, P.; Laycock, N. J.; Moayed, M. H.; Newman, R. C., The mechanism of lacy cover formation in pitting. *Corrosion Science* **1997,** *39* (6), 1133-1136.

127. Bruellhoff, K.; Fiedler, J.; Moller, M.; Groll, J.; Brenner, R. E., Surface coating strategies to prevent biofilm formation on implant surfaces. *Int J Artif Organs* **2010,** *33* (9), 646-653.

128. Kang, G. D.; Cao, Y. M., Development of antifouling reverse osmosis membranes for water treatment: A review. *Water Res* **2012,** *46* (3), 584-600.

129. Marcato-Romain, C. E.; Pechaud, Y.; Paul, E.; Girbal-Neuhauser, E.; Dossat-Letisse, V., Removal of microbial multi-species biofilms from the paper industry by enzymatic treatments. *Biofouling* **2012,** *28* (3), 305-314.

130. Bott, T. R., Chapter 1 - Industrial biofouling. In *Industrial Biofouling*, Elsevier: Amsterdam, 2011; pp 1-5.

131. Bott, T. R., Chapter 7 - Biofilms in industry. In *Industrial Biofouling*, Elsevier: Amsterdam, 2011; pp 181-201.

132. Ji, X. Y.; Fei, C. N.; Zhang, Y.; Zhang, W.; Liu, J.; Dong, J., Evaluation of bacterial contamination of dental unit waterlines and use of a newly designed measurement device to assess retraction of a dental chair unit. *Int Dent J* **2016,** *66* (4), 208-214.

133. Szymanska, J.; Sitkowska, J., Bacterial contamination of dental unit waterlines. *Environ Monit Assess* **2013,** *185* (5), 3603-3611.

134. Simoes, L. C.; Simoes, M.; Vieira, M. J., Adhesion and biofilm formation on polystyrene by drinking water-isolated bacteria. *Anton Leeuw Int J G* **2010,** *98* (3), 317-329.

135. Tuson, H. H.; Weibel, D. B., Bacteria-surface interactions. *Soft Matter* **2013,** *9* (17), 4368-4380.

136. vanOss, C. J., Hydrophobicity and hydrophilicity of biosurfaces. *Current Opinion in Colloid & Interface Science* **1997,** *2* (5), 503-512.

137. Qian, X.; Metallo, S. J.; Choi, I. S.; Wu, H.; Liang, M. N.; Whitesides, G. M., Arrays of self-assembled monolayers for studying inhibition of bacterial adhesion. *Analytical Chemistry* **2002,** *74* (8), 1805-1810.

138. Garrett, T. R.; Bhakoo, M.; Zhang, Z. B., Bacterial adhesion and biofilms on surfaces. *Progress in Natural Science* **2008,** *18* (9), 1049-1056.

139. Nishino, T.; Nayak, B. B.; Kogure, K., Density-dependent sorting of physiologically different cells of Vibrio parahaemolyticus. *Applied and Environmental Microbiology* **2003,** *69* (6), 3569-3572.

140. Boks, N. P.; Kaper, H. J.; Norde, W.; Busscher, H. J.; van der Mei, H. C., Residence time dependent desorption of Staphylococcus epidermidis from hydrophobic and hydrophilic substrata. *Colloid Surface B* **2008,** *67* (2), 276-278.

141. Xu, C. P.; Boks, N. P.; de Vries, J.; Kaper, H. J.; Norde, W.; Busscher, H. J.; van der Mei, H. C., Staphylococcus aureus-Fibronectin Interactions with and without Fibronectin-Binding Proteins and Their Role in Adhesion and Desorption. *Applied and Environmental Microbiology* **2008,** *74* (24), 7522-7528.

142. Renner, L. D.; Weibel, D. B., Physicochemical regulation of biofilm formation. *MRS Bulletin* **2011,** *36* (5), 347-355.

143. Renner, L. D.; Weibel, D. B., Cardiolipin microdomains localize to negatively curved regions of Escherichia coli membranes. *Proceedings of the National Academy of Science* **2011,** *108* (15), 6264-6269.

144. Renner, L. D.; Weibel, D. B., The role of cardiolipin domains in protein localization in bacterial cells. *Biophysical Journal* **2011,** *100* (3), 526-526.

145. Marshall, K. C.; Stout, R.; Mitchell, R., Mechanism of initial events in sorption of marine bacteria to surfaces. *Journal of General Microbiology* **1971,** *68*, 337-348.

146. Vanoss, C. J., Hydrophobicity of biosurfaces - origin, quantitative-determination and interaction energies. *Colloid Surface B* **1995,** *5* (3-4), 91-110.

147. Vigeant, M. A. S.; Ford, R. M.; Wagner, M.; Tamm, L. K., Reversible and irreversible adhesion of motile Escherichia coli cells analyzed by total internal reflection aqueous fluorescence microscopy. *Applied and Environmental Microbiology* **2002,** *68* (6), 2794-2801.

148. Fonseca, A. P.; Granja, P. L.; Nogueira, J. A.; Oliveira, D. R.; Barbosa, M. A., Staphylococcus epidermidis RP62A adhesion to chemically modified cellulose derivatives. *Journal of Materials Science-Materials in Medicine* **2001,** *12* (6), 543-548.

149. Chao, Y.; Zhang, T., Probing roles of lipopolysaccharide, Type 1 fimbria, and colanic acid in the attachment of escherichia coli strains on inert surfaces. *Langmuir* **2011,** *27* (18), 11545-11553.

150. Goulter-Thorsen, R. M.; Taran, E.; Gentle, I. R.; Gobius, K. S.; Dykes, G. A., CsgA production by escherichia coli O157:H7 alters attachment to abiotic surfaces in some growth environments. *Applied and Environmental Microbiology* **2011,** *77* (20), 7339-7344.

151. Tiller, J. C.; Liao, C.-J.; Lewis, K.; Klibanov, A. M., Designing surfaces that kill bacteria on contact. *Proceedings of the National Academy of Sciences* **2001,** *98* (11), 5981-5985.

152. Knetsch, M. L. W.; Koole, L. H., New strategies in the development of antimicrobial coatings: the example of increasing usage of silver and silver nanoparticles. *Polymers-Basel* **2011,** *3* (1), 340-366.

153. Kenawy, E.-R.; Worley, S. D.; Broughton, R., The chemistry and applications of antimicrobial polymers: a state-of-the-art review. *Biomacromolecules* **2007,** *8* (5), 1359-1384.

154. Roosjen, A.; van der Mei, H. C.; Busscher, H. J.; Norde, W., Microbial adhesion to poly(ethylene oxide) brushes: influence of polymer chain length and temperature. *Langmuir* **2004,** *20* (25), 10949-10955.

155. Yu, K.; Lo, J. C. Y.; Mei, Y.; Haney, E. F.; Siren, E.; Kalathottukaren, M. T.; Hancock, R. E. W.; Lange, D.; Kizhakkedathu, J. N., Toward Infection-Resistant Surfaces: Achieving High Antimicrobial Peptide Potency by Modulating the Functionality of Polymer Brush and Peptide. *ACS Applied Materials & Interfaces* **2015,** *7* (51), 28591-28605.

156. Nejadnik, M. R.; van der Mei, H. C.; Norde, W.; Busscher, H. J., Bacterial adhesion and growth on a polymer brush-coating. *Biomaterials* **2008,** *29* (30), 4117-4121.

157. Senaratne, W.; Andruzzi, L.; Ober, C. K., Self-assembled monolayers and polymer brushes in biotechnology: current applications and future perspectives. *Biomacromolecules* **2005,** *6* (5), 2427-2448.

158. Fu, H.; Hong, X.; Wan, A.; Batteas, J. D.; Bergbreiter, D. E., Parallel effects of cations on PNIPAM graft wettability and PNIPAM solubility. *ACS Applied Materials & Interfaces* **2010,** *2* (2), 452-458.

159. Ista, L. K.; López, G. P., Lower critical solubility temperature materials as biofouling release agents. *Journal of Industrial Microbiology and Biotechnology* **1998,** *20* (2), 121-125.

160. Dalsin, J. L.; Messersmith, P. B., Bioinspired antifouling polymers. *Materials Today* **2005,** *8* (9), 38-46.

161. Chung, K. K.; Schumacher, J. F.; Sampson, E. M.; Burne, R. A.; Antonelli, P. J.; Brennana, A. B., Impact of engineered surface microtopography on biofilm formation of Staphylococcus aureus. *Biointerphases* **2007,** *2* (2), 89-94.

162. Epstein, A. K.; Wong, T. S.; Belisle, R. A.; Boggs, E. M.; Aizenberg, J., Liquid-infused structured surfaces with exceptional anti-biofouling performance. *Proceedings of the National Academy of Sciences* **2012,** *109* (33), 13182-13187.

163. Diaz, C.; de Mele, M. A. F. L.; Schilardi, P. L., Comment on "The interaction of cells and bacteria with surfaces structured at the nanometre scale". *Acta Biomaterialia* **2011,** *7* (4), 1934-1935.

164. Anselme, K.; Davidson, P.; Popa, A. M.; Giazzon, M.; Liley, M.; Ploux, L., The interaction of cells and bacteria with surfaces structured at the nanometre scale. *Acta Biomaterialia* **2010,** *6* (10), 3824-3846.

165. Kim, S.; Jung, U. T.; Kim, S. K.; Lee, J. H.; Choi, H. S.; Kim, C. S.; Jeong, M. Y., Nanostructured multifunctional surface with antireflective and antimicrobial characteristics. *ACS Applied Materials & Interfaces* **2015,** *7* (1), 326-331.

166. Wu, S. M.; Zuber, F.; Brugger, J.; Maniura-Weber, K.; Ren, Q., Antibacterial Au nanostructured surfaces. *Nanoscale* **2016,** *8* (5), 2620-2625.

167. Feng, G.; Cheng, Y.; Wang, S.-Y.; Hsu, L. C.; Feliz, Y.; Borca-Tasciuc, D. A.; Worobo, R. W.; Moraru, C. I., Alumina surfaces with nanoscale topography reduce attachment and biofilm formation by Escherichia coli and Listeria spp. *Biofouling* **2014,** *30* (10), 1253-1268.

168. Feng, G.; Cheng, Y.; Wang, S.-Y.; Borca-Tasciuc, D. A.; Worobo, R. W.; Moraru, C. I., Bacterial attachment and biofilm formation on surfaces are reduced by small-

diameter nanoscale pores: how small is small enough? *Npj Biofilms And Microbiomes* **2015,** *1*, 15022.

169. Ivanova, E. P.; Hasan, J.; Webb, H. K.; Truong, V. K.; Watson, G. S.; Watson, J. A.; Baulin, V. A.; Pogodin, S.; Wang, J. Y.; Tobin, M. J.; Lobbe, C.; Crawford, R. J., Natural bactericidal surfaces: mechanical rupture of pseudomonas aeruginosa cells by cicada wings. *Small* **2012,** *8* (16), 2489-2494.

170. Ivanova, E. P.; Hasan, J.; Webb, H. K.; Gervinskas, G.; Juodkazis, S.; Truong, V. K.; Wu, A. H. F.; Lamb, R. N.; Baulin, V. A.; Watson, G. S.; Watson, J. A.; Mainwaring, D. E.; Crawford, R. J., Bactericidal activity of black silicon. *Nature Communications* **2013,** *4*.

171. An, Y. H.; Friedman, R. J., Laboratory methods for studies of bacterial adhesion. *Journal of Microbiological Methods* **1997,** *30* (2), 141-152.

172. Ladd, T. I.; Costerton, J. W., Methods for studying biofilm bacteria. In *Methods in Microbiology*, Grigorova, R.; Norris, J. R., Eds. Academic Press: 1990; Vol. Volume 22, pp 285-307.

173. Fry, J. C., Direct methods and biomass estimation. In *Methods in Microbiology*, Grigorova, R.; Norris, J. R., Eds. Academic Press: 1990; Vol. Volume 22, pp 41-85.

174. Allison, D. G.; Sutherland, I. W., A staining technique for attached bacteria and its correlation to extracellular carbohydrate production. *Journal of Microbiological Methods* **1984,** *2* (2), 93-99.

175. Caldwell, D. E.; Germida, J. J., Evaluation of difference imagery for visualizing and quantitating microbial growth. *Canadian Journal of Microbiology* **1985,** *31* (1), 35-44.

176. Herbert, R. A., Methods for enumerating microorganisms and determining biomass in natural environments. In *Methods in Microbiology*, Grigorova, R.; Norris, J. R., Eds. Academic Press: 1990; Vol. Volume 22, pp 1-39.

177. Gotman, I., Characteristics of metals used in implants. *Journal of Endourology* **1997,** *11* (6), 383-389.

178. Ionescu, R.; Mardare, M.; Dorobantu, A.; Vermesan, S.; Marinescu, E.; Saban, R.; Antoniac, I.; Ciocan, D. N.; Ceausu, M., Correlation between materials, design and clinical issues in the case of associated use of different stainless steels as implant materials. *Key Engineering Materials* **2014,** *583*, 41-44.

179. Parker, A. R.; Lawrence, C. R., Water capture by a desert beetle. *Nature* **2001,** *414* (6859), 33-34.

180. Seo, J.; Lee, S.; Lee, J.; Lee, T., Guided transport of water droplets on superhydrophobic–hydrophilic patterned Si nanowires. *ACS Applied Materials & Interfaces* **2011,** *3* (12), 4722-4729.

181. Yong, J.; Chen, F.; Yang, Q.; Zhang, D.; Du, G.; Si, J.; Yun, F.; Hou, X., Femtosecond laser weaving superhydrophobic patterned PDMS surfaces with tunable adhesion. *The Journal of Physical Chemistry C* **2013,** *117* (47), 24907-24912.

182. Her, E. K.; Ko, T.-J.; Lee, K.-R.; Oh, K. H.; Moon, M.-W., Bioinspired steel surfaces with extreme wettability contrast. *Nanoscale* **2012,** *4* (9), 2900-2905.

183. Garrod, R. P.; Harris, L. G.; Schofield, W. C. E.; McGettrick, J.; Ward, L. J.; Teare, D. O. H.; Badyal, J. P. S., Mimicking a Stenocara Beetle's back for microcondensation using plasmachemical patterned superhydrophobic−superhydrophilic surfaces. *Langmuir* **2007,** *23* (2), 689-693.

184. Balu, B.; Berry, A. D.; Hess, D. W.; Breedveld, V., Patterning of superhydrophobic paper to control the mobility of micro-liter drops for two-dimensional lab-on-paper applications. *Lab on a Chip* **2009,** *9* (21), 3066-3075.

185. Chen, X.; Kong, L.; Dong, D.; Yang, G.; Yu, L.; Chen, J.; Zhang, P., Fabrication of functionalized copper compound hierarchical structure with bionic superhydrophobic properties. *The Journal of Physical Chemistry C* **2009,** *113* (14), 5396-5401.

186. Qian, B.; Shen, Z., Fabrication of superhydrophobic surfaces by dislocation-selective chemical etching on aluminum, copper, and zinc substrates. *Langmuir* **2005,** *21* (20), 9007-9009.

187. Liu, L.; Xu, F.; Ma, L., Facile fabrication of a superhydrophobic Cu surface via a selective etching of high-energy facets. *The Journal of Physical Chemistry C* **2012,** *116* (35), 18722-18727.

188. Hao, L.; Chen, Z.; Wang, R.; Guo, C.; Zhang, P.; Pang, S., A non-aqueous electrodeposition process for fabrication of superhydrophobic surface with hierarchical micro/nano structure. *Applied Surface Science* **2012,** *258* (22), 8970-8973.

189. Priyanka, B.; Smita, G.; Javed, M.; Shankar, G.; Pushan, A., Universal, geometry-driven hydrophobic behaviour of bare metal nanowire clusters. *Nanotechnology* **2008,** *19* (7), 075709.

190. Qiao bao, Z.; Daguo, X.; Tak Fu, H.; Kaili, Z., Facile synthesis, growth mechanism and reversible superhydrophobic and superhydrophilic properties of non-flaking CuO nanowires grown from porous copper substrates. *Nanotechnology* **2013,** *24* (6), 065602.

191. Mumm, F.; van Helvoort, A. T. J.; Sikorski, P., Easy route to superhydrophobic copper-based wire-guided droplet microfluidic systems. *ACS Nano* **2009,** *3* (9), 2647-2652.

192. Barthwal, S.; Lim, S.-H., Fabrication of long-term stable superoleophobic surface based on copper oxide/cobalt oxide with micro-nanoscale hierarchical roughness. *Applied Surface Science* **2015,** *328*, 296-305.

193. Yao, X.; Chen, Q.; Xu, L.; Li, Q.; Song, Y.; Gao, X.; Quéré, D.; Jiang, L., Bioinspired ribbed nanoneedles with robust superhydrophobicity. *Advanced Functional Materials* **2010,** *20* (4), 656-662.

194. Yao, X.; Gao, J.; Song, Y.; Jiang, L., Superoleophobic surfaces with controllable oil adhesion and their application in oil transportation. *Advanced Functional Materials* **2011,** *21* (22), 4270-4276.

195. Huang, D.-J.; Leu, T.-S., Fabrication of high wettability gradient on copper substrate. *Applied Surface Science* **2013,** *280*, 25-32.

196. Zhu, X.; Zhang, Z.; Men, X.; Yang, J.; Xu, X.; Zhou, X., Plasma/thermal-driven the rapid wettability transition on a copper surface. *Applied Surface Science* **2011,** *257* (8), 3753-3757.

197. Qinmin, P.; Haizu, J.; Hongbo, W., Fabrication of superhydrophobic surfaces on interconnected Cu(OH) 2 nanowires via solution-immersion. *Nanotechnology* **2007,** *18* (35), 355605.

198. Haghdoost, A.; Pitchumani, R., Fabricating superhydrophobic surfaces via a two-step electrodeposition technique. *Langmuir* **2014,** *30* (14), 4183-4191.

199. Chavez, K. L.; Hess, D. W., A novel method of etching copper oxide using acetic acid. *Journal of The Electrochemical Society* **2001,** *148* (11), G640-G643.

200. Zhang, W.; Wen, X.; Yang, S., Controlled reactions on a copper surface: synthesis and characterization of nanostructured copper compound films. *Inorganic Chemistry* **2003,** *42* (16), 5005-5014.

201. Quéré, D., Rough ideas on wetting. *Physica A: Statistical Mechanics and its Applications* **2002,** *313* (1–2), 32-46.

202. Nishino, T.; Meguro, M.; Nakamae, K.; Matsushita, M.; Ueda, Y., The lowest surface free energy based on −CF3 alignment. *Langmuir* **1999,** *15* (13), 4321-4323.

203. Tuteja, A.; Choi, W.; Ma, M.; Mabry, J. M.; Mazzella, S. A.; Rutledge, G. C.; McKinley, G. H.; Cohen, R. E., Designing superoleophobic surfaces. *Science* **2007,** *318* (5856), 1618-1622.

204. Tuteja, A.; Choi, W.; Mabry, J. M.; McKinley, G. H.; Cohen, R. E., Robust omniphobic surfaces. *Proceedings of the National Academy of Sciences* **2008**.

205. Jellali, R.; Kromkamp, J. C.; Campistron, I.; Laguerre, A.; Lefebvre, S.; Perkins, R. G.; Pilard, J.-F.; Mouget, J.-L., Antifouling action of polyisoprene-based coatings by inhibition of photosynthesis in microalgae. *Environmental Science & Technology* **2013,** *47* (12), 6573-6581.

206. Sansone, V.; Pagani, D.; Melato, M., The effects on bone cells of metal ions released from orthopaedic implants. A review. *Clinical Cases in Mineral and Bone Metabolism* **2013,** *10* (1), 34-40.

207. Sivakumar, M.; Mudali, U. K.; Rajeswari, S., Compatibility of ferritic and duplex stainless steels as implant materials: in vitro corrosion performance. *Journal of Materials Science* **1993,** *28* (22), 6081-6086.

208. Hofmann, J.; Michel, R.; Holm, R.; Zilkens, J., Corrosion behaviour of stainless steel implants in biological media. *Surface and Interface Analysis* **1981,** *3* (3), 110-117.

209. Eric Jones, J.; Chen, M.; Yu, Q., Corrosion resistance improvement for 316L stainless steel coronary artery stents by trimethylsilane plasma nanocoatings. *Journal of Biomedical Materials Research Part B: Applied Biomaterials* **2014,** *102* (7), 1363-1374.

210. Williams, R. L.; Brown, S. A.; Merritt, K., Electrochemical studies on the influence of proteins on the corrosion of implant alloys. *Biomaterials* **1988,** *9* (2), 181-186.

211. Kocijan, A.; Milošev, I.; Pihlar, B., The influence of complexing agent and proteins on the corrosion of stainless steels and their metal components. *Journal of Materials Science: Materials in Medicine* **2003,** *14* (1), 69-77.

VITA

Won Tae Choi

Won Tae Choi was born in Seoul, South Korea. He received a B.S. (Summa Cum Laude) in Chemical Engineering from Hanyang University in Seoul, Korea in 2009. He earned a M.S. in Chemical Engineering from Seoul National University before joining to Georgia Tech to pursue a doctorate in Chemical Engineering. When he is not working in the lab, Won Tae enjoys spending time with his friends and dating with his wife, Yeongseon.